Linköping Studies in Science and Technology
Thesis No. 564

Driveline Modeling and Principles for Speed Control and Gear-Shift Control

Magnus Pettersson

Division of Vehicular Systems
Department of Electrical Engineering
Linköping University, S–581 83 Linköping, Sweden

Linköping 1996

Driveline Modeling and Principles for Speed Control and Gear-Shift Control

magnusp@isy.liu.se
Department of Electrical Engineering
Linköping University
S–581 83 Linköping
Sweden

ISBN 91-7871-744-2
ISSN 0280-7971
LiU-TEK-LIC-1996:29

To Anna and Oscar

Abstract

A vehicular driveline consists of engine, clutch, transmission, shafts, and wheels, which are controlled by a driveline management system.

Experiments and modeling using a heavy truck show that there are significant torsional resonances in the driveline. A linear model with a drive shaft flexibility is able to sufficiently explain the measured engine speed and wheel speed.

Engine control for automatic gear shifting is an approach at the leading edge of technology. A critical step is the controlling of the engine such that the transmission transfers zero torque, whereafter neutral gear can be engaged. Driveline oscillations is a limiting factor in this system. A model of the transmission torque is developed and a state-feedback controller is used to drive this torque to zero. The result is a possibility to optimize the time needed for a gear shift. Furthermore, neutral gear can successfully be engaged also when facing load disturbances and initial driveline oscillations.

Traditionally in diesel trucks, the engine speed is controlled by a system called RQV. This system has the desired property of a load dependent stationary error, and the undesired property of vehicle shuffle following a change in pedal position. A model based state-feedback controller is derived that actively reduces wheel speed oscillations. The performance and driveability is significantly improved, while maintaining the desired load characteristics for RQV control.

In conclusion, the proposed strategies improve performance and driveability in both speed control and gear-shift control.

Acknowledgment

This work has been carried out under the excellent guidance of Professor Lars Nielsen at Vehicular Systems, Linköping University, Sweden. By inspiring me and taking time for many discussions he has contributed to this work in many ways.

I am indebted to Lars-Gunnar Hedström, Anders Björnberg, Kjell Gestlöv, and Björn Westman at Scania in Södertälje for the help during this work, and for interesting discussions regarding control and modeling in heavy trucks.

I am also grateful to Simon Edlund, Lars Eriksson, and Mattias Nyberg for reading the manuscript. Thanks for the remarks and suggested improvements. Thanks also to Tomas Henriksson, my former office colleague, for our many discussions regarding research and courses.

I am indebted to Dr Joakim Petersson, Dr Fredrik Gustafsson, Dr Anders Helmersson, and Dr Tomas McKelvey for help and discussions.

Thanks to Dr Peter Lindskog and Magnus Sundstedt for support on computers and LaTeX.

I am very grateful to my parents Birgitta and Nils and my sister Katharina for their love and support in whatever I do.

Finally, I would like to express my deepest gratitude to my wife Anna and our son Oscar for their encouragements, patience, and love during this work.

Linköping, April 1996

Magnus Pettersson

Contents

1

Introduction

The main parts of a vehicular driveline are engine, clutch, transmission, shafts, and wheels. Since these parts are elastic, mechanical resonances may occur. The handling of such resonances is of course basic for driveability, but is also otherwise becoming increasingly important since it is a linking factor in development of new driveline management systems. Two systems where driveline oscillations limit performance is speed control and automatic gear shifting.

Fundamental driveline equations are obtained by using Newton's second law. The result is a series of models consisting of rotating inertias, connected with damped torsional flexibilities. Experiments are performed with a heavy truck with different gears and road slopes. The aim of the modeling and experiments is to find the most important physical effects that contribute to driveline oscillations. Some open questions are discussed, regarding influence of sensor dynamics and nonlinear effects.

The first problem is wheel speed oscillations following a change in accelerator pedal position, known as vehicle shuffle (Mo, Beaumount, and Powell 1996; Pettersson and Nielsen 1995). Traditionally in diesel trucks, the fuel metering is governed by a system called RQV. With RQV, there is no active damping of wheel speed oscillations resulting in vehicle shuffle. Another property is that a load dependent stationary error results from downhill and uphill driving. The thesis treats model based speed control with active damping of wheel speed oscillations while maintaining the stationary error characteristic for RQV control.

Engine controlled gear shifting without disengaging the clutch is an approach at the leading edge of technology (Orehall 1995). The engine is controlled such that the transmission transfers zero torque, whereafter neutral gear can be engaged.

The engine speed is then controlled to a speed such that the new gear can be engaged. A critical part in this scheme is the controlling of the engine such that the transmission torque is zero. In this state, the vehicle is free rolling, which must be handled. Driveline oscillations is a limiting factor in optimizing this step. In this thesis the transmission torque is modeled, and controlled to zero by using state feedback. With this approach, it is possible to optimize the time needed for a gear shift, also when facing existing initial driveline oscillations.

A common architectural issue in the two applications described above is the issue of sensor location. Different sensor locations result in different control problems. A comparison is made between using feedback from the engine speed sensor or the wheel speed sensor, and the influence in control design is investigated.

1.1 Outline and Contributions

In Chapters 2 and 3, a set of three driveline models is derived. Experiments with a heavy truck are described together with the modeling conclusions. The contribution of the chapter is that a linear model with one torsional flexibility and two inertias is able to fit the measured engine speed and wheel speed within the bandwidth of interest. Parameter estimation of a model with a nonlinear clutch and sensor dynamics explains that the difference between experiments and model occurs when the clutch transfers zero torque.

Control of resonant systems with simple controllers is, from other technical fields, known to have different properties with respect to sensor location. These results are reviewed in Chapter 4. The extension to more advanced control design methods is a little studied topic. The contribution of the chapter is a demonstration of the influence of sensor location in driveline control when using LQG/LTR.

Chapters 5 treats the design and simulation of the speed controller. A key contribution in this chapter is the formulation of a criterion for the speed control concept described above with active damping and retained RQV feeling. A simulation study shows significantly improved performance and driveability.

Chapters 6 deals with the design and simulation of the gear-shift controller. A major contribution in this thesis is a gear shifting strategy, based on a model describing the transmission torque, and a criterion for a controller that drives this torque to zero. The design improves the performance also in the case of load disturbances and initial driveline oscillations. Conclusions are summarized in Chapter 7.

2

Driveline Modeling

The driveline is a fundamental part of a vehicle and its dynamics has been modeled in different ways depending on the purpose. The frequency range treated in this work is the regime interesting for control design (Mo, Beaumount, and Powell 1996; Pettersson and Nielsen 1995). Vibrations and noise contribute to a higher frequency range (Suzuki and Tozawa 1992; Gillespie 1992) which is not treated here. This chapter deals with building models of a truck driveline. The generalized Newton's second law is used together with assumptions about how different parts in the driveline contribute to the model. The aim of these assumptions is to find the most important physical effects, contributing to driveline oscillations. Modeling is an iterative process in reality. Nevertheless, a set of three models of increasing complexity is presented. Next chapter will validate the choices.

First, a linear model with flexible drive shafts is derived. Assumptions about stiff clutch, stiff propeller shaft, viscous friction in transmission and final drive, together with a linear model of the air drag constitute the model. A second linear model is given by using the assumptions made above, and adding a second flexibility which is the clutch. Finally, a more complete nonlinear model is derived which includes a clutch model with a static nonlinearity.

2.1 Basic Equations

A vehicular driveline is depicted in Figure 2.1. It consists of an engine, clutch, transmission, propeller shaft, final drive, drive shafts, and wheels. In this section fundamental equations for the driveline will be derived. Furthermore, some basic equations regarding the forces acting on the wheel, are obtained. These equations

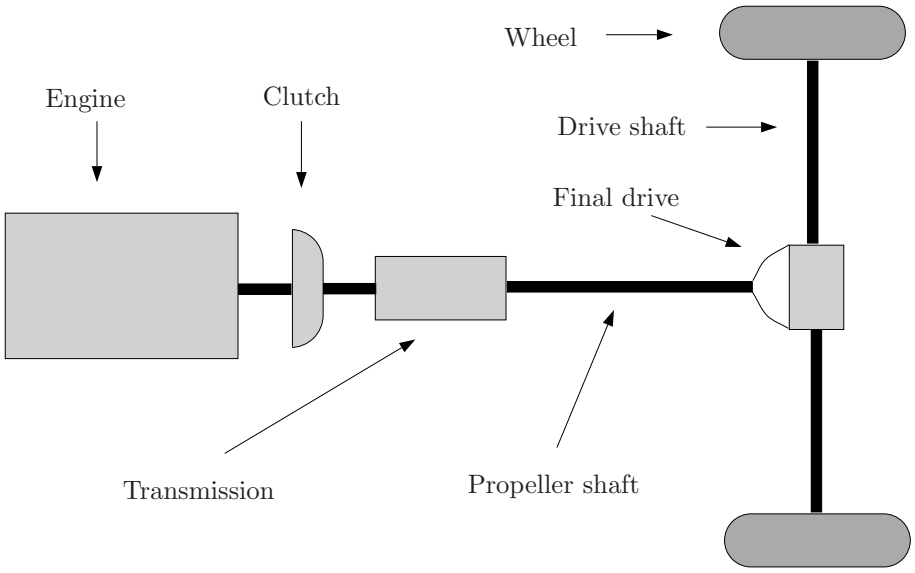

Figure 2.1 *A vehicular driveline.*

are influenced by the complete dynamics of the vehicle. This means that effects from, for instance, vehicle mass and trailer will be described by the equation describing the wheel. Next, a relation between the inputs and outputs of each part is obtained, in order to get a complete physical model. Inputs and outputs of each subsystem are labeled according to Figure 2.2.

Engine: The output torque of the engine is characterized by the driving torque (M_m) resulting from the combustion, the internal friction from the engine ($M_{fr:m}$), and the external load from the clutch (M_c). The generalized Newton's second law of motion (Meriam and Kraige 1987) gives the following model

$$J_m\ddot{\theta}_m = M_m - M_{fr:m} - M_c \tag{2.1}$$

where J_m is the mass moment of inertia of the engine and θ_m is the angle of the flywheel.

Clutch: A friction clutch found in vehicles equipped with a manual transmission consists of a clutch disk connecting the flywheel of the engine and the transmission's input shaft. When the clutch is engaged, no internal friction is assumed, giving $M_c = M_t$, according to Figure 2.2. The transmitted torque is a function of the angular difference $(\theta_m - \theta_c)$ and the angular velocity difference $(\dot{\theta}_m - \dot{\theta}_c)$ over the clutch

$$M_c = M_t = f_c(\theta_m - \theta_c,\ \dot{\theta}_m - \dot{\theta}_c) \tag{2.2}$$

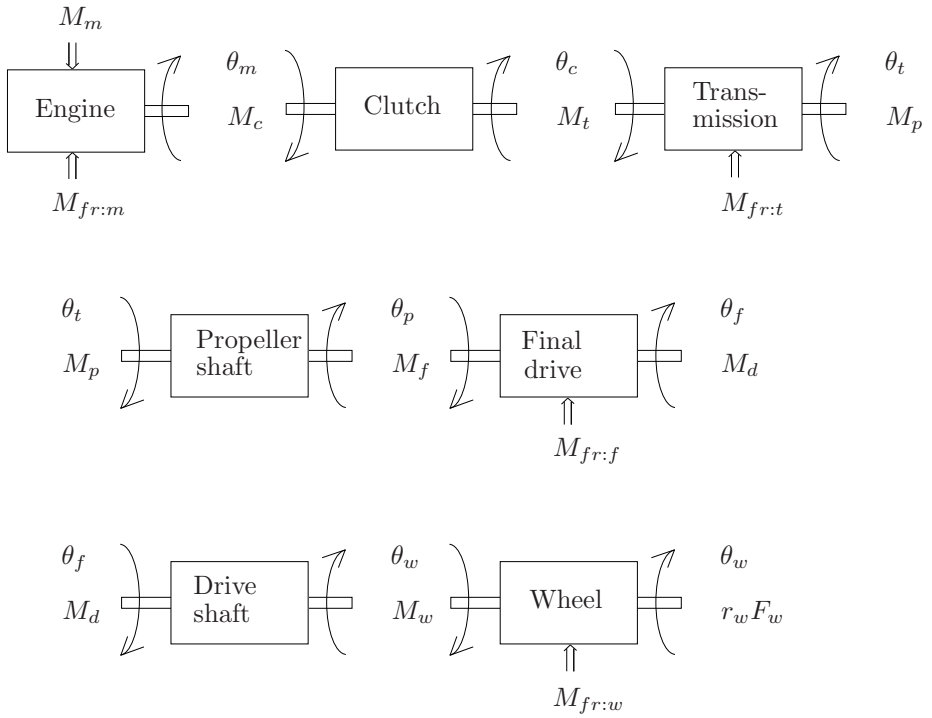

Figure 2.2 *Subsystems of a vehicular driveline with its input and output angle and torque.*

Transmission: A transmission has a set of gears, each with a conversion ratio i_t. This gives the following relation between the input and output torque of the transmission

$$M_p = f_t(M_t,\ M_{fr:t},\ \theta_c - \theta_t i_t,\ \dot{\theta}_c - \dot{\theta}_t i_t,\ i_t) \tag{2.3}$$

where the internal friction torque of the transmission is labeled $M_{fr:t}$. The reason for considering the angle difference $\theta_c - \theta_t i_t$ in (2.3) is the possibility of having torsional effects in the transmission.

Propeller shaft: The propeller shaft connects the transmission's output shaft with the final drive. No friction is assumed ($M_p = M_f$), giving the following model of the torque input to the final drive

$$M_p = M_f = f_p(\theta_t - \theta_p,\ \dot{\theta}_t - \dot{\theta}_p) \tag{2.4}$$

Final drive: The final drive is characterized by a conversion ratio i_f in the same way as the transmission. The following relation for the input and output torque holds

$$M_d = f_f(M_f,\ M_{fr:f},\ \theta_p - \theta_f i_f,\ \dot{\theta}_p - \dot{\theta}_f i_f, i_f) \tag{2.5}$$

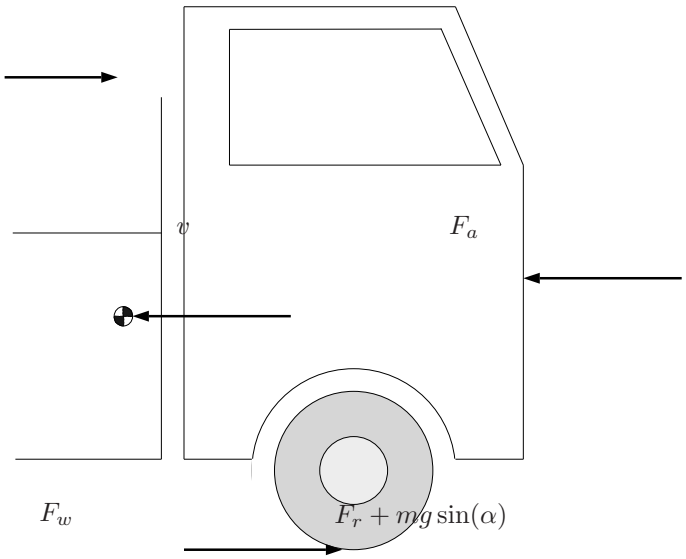

Figure 2.3 *Forces acting on a vehicle.*

where the internal friction torque of the final drive is labeled $M_{fr:f}$.

Drive shafts: The drive shafts connects the wheels to the final drive. Here it is assumed that the wheel speed is the same for the two wheels. Therfore, the drive shafts are modeled as one shaft. When the vehicle is turning and the speed differs between the wheels, both drive shafts have to be modeled. No friction ($M_w = M_d$) gives the model equation

$$M_w = M_d = f_d(\theta_f - \theta_w,\ \dot{\theta}_f - \dot{\theta}_w) \tag{2.6}$$

Wheel: In Figure 2.3 the forces acting on a vehicle with mass m and speed v is shown. Newton's second law in the longitudinal direction gives

$$F_w = m\dot{v} + F_a + F_r + mg\sin(\alpha) \tag{2.7}$$

The friction force (F_w) is described by the sum of the following quantities (Gillespie 1992).

- F_a, the air drag, is approximated by

$$F_a = \frac{1}{2} c_w A_a \rho_a v^2 \tag{2.8}$$

  where c_w is the drag coefficient, A_a the maximum vehicle cross section area, and ρ_a the air density. However, effects from, for instance, open or closed windows will make the force difficult to model.

- F_r, the rolling resistance, is approximated by

$$F_r = m(c_{r1} + c_{r2}v) \tag{2.9}$$

  where c_{r1} and c_{r2} depends on, for instance, tires and tire pressure.

- $mg\sin(\alpha)$, the gravitational force, where α is the slope of the road.

The coefficients of air drag and rolling resistance, (2.8) and (2.9), can be identified e.g. by a identification scheme (Henriksson, Pettersson, and Gustafsson 1993).

The resulting torque due to F_w is equal to $F_w r_w$, where r_w is the wheel radius. Newton's second law gives

$$J_w\ddot{\theta}_w = M_w - F_w r_w - M_{fr:w} \tag{2.10}$$

where J_w is the mass moment of inertia of the wheel, M_w is given by (2.6), and $M_{fr:w}$ is the friction torque. Including (2.7) to (2.9) in (2.10) together with $v = r_w\dot{\theta}_w$ gives

$$\begin{aligned}(J_w + mr_w^2)\ddot{\theta}_w &= M_w - M_{fr:w} - \frac{1}{2}c_w A_a \rho_a r_w^3 \dot{\theta}_w^2 \\ &\quad -r_w m(c_{r1} + c_{r2} r_w \dot{\theta}_w) - r_w mgsin(\alpha)\end{aligned} \tag{2.11}$$

A complete model for the driveline with the clutch engaged is described by Equations (2.1) to (2.11). So far the functions f_c, f_t, f_p, f_f, f_d, and the friction torques $M_{fr:t}$, $M_{fr:f}$, and $M_{fr:w}$ are unknown. In the following section assumptions will be made about the unknowns, resulting in a series of driveline models, with different complexities.

2.2 Shaft Flexibilities

In the following two sections, assumptions will be made about the unknowns. First, a model with one torsional flexibility (the drive shaft) will be considered, and then a model with two torsional flexibilities (the drive shaft and propeller shaft) will be considered.

2.2.1 Model 1: Drive Shaft Flexibility

Assumptions about the fundamental equations in Section 2.1 are made in order to obtain a model with drive shaft flexibility. Labels are according to Figure 2.2. The clutch and the propeller shafts are assumed to be stiff, and the drive shaft is described as a damped torsional flexibility. The transmission and the final drive are assumed to multiply the torque with the conversion ratio, without losses.

Clutch: The clutch is assumed to be stiff, which gives the following equations for the torque and the angle

$$M_c = M_t, \quad \theta_m = \theta_c \tag{2.12}$$

Transmission: The transmission is described by one rotating inertia J_t. The friction torque is assumed to be described by a viscous damping coefficient b_t. The model of the transmission, corresponding to (2.3), is

$$\begin{aligned} \theta_c &= \theta_t i_t & (2.13)\\ J_t\ddot{\theta}_t &= M_t i_t - b_t\dot{\theta}_t - M_p & (2.14) \end{aligned}$$

By using (2.12) and (2.13), the model can be rewritten as

$$J_t\ddot{\theta}_m = M_c i_t^2 - b_t\dot{\theta}_m - M_p i_t \tag{2.15}$$

Propeller shaft: The propeller shaft is also assumed to be stiff, which gives the following equations for the torque and the angle

$$M_p = M_f, \quad \theta_t = \theta_p \tag{2.16}$$

Final drive: In the same way as the transmission, the final drive is modeled by one rotating inertia J_f. The friction torque is assumed to be described by a viscous damping coefficient b_f. The model of the final drive, corresponding to (2.5), is

$$\begin{aligned} \theta_p &= \theta_f i_f & (2.17)\\ J_f\ddot{\theta}_f &= M_f i_f - b_f\dot{\theta}_f - M_d & (2.18) \end{aligned}$$

Equation (2.18) can be rewritten with (2.16) and (2.17) which gives

$$J_f\ddot{\theta}_t = M_p i_f^2 - b_f\dot{\theta}_t - M_d i_f \tag{2.19}$$

Reducing (2.19) to engine speed is done by using (2.12) and (2.13) resulting in

$$J_f\ddot{\theta}_m = M_p i_f^2 i_t - b_f\dot{\theta}_m - M_d i_f i_t \tag{2.20}$$

By replacing M_p in (2.20) with M_p in (2.15), a model for the lumped transmission, propeller shaft, and final drive is obtained

$$(J_t i_f^2 + J_f)\ddot{\theta}_m = M_c i_t^2 i_f^2 - b_t\dot{\theta}_m i_f^2 - b_f\dot{\theta}_m - M_d i_f i_t \tag{2.21}$$

Drive shaft: The drive shaft is modeled as a damped torsional flexibility, having stiffness k, and internal damping c. Hence, (2.6) becomes

$$\begin{aligned} M_w = M_d &= k(\theta_f - \theta_w) + c(\dot{\theta}_f - \dot{\theta}_w) = k(\theta_m/i_t i_f - \theta_w) & (2.22)\\ &+ c(\dot{\theta}_m/i_t i_f - \dot{\theta}_w) \end{aligned}$$

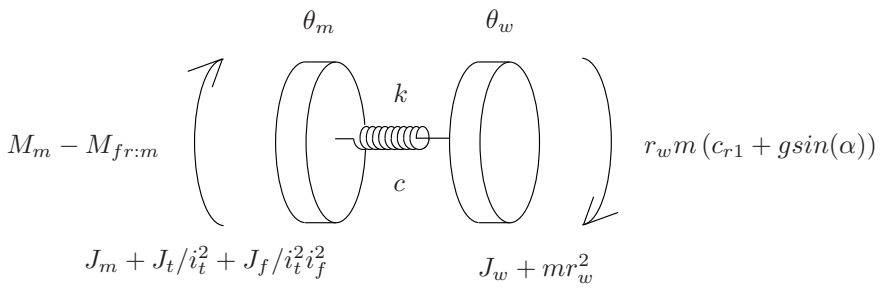

Figure 2.4 *Model 1: Stiff clutch and drive shaft torsional flexibility.*

where (2.12), (2.13), (2.16), and (2.17) are used. By replacing M_d in (2.21) with (2.22) the equation describing the transmission, propeller shaft, final drive, and drive shaft, becomes

$$\begin{aligned}(J_t i_f^2 + J_f)\ddot{\theta}_m &= M_c i_t^2 i_f^2 - b_t \dot{\theta}_m i_f^2 - b_f \dot{\theta}_m \\ &\quad -k(\theta_m - \theta_w i_t i_f) - c(\dot{\theta}_m - \dot{\theta}_w i_t i_f)\end{aligned} \tag{2.23}$$

Wheel: If (2.11) is combined with (2.22), and if the linear part of the air drag in (2.11) is used, the following equation for the wheel results

$$\begin{aligned}(J_w + mr_w^2)\ddot{\theta}_w &= k(\theta_m/i_t i_f - \theta_w) + c(\dot{\theta}_m/i_t i_f - \dot{\theta}_w) \\ &\quad -b_w\dot{\theta}_w - c_w A_a \rho_a r_w^3 \dot{\theta}_w - mc_{r2} r_w^2 \dot{\theta}_w - r_w m\,(c_{r1} + gsin(\alpha))\end{aligned} \tag{2.24}$$

where the friction torque is described as viscous damping, with label b_w.

The complete model is obtained by inserting M_c from (2.23) into (2.1), together with (2.24), which gives the following equations. An illustration of the model can be seen in Figure 2.4.

Definition 2.1 *Resulting equations for Model 1 - drive shaft flexibility.*

$$\begin{aligned}(J_m + J_t/i_t^2 + J_f/i_t^2 i_f^2)\ddot{\theta}_m &= M_m - M_{fr:m} - (b_t/i_t^2 + b_f/i_t^2 i_f^2)\dot{\theta}_m \\ &\quad -k(\theta_m/i_t i_f - \theta_w)/i_t i_f \\ &\quad -c(\dot{\theta}_m/i_t i_f - \dot{\theta}_w)/i_t i_f\end{aligned} \tag{2.25}$$

$$\begin{aligned}(J_w + mr_w^2)\ddot{\theta}_w &= k(\theta_m/i_t i_f - \theta_w) + c(\dot{\theta}_m/i_t i_f - \dot{\theta}_w) \\ &\quad -(b_w + c_w A_a \rho_a r_w^3 + mc_{r2} r_w^2)\dot{\theta}_w \\ &\quad -r_w m\,(c_{r1} + gsin(\alpha))\end{aligned} \tag{2.26}$$

Possible states describing Model 1 are $\dot{\theta}_m$, $\dot{\theta}_w$, and $\theta_m/i_t i_f - \theta_w$.

2.2.2 Model 1 Extended with a Flexible Propeller Shaft

It is also possible to consider two torsional flexibilities, the propeller shaft and the drive shaft. In the derivation of the model, the clutch is assumed stiff, and the propeller and drive shafts are modeled as damped torsional flexibilities. As in the derivation of Model 1, the transmission and final drive are assumed to multiply the torque with the conversion ratio, without losses.

The derivation of Model 1 is repeated here with the difference that the model for the propeller shaft (2.16) is replaced by a model of a flexibility with stiffness k_p and internal damping c_p

$$M_p = M_f = k_p(\theta_t - \theta_p) + c_p(\dot{\theta}_t - \dot{\theta}_p) = k_p(\theta_m/i_t - \theta_p) + c_p(\dot{\theta}_m/i_t - \dot{\theta}_p) \quad (2.27)$$

where (2.12) and (2.13) are used in the last equality. This means that there are two torsional flexibilities, the propeller shaft and the drive shaft. Inserting (2.27) into (2.15) gives

$$J_t\ddot{\theta}_m = M_c i_t^2 - b_t\dot{\theta}_m - \Big(k_p(\theta_m/i_t - \theta_p) + c_p(\dot{\theta}_m/i_t - \dot{\theta}_p)\Big)\, i_t \quad (2.28)$$

By combining this with (2.1) the following differential equation describing the lumped engine and transmission results

$$\begin{aligned}(J_m + J_t/i_t^2)\ddot{\theta}_m &= M_m - M_{fr:m} - b_t/i_t^2\dot{\theta}_m \\ &\quad -\frac{1}{i_t}\Big(k_p(\theta_m/i_t - \theta_p) + c_p(\dot{\theta}_m/i_t - \dot{\theta}_p)\Big)\end{aligned} \quad (2.29)$$

The final drive is described by inserting (2.27) in (2.18), and repeating (2.17)

$$\theta_p = \theta_f i_f \quad (2.30)$$

$$J_f\ddot{\theta}_f = i_f\Big(k_p(\theta_m/i_t - \theta_p) + c_p(\dot{\theta}_m/i_t - \dot{\theta}_p)\Big) - b_f\dot{\theta}_f - M_d \quad (2.31)$$

Including (2.30) in (2.31) gives

$$J_f\ddot{\theta}_p = i_f^2\Big(k_p(\theta_m/i_t - \theta_p) + c_p(\dot{\theta}_m/i_t - \dot{\theta}_p)\Big) - b_f\dot{\theta}_p - i_f M_d \quad (2.32)$$

The equation for the drive shaft (2.22) is repeated with new labels

$$M_w = M_d = k_d(\theta_f - \theta_w) + c_d(\dot{\theta}_f - \dot{\theta}_w) = k_d(\theta_p/i_f - \theta_w) + c_d(\dot{\theta}_p/i_f - \dot{\theta}_w) \quad (2.33)$$

where (2.30) is used in the last equality.

The equation for the final drive (2.32) now becomes

$$\begin{aligned}J_f\ddot{\theta}_p &= i_f^2\Big(k_p(\theta_m/i_t - \theta_p) + c_p(\dot{\theta}_m/i_t - \dot{\theta}_p)\Big) - b_f\dot{\theta}_p \\ &\quad -i_f\Big(k_d(\theta_p/i_f - \theta_w) + c_d(\dot{\theta}_p/i_f - \dot{\theta}_w)\Big)\end{aligned} \quad (2.34)$$

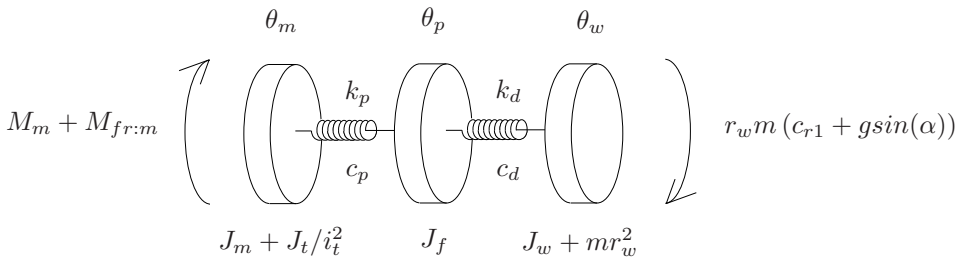

Figure 2.5 *Model with stiff clutch and two torsional flexibilities.*

The equation for the wheel is derived by combining (2.11) with (2.33). If the linear part of the of the air drag in (2.11) is used, the following equation for the wheel results

$$\begin{aligned}(J_w + mr_w^2)\ddot{\theta}_w = {} & k_d(\theta_p/i_f - \theta_w) + c_d(\dot{\theta}_p/i_f - \dot{\theta}_w) \\ & -b_w\dot{\theta}_w - c_w A_a \rho_a r_w^3 \dot{\theta}_w - mc_{r2}r_w^2\dot{\theta}_w - r_w m\,(c_{r1} + gsin(\alpha))\end{aligned} \tag{2.35}$$

where again the friction torque is assumed to be described by a viscous damping coefficient b_w. The complete model with drive shaft and propeller shaft flexibilities is the following, which can be seen in Figure 2.5.

$$\begin{aligned}(J_m + J_t/i_t^2)\ddot{\theta}_m &= M_m - M_{fr:m} - b_t/i_t^2\dot{\theta}_m \\ &\quad -\frac{1}{i_t}\Big(k_p(\theta_m/i_t - \theta_p) + c_p(\dot{\theta}_m/i_t - \dot{\theta}_p)\Big)\end{aligned} \tag{2.36}$$

$$\begin{aligned}J_f\ddot{\theta}_p &= i_f^2\Big(k_p(\theta_m/i_t - \theta_p) + c_p(\dot{\theta}_m/i_t - \dot{\theta}_p)\Big) - b_f\dot{\theta}_p \\ &\quad -i_f\Big(k_d(\theta_p/i_f - \theta_w) + c_d(\dot{\theta}_p/i_f - \dot{\theta}_w)\Big)\end{aligned} \tag{2.37}$$

$$\begin{aligned}(J_w + mr_w^2)\ddot{\theta}_w &= k_d(\theta_p/i_f - \theta_w) + c_d(\dot{\theta}_p/i_f - \dot{\theta}_w) \\ &\quad -(b_w + c_w A_a \rho_a r_w^3 + mc_{r2}r_w^2)\dot{\theta}_w - r_w m\,(c_{r1} + gsin(\alpha))\end{aligned} \tag{2.38}$$

2.3 Models Including the Clutch

The clutch is so far considered to be stiff and lumped together with the engine mass moment of inertia. In this section this assumption is relaxed and first, the clutch is modeled as a linear flexibility. Secondly, a nonlinear model of the clutch is derived.

2.3.1 Model 2: Flexible Clutch and Drive Shafts

A model with a linear clutch and one torsional flexibility (the drive shaft) is derived by repeating the procedure for Model 1 with the difference that the model for the

clutch is a flexibility with stiffness k_c and internal damping c_c

$$M_c = M_t = k_c(\theta_m - \theta_c) + c_c(\dot{\theta}_m - \dot{\theta}_c) = k_c(\theta_m - \theta_t i_t) + c_c(\dot{\theta}_m - \dot{\theta}_t i_t) \quad (2.39)$$

where (2.13) is used in the last equality. By inserting this into (2.1) the equation describing the engine inertia is given by

$$J_m\ddot{\theta}_m = M_m - M_{fr:m} - \Big(k_c(\theta_m - \theta_t i_t) + c_c(\dot{\theta}_m - \dot{\theta}_t i_t)\Big) \quad (2.40)$$

Also by inserting (2.39) into (2.14), the equation describing the transmission is

$$J_t\ddot{\theta}_t = i_t\Big(k_c(\theta_m - \theta_t i_t) + c_c(\dot{\theta}_m - \dot{\theta}_t i_t)\Big) - b_t\dot{\theta}_t - M_p \quad (2.41)$$

M_p is derived from (2.19) giving

$$(J_t + J_f/i_f^2)\ddot{\theta}_t = i_t\Big(k_c(\theta_m - \theta_t i_t) + c_c(\dot{\theta}_m - \dot{\theta}_t i_t)\Big) - (b_t + b_f/i_f^2)\dot{\theta}_t - M_d/i_f \quad (2.42)$$

which is the lumped transmission, propeller shaft, and final drive inertia.

The drive shaft is modeled according to (2.22) as

$$M_w = M_d = k_d(\theta_f - \theta_w) + c_d(\dot{\theta}_f - \dot{\theta}_w) = k_d(\theta_t/i_f - \theta_w) + c_d(\dot{\theta}_t/i_f - \dot{\theta}_w) \quad (2.43)$$

where (2.16) and (2.17) is used in the last equality.

The complete model is obtained by inserting (2.43) into (2.42) and (2.11), and using the linear part of the air drag. An illustration of the model can be seen in Figure 2.6.

Definition 2.2 *Resulting equations for Model 2 - flexible clutch and drive shaft flexibility.*

$$\begin{aligned}
J_m\ddot{\theta}_m &= M_m - M_{fr:m} - \Big(k_c(\theta_m - \theta_t i_t) + c_c(\dot{\theta}_m - \dot{\theta}_t i_t)\Big) && (2.44)\\
(J_t + J_f/i_f^2)\ddot{\theta}_t &= i_t\Big(k_c(\theta_m - \theta_t i_t) + c_c(\dot{\theta}_m - \dot{\theta}_t i_t)\Big) && (2.45)\\
&\quad -(b_t + b_f/i_f^2)\dot{\theta}_t - \frac{1}{i_f}\Big(k_d(\theta_t/i_f - \theta_w) + c_d(\dot{\theta}_t/i_f - \dot{\theta}_w)\Big)\\
(J_w + mr_w^2)\ddot{\theta}_w &= k_d(\theta_t/i_f - \theta_w) + c_d(\dot{\theta}_t/i_f - \dot{\theta}_w) && (2.46)\\
&\quad -(b_w + c_w A_a\rho_a r_w^3 + c_{r2}r_w)\dot{\theta}_w - r_w m\,(c_{r1} + gsin(\alpha))
\end{aligned}$$

2.3.2 Model 3: Nonlinear Clutch and Drive Shaft Flexibility

When studying a clutch in more detail it is seen that the torsional flexibility comes from an arrangement of smaller springs in series with springs with much higher stiffness. The reason for this arrangement is vibration insulation. When the angle difference over the clutch starts from zero and increases, the smaller springs, with

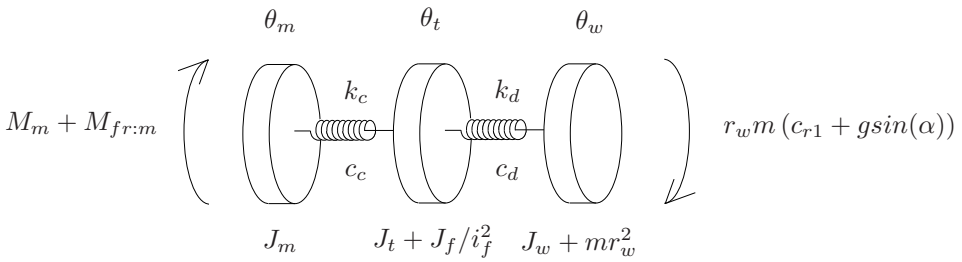

Figure 2.6 *Model 2: Linear clutch and drive shaft torsional flexibility.*

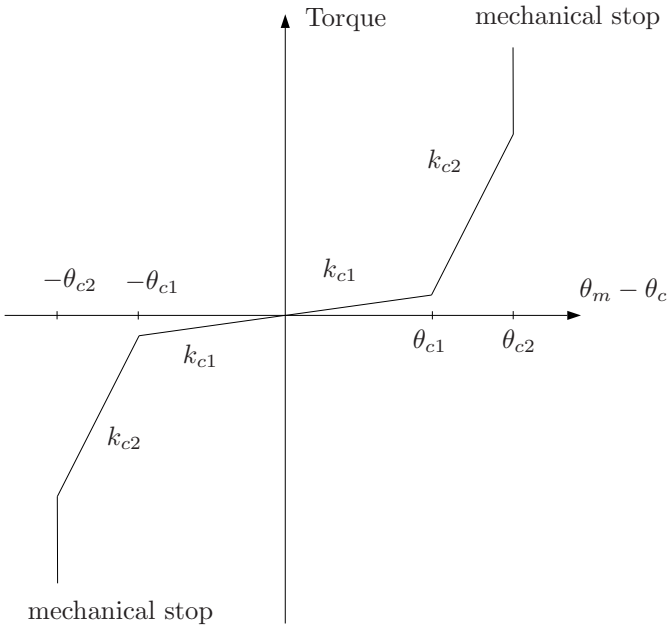

Figure 2.7 *Nonlinear clutch characteristics.*

stiffness k_{c1}, are being compressed. This ends when they are fully compressed at θ_{c1} radians. If the angle is increased further, the stiffer springs, with stiffness k_{c2}, are beginning to be compressed. When θ_{c2} is reached, the clutch hits a mechanical stop. This clutch characteristics can be modeled as in Figure 2.7. The resulting stiffness $k_c(\theta_m - \theta_c)$ of the clutch is given by

$$k_c(x) = \begin{cases} k_{c1} & \text{if } |x| \le \theta_{c1} \\ k_{c2} & \text{if } \theta_{c1} < |x| \le \theta_{c2} \\ \infty & \text{otherwise} \end{cases} \tag{2.47}$$

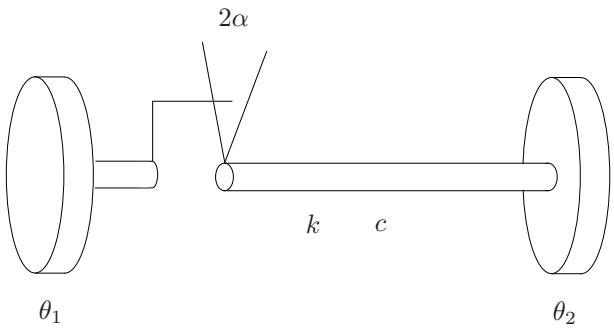

Figure 2.8 *A shaft with stiffness k and internal damping c with a backlash of* 2α *rad.*

The torque $M_{kc}(\theta_m - \theta_c)$ from the clutch nonlinearity is

$$M_{kc}(x) = \begin{cases} k_{c1}x & \text{if } |x| \leq \theta_{c1} \\ k_{c1}\theta_{c1} + k_{c2}(x - \theta_{c1}) & \text{if } \theta_{c1} < x \leq \theta_{c2} \\ -k_{c1}\theta_{c1} + k_{c2}(x + \theta_{c1}) & \text{if } -\theta_{c2} < x \leq -\theta_{c1} \\ \infty & \text{otherwise} \end{cases} \tag{2.48}$$

The nonlinear model is given by the following equations. The linear part of the air drag is included, as in the previous models.

Definition 2.3 *Resulting equations for Model 3 - nonlinear clutch and drive shaft flexibility.*

$$\begin{aligned} J_m\ddot{\theta}_m &= M_m - M_{fr:m} - M_{kc}(\theta_m - \theta_t i_t) \\ &\quad -c_c(\dot{\theta}_m - \dot{\theta}_t i_t) \end{aligned} \tag{2.49}$$

$$\begin{aligned} (J_t + J_f/i_f^2)\ddot{\theta}_t &= i_t\left(M_{kc}(\theta_m - \theta_t i_t) + c_c(\dot{\theta}_m - \dot{\theta}_t i_t)\right) \\ &\quad -(b_t + b_f/i_f^2)\dot{\theta}_t - \frac{1}{i_f}\left(k_d(\theta_t/i_f - \theta_w) + c_d(\dot{\theta}_t/i_f - \dot{\theta}_w)\right) \end{aligned} \tag{2.50}$$

$$\begin{aligned} (J_w + mr_w^2)\ddot{\theta}_w &= k_d(\theta_t/i_f - \theta_w) + c_d(\dot{\theta}_t/i_f - \dot{\theta}_w) \\ &\quad -(b_w + mc_{r2}r_w + c_w A_a \rho_a r_w^3)\dot{\theta}_w - r_w m\left(c_{r1} + gsin(\alpha)\right) \end{aligned} \tag{2.51}$$

where $M_{kc}(\cdot)$ is given by (2.48) and c_c denotes the damping coefficient of the clutch.

2.4 Additional Dynamics

For high speeds, the linear part of the air drag, is not sufficient. Then the differential equation describing the wheel and the vehicle (2.26), (2.46), and (2.51) can be changed to include the nonlinear model of the air drag, described in (2.8). The

model describing the wheel is

$$\begin{aligned}(J_w + mr_w^2)\ddot{\theta}_w &= k_d(\theta_t/i_f - \theta_w) + c_d(\dot{\theta}_t/i_f - \dot{\theta}_w) \\ &\quad -(b_w + mc_{r2}r_w)\dot{\theta}_w - r_w m\,(c_{r1} + gsin(\alpha)) \\ &\quad -\frac{1}{2}c_w A_a \rho_a r_w^3 \dot{\theta}_w^2\end{aligned} \tag{2.52}$$

It is well known that elements like transmissions and drives introduce backlash. Throughout this thesis the dead zone model will be used (Liversidge 1952). The torque resulting from a shaft connected to a drive with backlash 2α is

$$M = \begin{cases} k(\theta_1 - \theta_2 - \alpha) + c(\dot{\theta}_1 - \dot{\theta}_2) & \text{if } \theta_1 - \theta_2 > \alpha \\ k(\theta_1 - \theta_2 + \alpha) + c(\dot{\theta}_1 - \dot{\theta}_2) & \text{if } \theta_1 - \theta_2 < -\alpha \\ 0 & \text{if } |\theta_1 - \theta_2| < \alpha \end{cases} \tag{2.53}$$

where k is the stiffness and c is the internal damping of the shaft, according to Figure 2.8.

3

Field Trials and Modeling

Field trials are performed with a Scania truck. Different road slopes and gears are tested to study driveline resonances. The driving torque, engine speed, transmission speed, and wheel speed are measured. As mentioned already in Chapter 2, these measurements are used to build models by extending an initial model structure by adding the effect that seems to be the major cause for the deviation still left. There has been some open questions regarding model structure in this study. One such question is whether differences in engine speed and transmission speed is due to clutch dynamics or has other causes. The parameters of the models are estimated. The result is a series of models that describe the driveline in increasing detail.

3.1 The Truck

Tests were performed with a Scania 144L530 truck (Figure 3.1) on test roads in Södertälje, Sweden, September 1995. The 6x2 truck (6 wheels, 2 driven) has a 14 liter V8 diesel engine (Figure 3.2) with maximum power of 530 Hp and maximum torque of 2300 Nm. The DSC14 engine is connected to a manual range-splitter transmission (Figure 3.3) via a clutch. The transmission has 14 gears and a hydraulic retarder. It is also equipped with the gear shifting system Opticruise (Orehall 1995). A propeller shaft connects the output shaft of the transmission with the final drive. The drive shafts connect the final drive to the wheels which has a radius of $r_w = 0.52$ m. The weight of the truck is $m = 24$ ton and the front area is $A_a = 9\ m^2$. The drag coefficient is equal to $c_w = 0.6$.

Figure 3.1 *Scania 6x2 144L530 truck.*

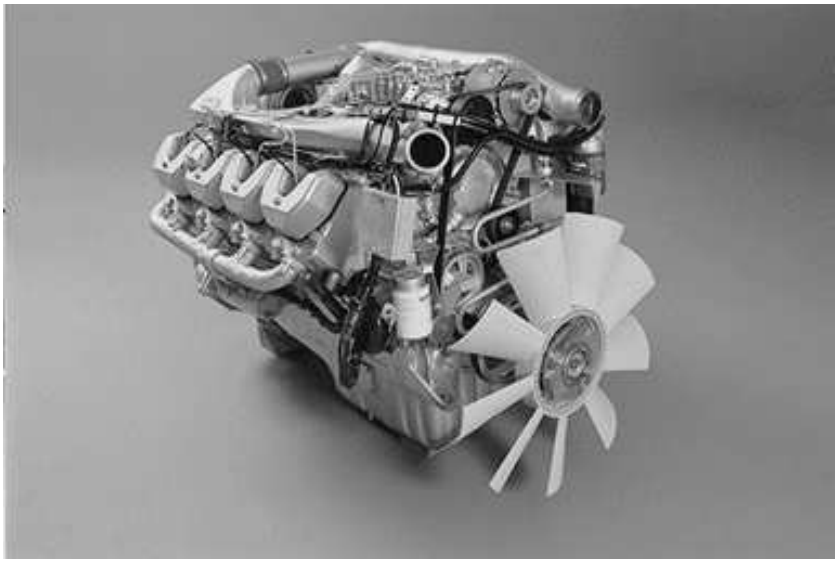

Figure 3.2 *Scania DSC14 engine.*

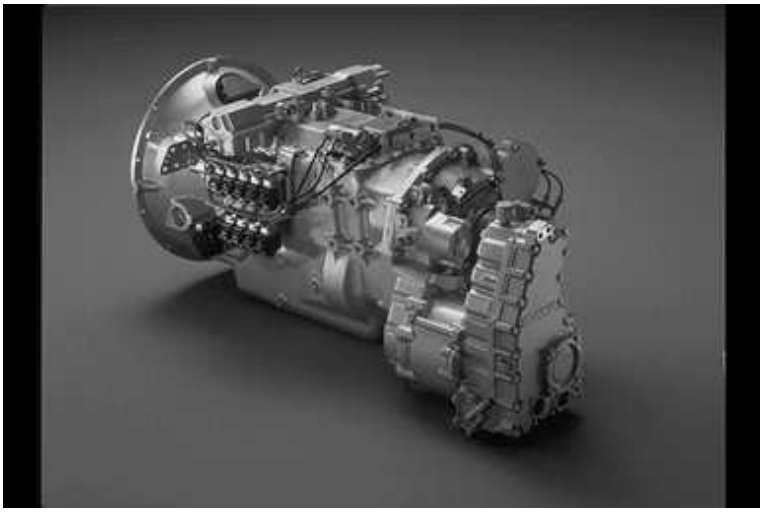

Figure 3.3 *Scania GRS900R range-splitter transmission with retarder and Opticruise gear changing system.*

3.2 Measurement Description

The truck is equipped with three sensors measuring the angle of the flywheel of the engine (θ_m), the output shaft from the transmission (θ_t), and the driving wheel (θ_w). The velocity of a rotating part is measured by using an inductive sensor (Nwagboso 1993), which detects the time when cogs from a rotating cogwheel are passing. This time sequence is then inverted to get the angle velocity. Hence, the bandwidth of the measured signal depends on the speed and the number of cogs the cogwheel is equipped with.

If the cogwheels of the three sensors are compared, the transmission speed sensor has fewer cogs than the other two sensors, indicating that the bandwidth of this signal is lower.

By measuring the amount of fuel that is fed to the engine, a measure of the driving torque (M_m) is obtained. The friction torque of the engine ($M_{fr:m}$) is also calculated online from a function given by Scania. From these two signals, the torque $u = M_m - M_{fr:m}$ acting on the driveline is calculated.

Hence, five signals are sampled ($\dot{\theta}_m, \dot{\theta}_t, \dot{\theta}_w, M_m, M_{fr:m}$) with the Scania sampling program "Truck-view". Sampling is not equidistant in time, and the sample period range from 0.05 s to 0.11 s (corresponding to sampling frequencies between 9 Hz and 20 Hz). The data has information up to half the sample period, which means that there is information up to 10 Hz frequency.

The four signals used in the following modeling are calculated from the five sampled signals. The four signals are ($\dot{\theta}_m, \dot{\theta}_t, \dot{\theta}_w, u = M_m - M_{fr:m}$).

In the rest of this thesis, the control signal $u = M_m - M_{fr:m}$ is assumed to be a

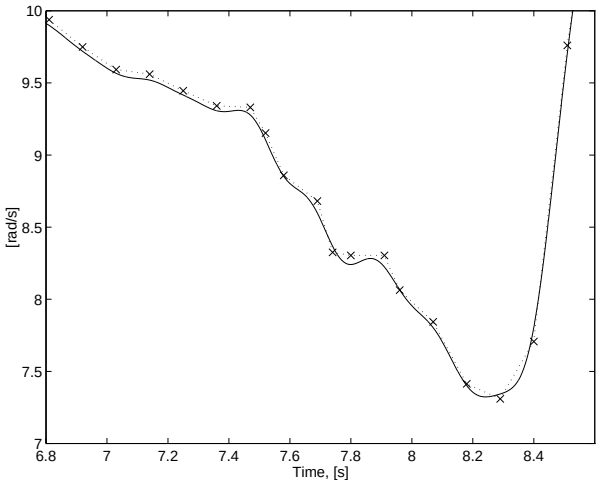

Figure 3.4 *Example of resampling a signal not equidistant in time (x). The dotted line is the linear interpolation between the samples and the straight line is the signal filtered with* 6 *Hz.*

continuous signal. This is reasonably for the frequency range considered for control design. A motivation for this is that an eight-cylinder engine makes 80 strokes/s at an engine speed of 1200 rev/min. The dynamics from fuel amount to engine torque is not considered in this work.

Preprocessing Data

Since the sampling is not equidistant in time, the data sets are resampled. A new data set is obtained by interpolating the old data using linear interpolation. This introduces higher frequencies than those in the original data set. Therefore, the interpolated data is low-pass filtered with a frequency corresponding to half the sampling frequency in the original data. This means a frequency in the interval 4.5 to 10 Hz. The chosen frequency is 6 Hz. This is done offline and therefore without phase shifts in the signals. An example of the resampling is seen in Figure 3.4.

Parameter Estimation Software

To estimate the parameters of the linear models derived in Chapter 2 the System Identification Toolbox (Ljung 1995) is used. The prediction error estimation method (PEM) for parameterized state-space representations is used to estimate the unknown parameters and initial conditions.

In order to estimate the parameters and initial condition of the nonlinear Model 3, the continuous model is discretized. This is done by using Euler's method.

For a continuous differential equation, $\dot{x} = f(x, u)$, the discrete version is

$$x_n = x_{n-1} + hf(x_{n-1}, u_{n-1}) \tag{3.1}$$

where h is the sampling time. The global truncation error with this method equals $O(h)$. Therefore it is necessary to keep h small. A too small h can give numerical problems and it also gives unnecessarily long iteration time. The data is resampled at a sampling frequency of 1 kHz. Furthermore, the five differential equations, describing Model 3, are scaled to be of the same magnitude.

For a given set of parameters, initial conditions, and control signal sequence u, the state vector is calculated at each sample. By comparing the model output (y_m, y_t, y_w) with the measured signals ($\dot{\theta}_m$, $\dot{\theta}_t$, $\dot{\theta}_w$) a cost function can be evaluated. The cost function used is

$$\sum_{\forall i} \Big((\dot{\theta}_m(i) - y_m(i))^2 + i_t^2 (\dot{\theta}_t(i) - y_t(i))^2 + i_t^2 i_f^2 (\dot{\theta}_w(i) - y_w(i))^2 \Big) \tag{3.2}$$

where $\forall i$ means that the sum is to taken over all samples in the estimation data. The optimal parameters and initial conditions are the ones minimizing (3.2). The data sets are divided into two parts to be used with the parameter estimation and validation respectively.

For Model 1 the following states are used in the parameter estimation

$$x_1 = \theta_m / i_t i_f - \theta_w, \quad x_2 = \dot{\theta}_m, \quad x_3 = \dot{\theta}_w \text{ and for Models 2 and 3,}$$
$$x_1 = \theta_m - \theta_t i_t, \quad x_2 = \theta_t / i_f - \theta_w, \quad x_3 = \dot{\theta}_m, \quad x_4 = \dot{\theta}_t, \quad x_5 = \dot{\theta}_w$$

are used. More details about the state-space representation can be found in Chapter 4.

3.3 Experiments

A number of roads at Scania were used for testing. They have different known slopes. The sensor outputs described above were logged, with the friction torque ($M_{fr:m}$) subtracted from the driving torque (M_m). Step input experiments were done by repeatedly pressing and releasing the accelerator, in order to excite driveline oscillations.

Trial 1: The test was performed with step inputs on the accelerator with gear 1. The road was almost flat. The data is seen in Figure 3.5.

Trial 2: The test was performed with step inputs on the accelerator with gear 5. The road was almost flat. The data is seen in Figure 3.6.

Trial 3: The test was performed with step inputs on the accelerator with gear 5. The road has 16 % slope. The data is seen in Figure 3.7.

Trial 4: The test was performed with step inputs on the accelerator with gear 8. The road was almost flat. The data is seen in Figure 3.8.

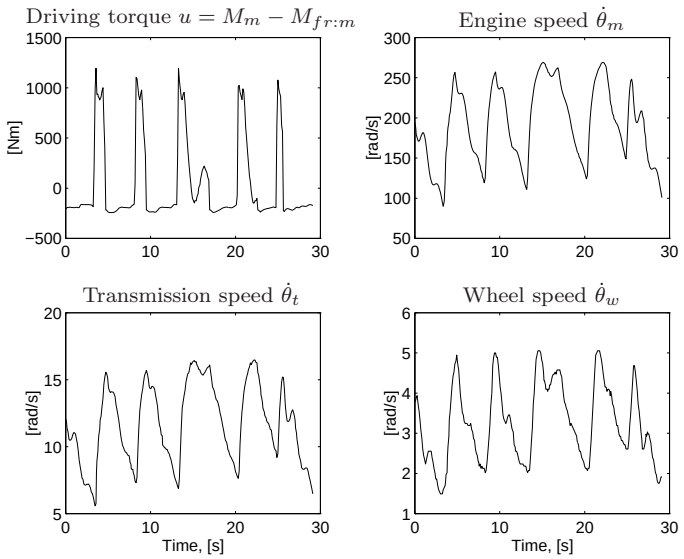

Figure 3.5 *Torque and angular velocities for a test with gear 1 and flat road.*

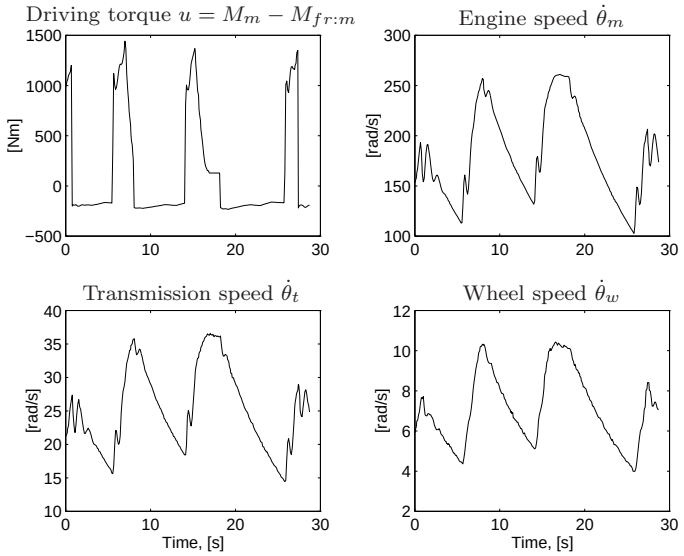

Figure 3.6 *Torque and angular velocities for a test with gear 5 and flat road.*

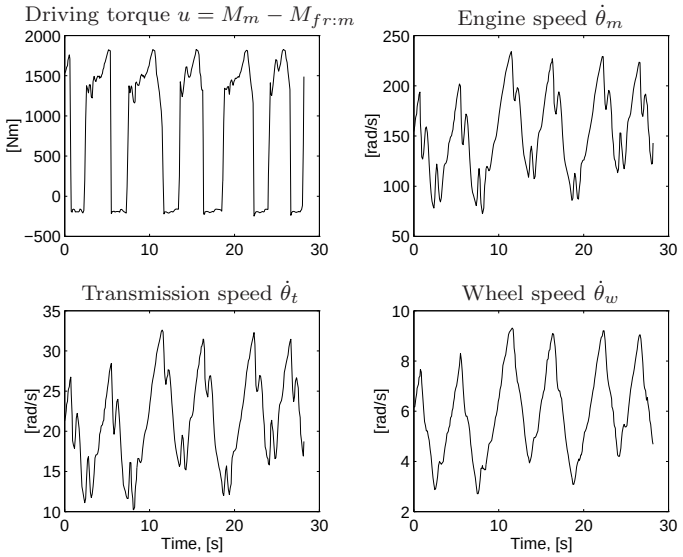

Figure 3.7 *Torque and angular velocities for a test with gear 5 and 16 % slope.*

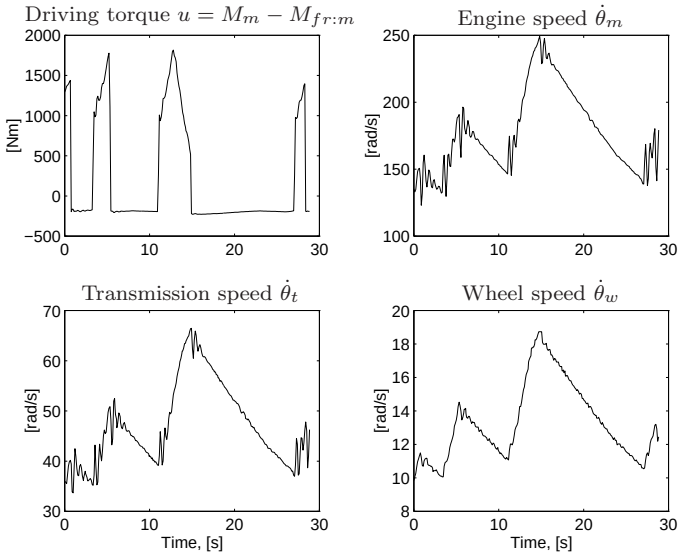

Figure 3.8 *Torque and angular velocities for a test with gear 8 and flat road.*

3.4 Models

A number of driveline models were developed in Chapter 2. The choices made in the modeling are now justified, by fitting the models to measured data. Besides the measured states ($\dot{\theta}_m$, $\dot{\theta}_t$, $\dot{\theta}_w$), the load and the states describing the torsion of the flexibilities are estimated by the models.

The data shown are from Trial 1, where the driveline oscillations are well excited. Similar results are obtained from the other trials.

3.4.1 Influence from the Drive Shaft

First, the influence from the drive shaft is investigated by estimating the parameters and initial conditions of Model 1. The engine speed and the wheel speed data is used to estimate the parameters. In Figure 3.9, the results from Trial 1 are shown. Here, also the transmission speed is plotted together with the model output engine speed scaled with the conversion ratio in the transmission (i_t). The plots are typical examples that show that a major part of the driveline dynamics in the frequency range up to 6 Hz is captured with a linear mass-spring model with the drive shafts as the main flexibility.

Result

- The main contribution to driveline dynamics from driving torque to engine speed and wheel speed is the drive shaft.
- The true angle difference ($x_1 = \theta_m/i_t i_f - \theta_w$) is unknown, but the value estimated by the model has physically reasonable values.
- The model output transmission speed (x_2/i_t) fits the measured transmission speed data well, but there are still deviations between model and measurement.

3.4.2 Influence from the Propeller Shaft

The model equations (2.36) to (2.38) describes Model 1 extended with the propeller shaft with stiffness k_p and damping c_p. The three inertias in the model are

$$\begin{aligned} J_1 &= J_m + J_t/i_t^2 \\ J_2 &= J_f \\ J_3 &= J_w + mr_w^2 \end{aligned} \tag{3.3}$$

If the size of the three inertias are compared, the inertia of the final drive (J_f) is considerably less than J_1 and J_2 in (3.3). Therefore, the model will act as if there are two damped springs in series. The total stiffness of two undamped springs in series is

$$k = \frac{k_p i_f^2 k_d}{k_p i_f^2 + k_d} \tag{3.4}$$

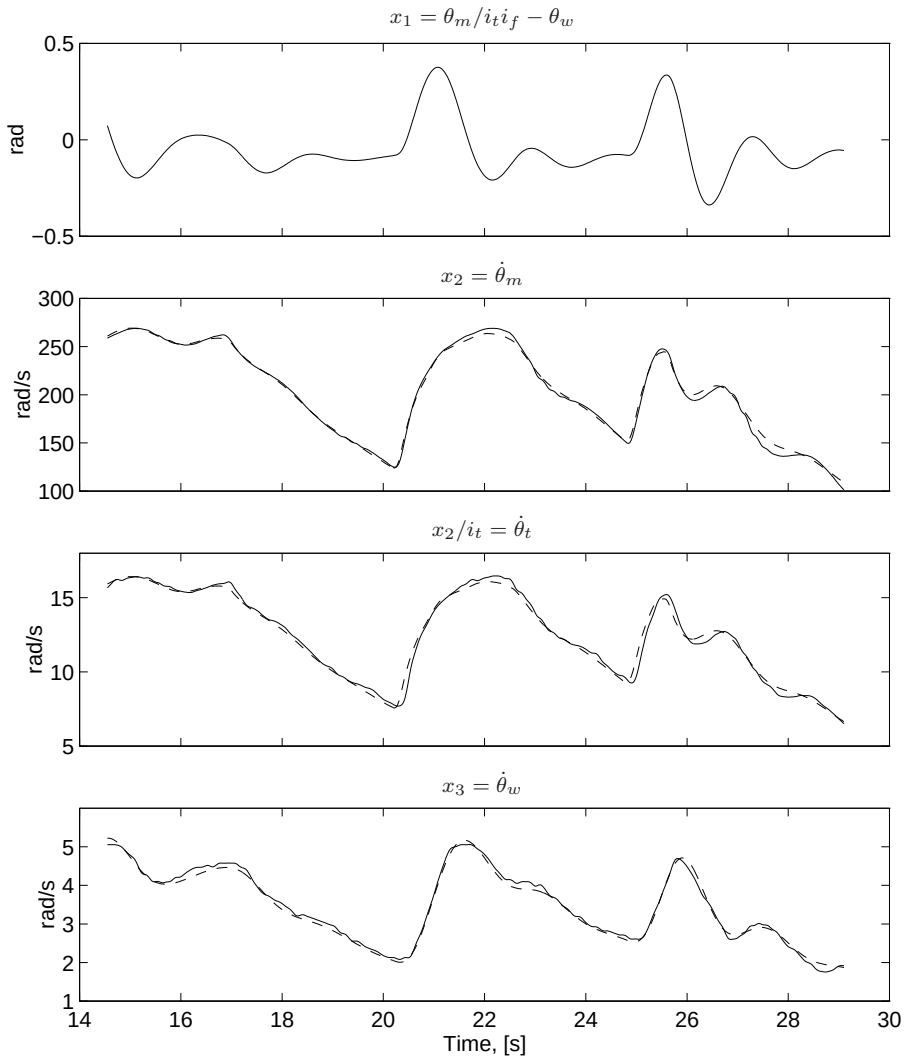

Figure 3.9 *Model 1 estimated on data from Trial 1. The top figure shows the drive shaft angle difference, and the bottom figures show the model outputs (x_2, x_3) in dashed lines, together with the measured data in solid. The plots are typical examples of that a major part of the dynamics is captured by a linear model with drive shaft flexibility.*

whereas the total damping of two dampers in series is

$$c = \frac{c_p i_f^2 c_d}{c_p i_f^2 + c_d} \tag{3.5}$$

The damping and the stiffness of the drive shaft in the previous section will thus typically be underestimated due to the flexibility of the propeller shaft. This effect will increase with lower conversion ratio in the final drive, i_f. The individual stiffness values obtained from parameter estimation are somewhat lower than the values obtained from material data.

3.4.3 Deviations between Engine Speed and Transmission Speed

As mentioned above, there is good agreement between model and experiments for $u = M_m - M_{fr:m}$, $\dot{\theta}_m$, and $\dot{\theta}_w$, but there is a slight deviation between measured and estimated transmission speed. This deviation has a character of a phase shift and some smoothing (signal levels and shapes agree). This indicates that there is some additional dynamics between engine speed, $\dot{\theta}_m$, and transmission speed, $\dot{\theta}_t$. Two natural candidates are additional mass-spring dynamics in the driveline, or sensor dynamics. The explanation is that there is a combined effect, with the major difference explained by the sensor dynamics. The motivation for this is that the high stiffness of the clutch flexibility (given from material data) can not result in a difference of a phase shift form. Neither can backlash in the transmission explain the difference, because then the engine and transmission speeds would be equal when the backlash is at its endpoint.

As mentioned before, the bandwidth of the measured transmission speed is lower than the measured engine and wheel speeds, due to fewer cogs in the sensor. It is assumed that the engine speed and wheel speed sensor dynamics are not influencing the data for frequencies up to 6 Hz. The speed dependence of the transmission sensor dynamics is neglected. The following sensor dynamics are assumed, after some comparison between sensor filters of different order,

$$\begin{aligned} f_m &= 1 \\ f_t &= \frac{1}{1+\alpha s} \\ f_w &= 1 \end{aligned} \tag{3.6}$$

where a first order filter with an unknown parameter α models the transmission sensor. Figure 3.10 shows the configuration with Model 1 and sensor filter f_m, f_t, and f_w. The outputs of the filters are y_m, y_t, and y_w.

Now the parameters, initial condition, and the unknown filter constant α can be estimated such that the model output (y_m, y_t, y_w) fits the measured data. The result of this is seen in Figure 3.11 for Trial 1. The conclusion is that the main part of the deviation between engine speed and transmission speed is due to sensor dynamics. In Figure 3.12, an enlarged plot of the transmission speed is seen, with the model output from Model 1 with and without sensor filtering.

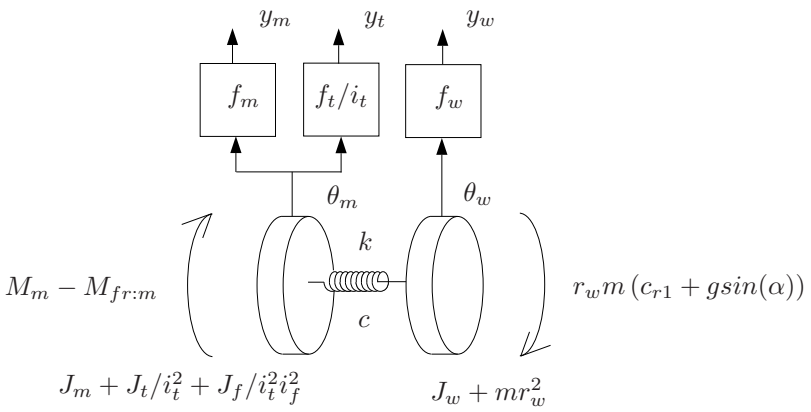

Figure 3.10 *Model 1 with sensor dynamics.*

Result

- If Model 1 is equipped with a first order sensor filter for the transmission speed, all three velocities ($\dot{\theta}_m$, $\dot{\theta}_t$, $\dot{\theta}_w$) are estimated by the model. The model output fits the data except for a number of time intervals where there are deviations between model and measured data (see Figure 3.12). However, these deviations will in the following be related to nonlinearities at low clutch torques.

3.4.4 Influence from the Clutch

So far the clutch has been assumed stiff, and the drawback with the models considered so far is that they are unable to estimate the angle difference over the clutch that actually exists. Model 2 and 3 on the other hand estimate a clutch angle difference.

Linear Clutch (Model 2)

The parameters and initial conditions of Model 2 are estimated with the sensor dynamics described above. A problem when estimating the parameters of Model 2 is that the bandwidth of 6 Hz in the data is not enough to estimate the stiffness k_c in the clutch. Therefore, the value of the stiffness given by Scania is used and fixed, and the rest of the parameters are estimated.

The resulting clutch angle difference ($x_1 = \theta_m - \theta_t i_t$) and the drive shaft angle difference ($x_2 = \theta_t/i_f - \theta_w$) are seen in Figure 3.13. The true values of these torsions are not known, but the figure shows that the drive shaft torsion have realistic values that agree with other experience. However, the clutch angle torsion does not have realistic values, which can be seen when comparing with the static nonlinearity in Figure 2.7. The model output velocities ($\dot{\theta}_m$, $\dot{\theta}_t$, $\dot{\theta}_w$) show

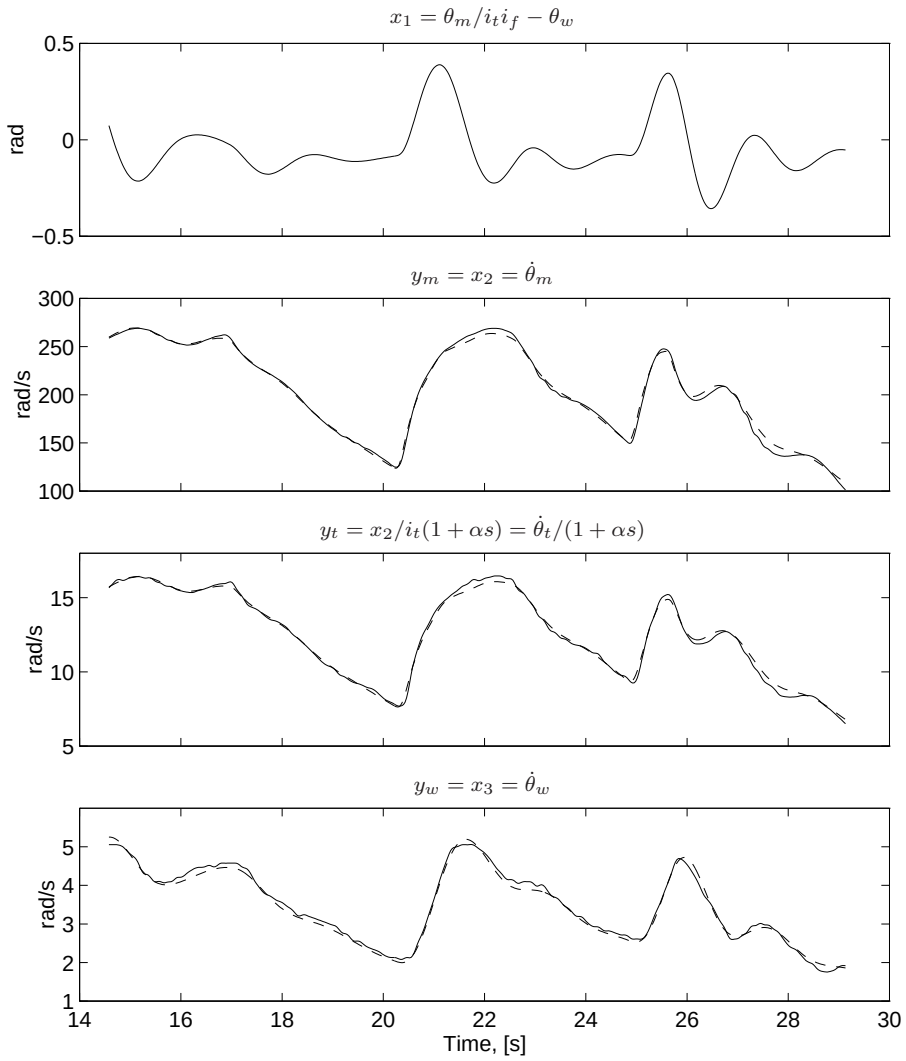

Figure 3.11 *Model as in Figure 3.9 but with sensor dynamics included. The top figure shows the angle difference over the drive shaft, and the bottom figures show the model outputs (y_m, y_t, y_w) in dashed, together with the measured data in solid. The main part of the deviation between engine speed and transmission speed is due to sensor dynamics. See also Figure 3.12.*

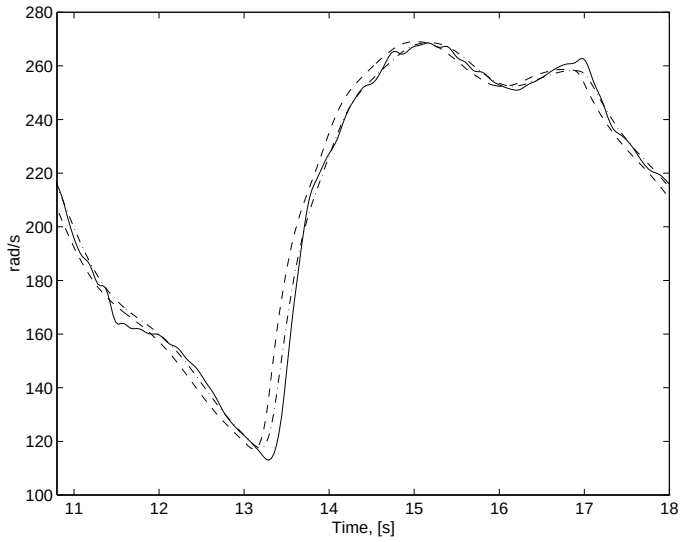

Figure 3.12 *Enlargement of part of Figure 3.11. Measured transmission speed (solid), output from Model 1 without sensor filtering (dashed), and output from Model 1 with sensor filtering (dash-dotted). The parameters are estimated on data from Trial 1.*

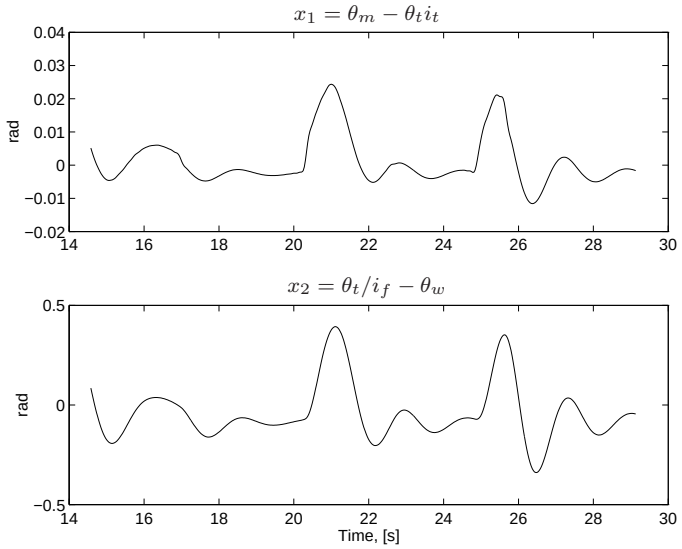

Figure 3.13 *Clutch angle difference (top figure) and drive shaft angle difference (bottom figure) resulting from parameter estimation of Model 2 with sensor filtering, on data from Trial 1. The true values of these torsions are not known, but the plots show that the drive shaft angle has realistic values.*

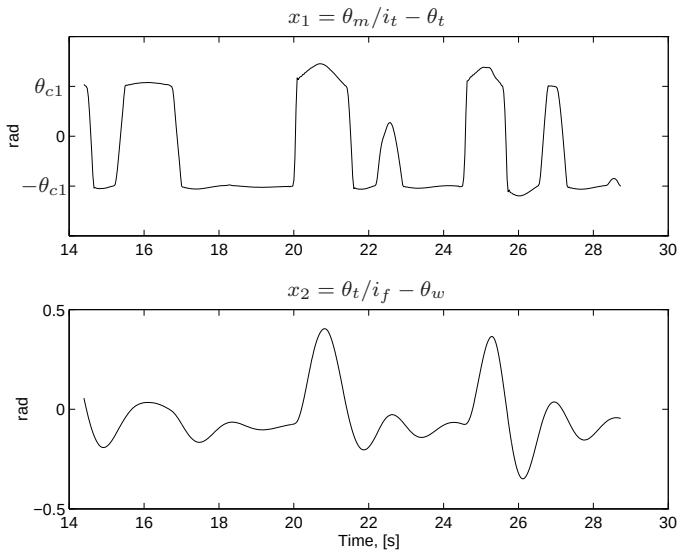

Figure 3.14 *Clutch angle difference (top figure) and drive shaft angle difference (bottom figure) resulting from parameter estimation of Model 3 with sensor filtering, on data from Trial 1. The true values of these torsions are not known, but the plots show that they have realistic values.*

no improvement compared to those generated by Model 1 with sensor dynamics, displayed in Figure 3.11.

Result

- The model including a linear clutch does not improve the data fit. The interpretation of this is that the clutch model does not add information for frequencies under 6 Hz.

Nonlinear Clutch (Model 3)

When estimating the parameters of Model 3, the clutch static nonlinearity is fixed with known physical values and the rest of the parameters are estimated, except for the sensor filter which is the same as in the previous model estimations.

The resulting clutch angle difference ($x_1 = \theta_m - \theta_t i_t$) and drive shaft angle difference ($x_2 = \theta_t/i_f - \theta_w$) after minimizing (3.2) are seen in Figure 3.14. The true values of these torsions are not known as mentioned before. However, the figure shows that both angles have realistic values that agree with other experience. The model output velocities ($\dot{\theta}_m$, $\dot{\theta}_t$, $\dot{\theta}_w$) show no improvement compared to those generated by Model 1 with sensor dynamics, displayed in Figure 3.11.

In Figure 3.12 it was seen that the model with the sensor filtering fitted the signal except for a number of time intervals with deviations. The question is if

this is a result of some nonlinearity. Figure 3.15 shows the transmission speed plotted together with the model output and the clutch angle torsion. It is clear from Figure 3.15 that the deviation between model and experiments occurs when the clutch angle passes the area with the low stiffness in the static nonlinearity (see Figure 2.7).

Result

- The model including the nonlinear clutch does not improve the data fit for frequencies up to 6 Hz.
- The model is able to estimate a clutch angle with realistic values.
- The estimated clutch angle shows that when the clutch passes the area with low stiffness in the nonlinearity, the model deviates from the data. The reason is unmodeled dynamics at low clutch torques (Björnberg, Pettersson, and Nielsen 1996).

3.4.5 Model Validity

As mentioned before, the data sets are divided into two parts. The parameters are estimated on the estimation data. The results are then evaluated on the validation data, and these are the results shown in this chapter.

In the parameter estimation, the unknown load l, which vary between the trials, is estimated. The load can be recalculated to estimate road slope, and the calculated values agree well with the known values of the road slopes at Scania. Furthermore, the estimation of the states describing the torsion of the clutch and the drive shaft shows realistic values. This gives further support to model structure and parameters.

The assumption about sensor dynamics in the transmission speed influencing the experiments, agrees well with the fact that the engine speed sensor and the wheel speed sensor have considerably higher bandwidth (more cogs) than the transmission speed sensor.

When estimating the parameters of the models investigated, there is a problem with identifying the viscous friction components b. The sensitivity in the model to variations in the friction parameters is low, and the same model fit can be obtained for a range of frictions parameters.

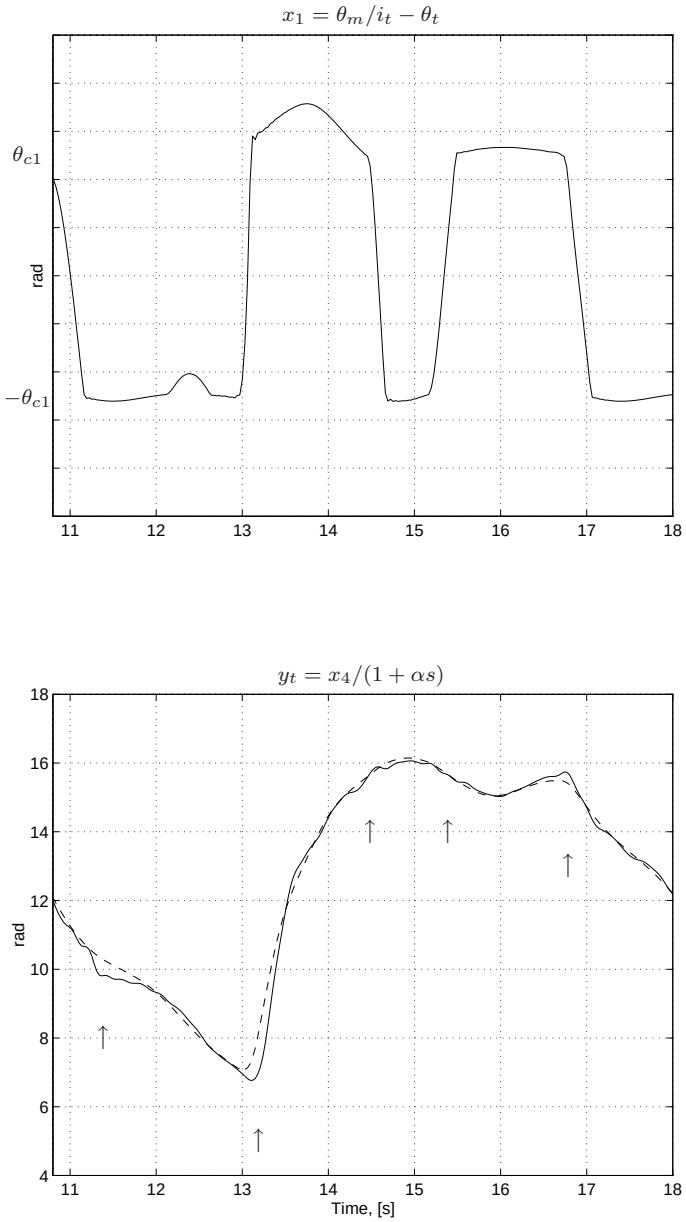

Figure 3.15 *Clutch angle difference (top figure) and measured and estimated transmission speed (bottom figure) from estimation of Model 3 with sensor dynamics on data from Trial 1. The result is that the miss fit occurs when the clutch angle passes the area with the low stiffness ($|\theta| < \theta_{c1}$) in the static nonlinearity.*

3.5 Summary

Parameter estimation of the models derived in Chapter 2 shows that a model with one torsional flexibility and two inertias is able to fit the measured engine speed and wheel speed. By considering the difference between the measured transmission speed and wheel speed it is reasonably to deduce that the main flexibility is the drive shafts.

In order for the model to fit the data from all three measured velocities, a first order sensor filter is added to the model, in accordance with properties of the sensory system. It is shown that all three velocities are fitted. Parameter estimation of a model with a nonlinear clutch explains that the difference between the measured data and the model occurs when the clutch transfers zero torque.

Further supporting facts of the models are that they give values to the non-measured variables, drive shaft and clutch torsion, that agree with experience from other sources. Furthermore, the known road slopes are well estimated.

The result is a series of models that describe the driveline in increasing detail by, in each extension, adding the effect that seems to be the major cause for the deviation still left.

The result, from a user perspective, is that, within the frequency regime interesting for control design, the mass-spring models with some sensor dynamics (Model 1 and Model 2) give good agreement with experiments. They are thus suitable for control design. The major deviations left are captured by the nonlinear effects in Model 3 which makes this model suitable for verifying simulation studies in control design.

4

Architectural Issues for Driveline Control

As seen in the previous chapters, there are significant torsional resonances in a driveline. Active control of these resonances is the topic of the rest of this thesis. Chapters 5 and 6 treats two different problems. Besides formulating the control problem in this chapter, there is one architectural issue that will be given special attention. There are different possible choices in driveline control between using different sensor locations, e.g. engine speed sensor, transmission speed sensor, or wheel speed sensor. If the driveline were rigid, the choice would not matter, since the sensor outputs would differ only by a scaling factor. However, it will be demonstrated that the presence of torsional flexibilities implies that sensor choice gives different control problems. The difference can be formulated in control theoretic terms e.g. by saying that the poles are the same, but the zeros differ both in number and values. The issue of sensor location seems to be a little studied topic (Kubrusly and Malebranche 1985; Ljung 1988), even though its relevance for control characteristics.

The driveline model equations in Chapter 2 are written in state-space form in Section 4.1. The formulation of performance output and controller structures used in the rest of the thesis are given in Section 4.2. Control of resonant systems with simple controllers is known to have structural properties e.g. with respect to sensor location (Spong and Vidyasagar 1989), as mentioned before. In Section 4.3, these differences are illustrated for driveline models. In Section 4.4, forming the main contribution of this chapter, an investigation about how these properties transfers when using more complicated controller structures like LQG/LTR is made. This part is based on the material in Pettersson and Nielsen (1995).

4.1 State-Space Formulation

The input to the open-loop driveline system is $u = M_m - M_{fr:m}$, the difference between the driving torque and the friction torque. Possible physical state variables in the models of Chapter 2 are torques, angle differences, and angle velocity of any inertia. In this work, the angle difference of each torsional flexibility and the angle velocity of each inertia is used as states. The state space representation is

$$\dot{x} = Ax + Bu + H\ l \tag{4.1}$$

where A, B, H, x, and l are defined next for the linear Models 1 and 2 in Chapter 2.

State-space formulation of Model 1:

$$\begin{aligned} x_1 &= \theta_m/i_t i_f - \theta_w \\ x_2 &= \dot{\theta}_m \\ x_3 &= \dot{\theta}_w \\ l &= r_w m\,(c_{r1} + gsin(\alpha)) \end{aligned} \tag{4.2}$$

giving

$$A = \begin{pmatrix} 0 & 1/i & -1 \\ -k/iJ_1 & -(b_1 + c/i^2)/J_1 & c/iJ_1 \\ k/J_2 & c/iJ_2 & -(c+b_2)/J_2 \end{pmatrix}, \tag{4.3}$$

$$B = \begin{pmatrix} 0 \\ 1/J_1 \\ 0 \end{pmatrix}, \quad H = \begin{pmatrix} 0 \\ 0 \\ -1/J_2 \end{pmatrix} \tag{4.4}$$

where

$$\begin{aligned} i &= i_t i_f \\ J_1 &= J_m + J_t/i_t^2 + J_f/i_t^2 i_f^2 \\ J_2 &= J_w + m r_w^2 \\ b_1 &= b_t/i_t^2 + b_f/i_t^2 i_f^2 \\ b_2 &= b_w + c_w A \rho r_w^3 + m c_{r2} r_w^2 \end{aligned} \tag{4.5}$$

according to Definition 2.1.

State-space formulation of Model 2:

$$\begin{aligned} x_1 &= \theta_m - \theta_t i_t \\ x_2 &= \theta_t/i_f - \theta_w \\ x_3 &= \dot{\theta}_m \\ x_4 &= \dot{\theta}_t \\ x_5 &= \dot{\theta}_w \end{aligned} \tag{4.6}$$

A is given by the matrix

$$\begin{pmatrix} 0 & 0 & 1 & -i_t & 0 \\ 0 & 0 & 0 & 1/i_f & -1 \\ -k_c/J_1 & 0 & -c_c/J_1 & c_c i_t/J_1 & 0 \\ k_c i_t/J_2 & -k_d/i_f J_2 & c_c i_t/J_2 & -(c_c i_t^2 + b_2 + c_d/i_f^2)/J_2 & c_d/i_f J_2 \\ 0 & k_d/J_3 & 0 & c_d/i_f J_3 & -(b_3 + c_d)/J_3 \end{pmatrix}$$

and

$$B = \begin{pmatrix} 0 \\ 0 \\ 1/J_1 \\ 0 \\ 0 \end{pmatrix}, \quad H = \begin{pmatrix} 0 \\ 0 \\ 0 \\ 0 \\ -1/J_2 \end{pmatrix} \tag{4.7}$$

where

$$\begin{aligned} J_1 &= J_m \\ J_2 &= J_t + J_f/i_f^2 \\ J_2 &= J_w + m r_w^2 \\ b_2 &= b_t + b_f/i_f^2 \\ b_3 &= b_w + c_w A \rho r_w^3 + c_{r2} r_w \end{aligned} \tag{4.8}$$

according to Definition 2.2.

4.1.1 Disturbance Description

The disturbance l can be seen as a slow-varying part resulting from the rolling resistance and the road slope plus and additive disturbance v. A second state disturbance n is a disturbance acting on the input of the system. This disturbance is considered because the firing pulses in the driving torque can be seen as an additive disturbance acting on the input. The state-space description is

$$\dot{x} = Ax + Bu + Bn + H\ l + Hv \tag{4.9}$$

with x, A, B, H, and l defined in (4.2) to (4.8).

4.1.2 Measurement Description

For controller synthesis it is of fundamental interest which physical variables of the process that can be measured. In the case of a vehicular driveline the normal sensor alternative is an inductive sensor mounted on a cog wheel measuring the angle, as mentioned before. Sensors that measure torque are expensive, and are seldom used in a production vehicular applications.

The output of the process is defined as a combination of the states given by the matrix C in

$$y = Cx + e \tag{4.10}$$

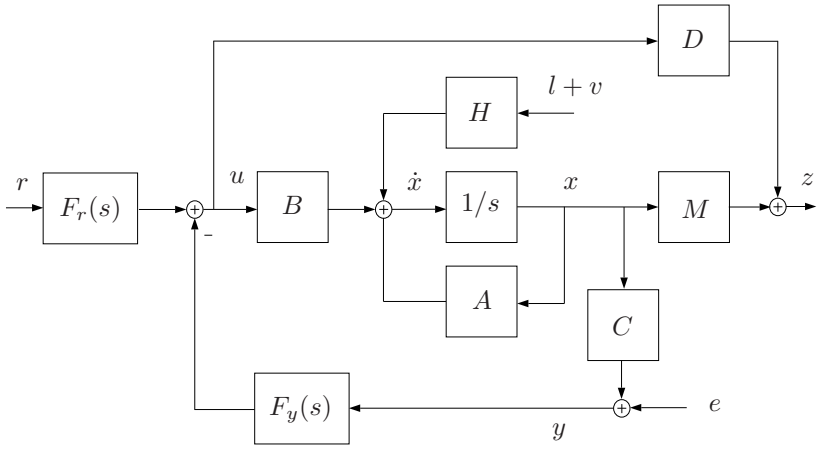

Figure 4.1 *Plant and controllers F_r and F_y.*

where e is a measurement disturbance.

In this work, only angle velocity sensors are considered, and therefore, the output of the process is one/some of the state variables defining an angle velocity. Especially, the following are defined (corresponding to a sensor on $\dot{\theta}_m$ and $\dot{\theta}_w$ for Model 1).

$$C_m = (0\ 1\ 0) \tag{4.11}$$
$$C_w = (0\ 0\ 1) \tag{4.12}$$

4.2 Controller Formulation

The performance output z is the combination of states that has requirements to behave in a certain way. This combination of the states is described by the matrices M and D in the following way

$$z = Mx + Du \tag{4.13}$$

The control problem can be seen as in Figure 4.1. The unknown controllers F_r and F_y are to be designed such that that the performance output (4.13) meets its requirements (defined later).

In this thesis controllers will be designed as state-feedback controllers extensively except for a few simple examples. The control signal u is a linear function of the states (if they are all measured) or else the state estimates, which are obtained from a Kalman filter,

$$u = l_0 r - K_c \hat{x} \tag{4.14}$$

where, r represents the commanded signal with the gain l_0, and K_c is the state-feedback matrix.

Identifying the matrices $F_r(s)$ and $F_y(s)$ in Figure 4.1 gives

$$\begin{aligned} F_y(s) &= K_c(sI - A + BK_c + K_fC)^{-1}K_f \\ F_r(s) &= l_0\left(1 - K_c(sI - A + BK_c + K_fC)^{-1}B\right) \end{aligned} \tag{4.15}$$

The closed-loop transfer functions from r, v, and e to the control signal u are given by

$$G_{ru} = \left(I - K_c(sI - A + BK_c)^{-1}B\right)l_0 r \tag{4.16}$$

$$\begin{aligned} G_{vu} &= K_c(sI - A + K_fC)^{-1}N - K_c(sI - A + BK_c)^{-1}N \\ &\quad -K_c(sI - A + BK_c)^{-1}BK_c(sI - A + K_fC)^{-1}N \end{aligned} \tag{4.17}$$

$$G_{eu} = K_c\left((sI - A + BK_c)^{-1}BK_c - I\right)(sI - A + K_fC)^{-1}K_f \tag{4.18}$$

The transfer functions to the performance output z are given by

$$G_{rz} = (M(sI - A)^{-1}B + D)G_{ru} \tag{4.19}$$

$$\begin{aligned} G_{vz} &= M(sI - A + BK_c)^{-1}BK_c(sI - A + K_fC)^{-1}N \\ &\quad +M(sI - A + BK_c)^{-1}N + DG_{wu} \end{aligned} \tag{4.20}$$

$$G_{ez} = (M(sI - A)^{-1}B + D)G_{vu} \tag{4.21}$$

Two return ratios results, which characterizes the closed-loop behavior at the plant output and input respectively

$$GF_y = C(sI - A)^{-1}BF_y \tag{4.22}$$

$$F_yG = F_yC(sI - A)^{-1}B \tag{4.23}$$

When only one sensor is used, these return ratios are scalar and thus equal.

LQG/LTR is not directly applicable to driveline control with more than one sensor as input to the observer. This is because there are unequal number of sensors and control signals. Therefore, it is important with the type of investigation about the structural properties made in this chapter, when extending to more sensors. This is however not considered in this work.

4.3 Some Feedback Properties

The performance output when controlling the driveline to a certain speed is the velocity of the wheel, defined as

$$z = \dot{\theta}_w = C_w x \tag{4.24}$$

When studying the closed-loop control problem with a sensor on $\dot{\theta}_m$ or $\dot{\theta}_w$, two different control problems results. In Figure 4.2 a root locus with respect to a P-controller gain is seen for two gears using velocity sensor $\dot{\theta}_m$ and $\dot{\theta}_w$ respectively. The open-loop transfer functions from u to engine speed G_{um} has three poles and

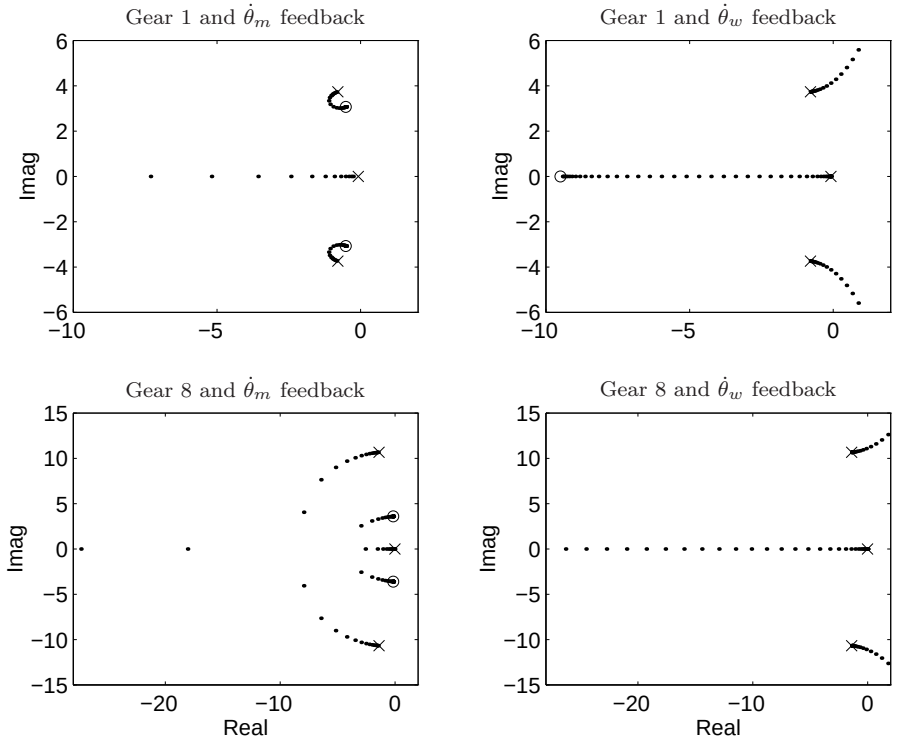

Figure 4.2 *Root locus with respect to a P controller gain, for gear 1 (top figures) and gear 8 (bottom figures) with sensor on $\dot{\theta}_m$ (left figures), and $\dot{\theta}_w$ (right figures). The cross represent the open-loop poles, while the rings represents the open-loop zeros. The system goes unstable when the $\dot{\theta}_w$ gain is increased, but is stable for all $\dot{\theta}_m$ gains.*

two zeros, as can be seen in Figure 4.2. G_{uw} on the other hand has one zero, and the same poles. Hence, the relative degree of G_{um} is one and G_{uw} has a relative degree of two. This means that when $\dot{\theta}_w$ feedback is used, and the gain is increased, two poles must go to infinity which makes the system unstable. When the velocity sensor $\dot{\theta}_m$ is used, the relative degree is one, and the closed-loop system is stable for all gains. (Remember that $\dot{\theta}_w$ is the performance output and thus desirable to use.)

The same effect can be seen in the step response when the P controller is used. Figure 4.3 demonstrates the problem with resonances that occurs with increasing gain for the two cases of feedback. When the engine speed sensor is used, the engine speed behaves well when the gain is increased, but the resonance in the drive shaft makes the wheel speed oscillate. When using $\dot{\theta}_w$ feedback it is difficult to increase

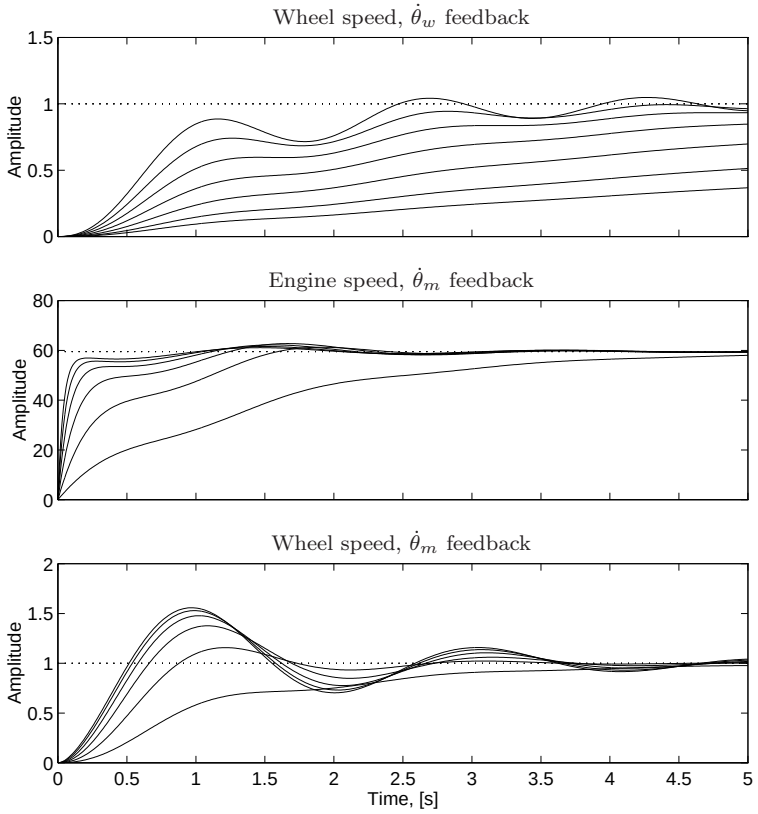

Figure 4.3 *Step responses using a P controller with different gains on Model 1 with gear 1. With $\dot{\theta}_w$ feedback (top figure), increased rise time results in instability. With $\dot{\theta}_m$ feedback (bottom figures), increased gain results in a well behaved engine speed, but an oscillating wheel speed.*

the bandwidth, since the poles moves closer to the imaginary axis, giving a resonant system.

The characteristic results in Figures 4.2 and 4.3 only depend on the relative degree, and are thus parameter independent. However, this observation may depend on feedback structure, and therefore a more detailed analysis is performed in the following sections.

4.4 Driveline Control with LQG/LTR

Different sensor locations result in different control problems with different inherent characteristics, as seen in the previous section. The topic of this section is to show how this influences control design when using LQG/LTR. The reason for using

LQG/LTR, in this principle study, is that it offers a control design method resulting in a controller and observer of the same order as the plant model, and it is also an easy method for obtaining robust controllers.

4.4.1 Transfer Functions

When comparing the control problem with using $\dot{\theta}_m$ or $\dot{\theta}_w$ as sensors, open-loop transfer functions G_{um} and G_{uw} results. These have the same number of poles but different number of zeros as mentioned before. Two different closed-loop systems results depending on which sensor that is used.

Feedback from $\dot{\theta}_w$

A natural feedback configuration is to use the performance output, $\dot{\theta}_w$. Then among others the following transfer functions results, where (4.16) to (4.21) are used together with the matrix inversion lemma

$$G_{rz} = \frac{G_{uw}F_yF_r}{1+G_{uw}F_y} = T_wF_r \tag{4.25}$$

$$G_{nu} = = \frac{1}{1+G_{uw}F_y} = S_w \tag{4.26}$$

where n is the input disturbance. The transfer functions S_w and T_w are, as usual, the *sensitivity* function and the *complementary sensitivity* function. Also, as usual,

$$S_w + T_w = 1 \tag{4.27}$$

Feedback from $\dot{\theta}_m$

The following transfer functions results if the sensor measures $\dot{\theta}_m$

$$G_{rz} = \frac{G_{uw}F_yF_r}{1+G_{um}F_y} \tag{4.28}$$

$$G_{nu} = \frac{1}{1+G_{um}F_y} \tag{4.29}$$

The difference between the two feedback configurations is that the return difference is $1+G_{uw}F_y$ or $1+G_{um}F_y$.

It is desirable to have sensitivity functions that corresponds to $y = \dot{\theta}_m$ and $z = \dot{\theta}_w$. The following transfer functions are defined

$$S_m = \frac{1}{1+G_{um}F_y}, \quad T_m = \frac{G_{um}F_y}{1+G_{um}F_y} \tag{4.30}$$

These transfer functions corresponds to a configuration where $\dot{\theta}_m$ is the output (i.e. $y = z = \dot{\theta}_m$). Using (4.28) it is natural to define $\overline{T}_m$ by

$$\overline{T}_m = \frac{G_{uw}F_y}{1+G_{um}F_y} = T_m\frac{G_{uw}}{G_{um}} \tag{4.31}$$

The functions S_m and $\overline{T}_m$ describe the design problem when feedback from θ_m is used.

When combining (4.30) and (4.31), the corresponding relation to (4.27) is

$$S_m + \overline{T}_m \frac{G_{um}}{G_{uw}} = 1 \tag{4.32}$$

If S_m is made zero for some frequencies in (4.32), then $\overline{T}_m$ will not be equal to one, as in (4.27). Instead, $\overline{T}_m = G_{uw}/G_{um}$ for these frequency domains.

Limitations on Performance

The relations (4.27) and (4.32) will be the fundamental relations for discussing design considerations. The impact of the ratio G_{uw}/G_{um} will be analyzed in the following sections.

Definition 4.1 *$\overline{T}_m$ in (4.31) is the modified complementary sensitivity function, and $G_{w/m} = G_{uw}/G_{um}$ is the dynamic output ratio.*

4.4.2 Design Example with a Simple Mass-Spring Model

Linear Quadratic Design with Loop Transfer Recovery will be treated in four cases, being combinations of two sensor locations, $\dot{\theta}_m$ or $\dot{\theta}_w$, and two models with the same structure, but with different parameters. Design without pre filter ($F_r = 1$) is considered.

The section covers a general plant with n inertias connected by $k-1$ torsional flexibilities, without damping and load, and with unit conversion ratio. There are $(2n-1)$ poles, and the location of the poles are the same for the different sensor locations. The number of zeros depends on which sensor that is used, and when using $\dot{\theta}_w$ there are no zeros. When using feedback from $\dot{\theta}_m$ there are $(2n-2)$ zeros. Thus, the transfer functions G_{um} and G_{uw}, have the same denominators, and a relative degree of 1 and $(2n-1)$ respectively.

Structural Properties of Sensor Location

The controller (4.15) has a relative degree of one. The relative degree of $G_{um}F_y$ is thus 2, and the relative degree of $G_{uw}F_y$ is $2n$. When considering design, a good alternative is to have relative degree one in GF_y, implying infinite gain margin and high phase margin.

When using $G_{um}F_y$, one pole has to be moved to infinity, and when using $G_{uw}F_y$, $2n-1$ poles have to be moved to infinity, in order for the ratio to resemble a first order system at high frequencies. It could be expected that a higher control signal is needed for $\dot{\theta}_w$ feedback in order to move the poles towards infinity.

When the return ratio behaves like a first order system, also the closed-loop transfer function behaves like one. This conflicts with the design goal of having

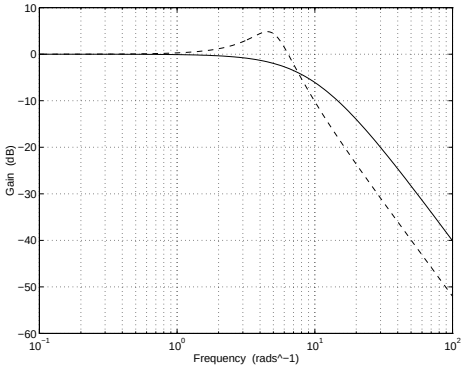

Figure 4.4 *$G_{w/m}$ for a) (solid) and b) (dashed).*

a steep roll-off rate for the closed-loop system in order to attenuate measurement noise. Hence, there is a trade-off when using $\dot{\theta}_w$ feedback.

When using $\dot{\theta}_m$ feedback, there is no trade-off, since the relative degree of G_{um} is one.

Structure of $G_{w/m}$

We have in the previous simple examples seen that the relative degree and the zeros are important. The dynamic output ratio contains exactly this information and nothing else.

For low frequencies the dynamic output ratio has gain equal to one,

$$\left|G_{w/m}(0)\right| = 1$$

(if the conversion ratio is equal to one). Furthermore, $G_{w/m}$ has a relative degree of $2n-2$ and thus, a high frequency gain roll-off rate of $20(2n-2)$ dB/decade. Hence, the dynamic output ratio gives the closed-loop transfer function $\overline{T}_m$ a high frequency gain roll-off rate of $q_m + 20(2n-2)$ dB/decade, where q_m is the roll-off rate of $G_{um}F_y$. When using $\dot{\theta}_w$ feedback, T_w will have the same roll-off rate as $G_{uw}F_y$.

Parametric properties of $G_{w/m}$

Typical parametric properties of $G_{w/m}$ can be seen in the following example.

Example 4.1 *Two different plants are considered:*
a) $J_1 = 0.0974$, $J_2 = 0.0280$, $k = 2.80$, $c = 0$, $b_1 = 0.0244$, $b_2 = 0.566$, $l = 0$.
b) $J_1 = 0.0974$, $J_2 = 0.220$, $k = 5.50$, $c = 0$, $b_1 = 1.70$, $b_2 = 0.660$, $l = 0$.
with labels according to the state-space formulation in Section 4.1. The shape of $G_{w/m}$ can be seen in Figure 4.4.

LQG Designs

Integral action is included by augmenting the state to attenuate step disturbances in v (Maciejowski 1989). The state-space realization A_a, B_a, M_a, C_{wa}, and C_{ma} results. The Kalman-filter gain, K_f, is derived using a Riccati equation (Maciejowski 1989)

$$P_f A^T + A P_f - P_f C^T V^{-1} C P_f + B W B^T = 0 \tag{4.33}$$

The covariances W and V, of v and e respectively, are adjusted until the return ratio

$$C(sI - A)^{-1} K_f, \quad K_f = P_f C^T V^{-1} \tag{4.34}$$

and the closed-loop transfer functions S and T show satisfactory performance. The Nyquist locus remains outside the unit circle centered at -1. This means that there is infinite gain margin, and a phase margin of at least 60°. Furthermore, the relative degree is one, and $|S| \leq 1$.

Design for $\dot{\theta}_w$ feedback. W is adjusted (and thus $F_y(s)$) such that S_w and T_w show a satisfactory performance, and that the desired bandwidth is obtained. The design in Example 4 is shown in Figure 4.5. Note that the roll-off rate of T_w is 20 dB/decade.

Design for $\dot{\theta}_m$ feedback. W is adjusted (and thus $F_y(s)$) such that S_m and T_m (and thus $\dot{\theta}_m$) show a satisfactory performance. Depending on the shape of $G_{w/m}$ for middle high frequencies, corrections in W must be taken such that $\overline{T}_m$ achieves the desired bandwidth. If there is a resonance peak in $G_{w/m}$, the bandwidth in $\overline{T}_m$ is chosen such that the peak is suppressed. Figure 4.5 shows such an example, $\dot{\theta}_m$ feedback in b), where the bandwidth is lower in order to suppress the peak in $G_{w/m}$. Note also the difference between S_w and S_m.

The parameters of the dynamic output ratio are thus important in the LQG step of the design.

Loop Transfer Recovery, LTR

The next step in the design process is to include K_c, and recover the satisfactory return ratio obtain previously. When using the combined state feedback and Kalman filter, the return ratio is $GF_y = C(sI - A)^{-1} B K_c (sI - A + B K_c + K_f C)^{-1} K_f$. A simplistic LTR can be obtained by using $K_c = \rho C$ and increasing ρ. As ρ is increased, $2n - 1$ poles move towards the open system zeros. The remaining poles move towards infinity (compare to Section 5.1). If the Riccati equation

$$A^T P_c + P_c A - P_c B R^{-1} B^T P_c + C^T Q C = 0 \tag{4.35}$$

is solved with $Q = \rho$, and $R = 1$, $K_c = \sqrt{\rho} C$ is obtained in the limit, and to guarantee stability, this K_c is used for recovery.

In Figures 4.6 and 4.7, the recovered closed-loop transfer functions, Nyquist locus, and control signal are seen.

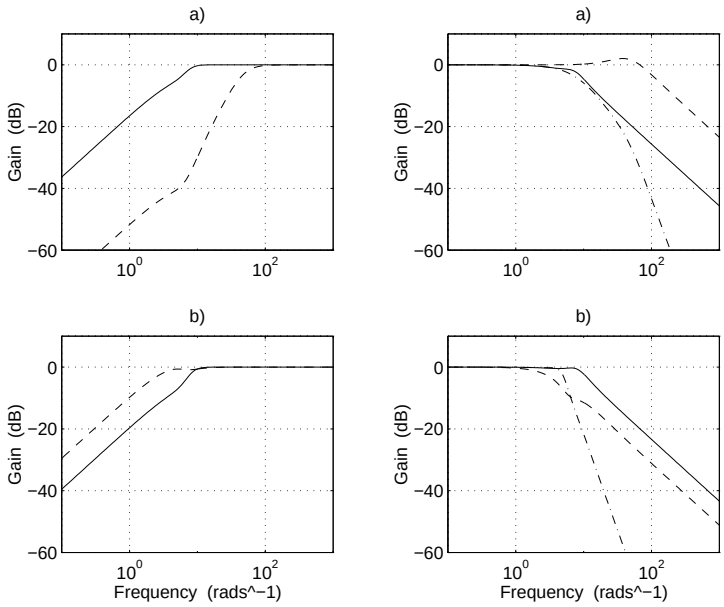

Figure 4.5 *Closed-loop transfer functions S (left figures), and T (right figures). Feedback from $\dot{\theta}_w$ in solid curves, and feedback from $\dot{\theta}_m$ in dashed curves. $\overline{T}_m$ is seen in right figures in dash-dot curves. $W = 15$ (θ_w, a), $W = 5 \cdot 10^4$ (θ_m, a), $W = 5 \cdot 10^2$ (θ_w, b), and $W = 50$ (θ_m, b).*

Recovery for $\dot{\theta}_w$ feedback. There is a trade-off when choosing an appropriate ρ. A low ρ gives good attenuation of measurement noise and a low control signal, but in order to have good stability margins, a high ρ must be chosen. This gives an increased control signal, and a 20 dB/decade roll-off rate in T_w for a wider frequency range.

Recovery for $\dot{\theta}_m$ feedback. There is no trade-off when choosing ρ. It is possible to achieve good recovery with reasonable stability margins and control signal, together with a steep roll-off rate.

The structural properties i.e. the relative degrees are thus dominant in determining the LTR step of the design.

4.5 Summary

Control and damping of torsional oscillations in vehicular drivelines is an important problem. Different sensor locations give different transfer functions, G_{um} or G_{uw}. These functions have the same poles, but have different relative degree and different zeros. The *dynamic output ratio*, $G_{w/m}$, exactly captures these differences and nothing else. The problem that the performance output signal is not the same

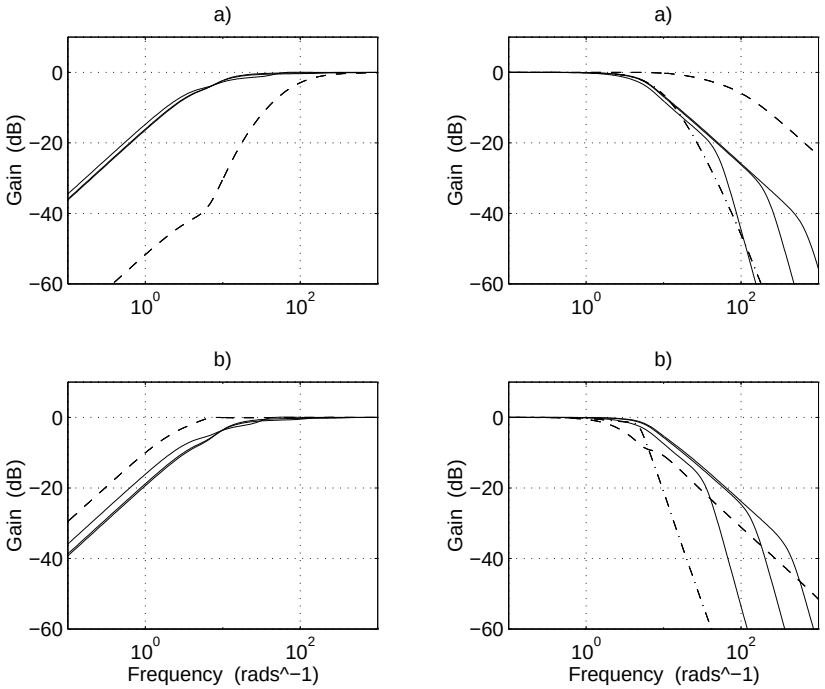

Figure 4.6 *Closed-loop transfer functions S (left figures), and T (right figures) after recovery. Feedback from $\dot{\theta}_w$ in solid curves, and feedback from $\dot{\theta}_m$ in dashed curves. $\overline{T}_m$ is seen in right figures in dash-dot curves. For the $\dot{\theta}_m$ design $\rho = 10^6$ (a) and $\rho = 10^5$ (b) is used, and for the $\dot{\theta}_w$ design $\rho = 10^4$, 10^8, and 10^{11} is used in both a) and b).*

as the measured output signal is handled by introducing a *modified complementary sensitivity* function, being modified with $G_{w/m}$. Both structural and parameter dependent aspects of sensor location have been characterized. In LQG/LTR, parameter dependent properties dominate in the LQG step of the design, whereas structural properties, i.e. sensor location, dominate in the LTR step.

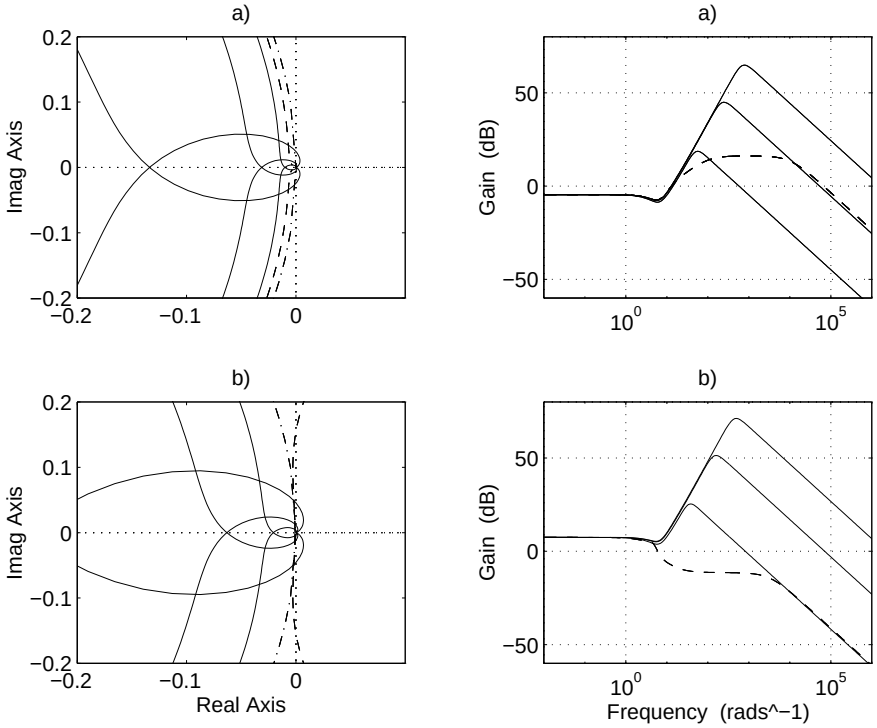

Figure 4.7 *Nyquist plot of return ratio (left figures) and $F_y/(1+G_{uw}F_y)$ (right figures). Feedback from $\dot{\theta}_w$ in solid curves, and feedback from $\dot{\theta}_m$ in dashed curves. For the $\dot{\theta}_m$ design $\rho = 10^6$ (a) and $\rho = 10^5$ (b) is used, and for the $\dot{\theta}_w$ design $\rho = 10^4$, 10^8, and 10^{11} is used in both a) and b). A dash-dotted circle with radius one and centered at -1, is also shown in the Nyquist plots.*

5

Speed Controller Design and Simulations

Driveline oscillations may occur in different modes of operation. Active damping in two modes will be treated in this and next chapter. The first problem is wheel speed oscillations following a change in accelerator pedal position, known as vehicle shuffle (Mo, Beaumount, and Powell 1996; Pettersson and Nielsen 1995). Traditionally in diesel powered trucks, the relation between the accelerator pedal and the amount of fuel metered by the diesel pump is governed by a system called RQV control. The RQV control gives a specific character to the driving feeling e.g. when going uphill and downhill. This driving character is important to maintain when extending speed control with active damping. Traditional RQV control is explained in Section 5.1. Thereafter, the speed control problem keeping RQV characteristics is formulated in Section 5.2. The sections following study the problem using available computationally powerful methods like LQG/LTR. Sensor location, influence from disturbances, and load estimations are treated.

5.1 RQV Control

RQV control is the traditional diesel engine control scheme steaming from the mechanical centrifugal governor, used to control the diesel pump (Bosch 1993). In todays electronically controlled engines, the RQV scheme is still used for controlling the fuel amount to the engine, since the driver wants the engine to behave as with the mechanical governor.

RQV control is essentially a P controller with the accelerator as reference value and a sensor measuring the engine speed. The RQV controller has no information about the load, and a nonzero load (e.g. going uphill or downhill) gives a stationary

error. The RQV controller is described by

$$u = u_0 + K_p(ri - \dot{\theta}_m) \tag{5.1}$$

where $i = i_t i_f$ is the conversion ratio of the driveline, K_p is the controller gain, and r is the reference velocity. The constant u_0 is a function of the speed, but not the load since this is unknown to the RQV controller. RQV control is demonstrated in the following example.

Example 5.1 *Consider the truck modeled in Chapters 2 and 3 traveling at a speed of 2 rad/s (3.6 km/h) with gear 1 and a total load of 3000 Nm ($\approx$ 2 % road slope). Let the new desired velocity be $r = 2.3$ rad/s. Figure 5.1 shows the RQV control law (5.1) applied to Model 1 with three gains K_p. In the plots, u_0 is calculated such that the stationary level is the same for the three gains. (Otherwise there would be a gain dependent stationary error.)*

When the controller gain is increased, the rise time and the overshoot is increasing. Hence, there is a trade-off between short rise time and little overshoot. Furthermore, the engine speed behaves well, but the flexibility of the driveline causes the wheel speed to oscillate, when the gain is increased.

Figure 5.2 shows the transfer functions from load and measurement disturbances v and e to the performance output, when the RQV controller is used. The resonance peak in the transfer functions is increasing when the controller gain is increased.

5.2 Problem Formulation

The performance output for the speed controller is the wheel speed, $z = \dot{\theta}_w$, as defined in Chapter 4. In Figure 5.3, the wheel speed z is seen for Models 1 and 2. Model 2 adds a second resonance peak from the clutch. Furthermore, the high frequency roll-off rate is steeper for Model 2 than for Model 1. Note that the transfer function from the load l to the performance output z is the same for the two models. This chapter deals with the development of a controller based on Model 1.

5.2.1 Mathematical Problem Formulation

A first possible attempt for speed control is a scheme of applying the engine torque to the driveline such that the following cost function is minimized

$$\lim_{T\to\infty} \int_0^T (z - r)^2 \tag{5.2}$$

where r is the reference velocity given by the driver. If a control law is to minimize the cost function, then (5.2) can be made arbitrarily small if there are no restrictions on the control signal u, since the plant model is linear. A diesel engine can only produce torque in a certain range, and therefore, (5.2) is extended such that a large control signal adds to the cost function.

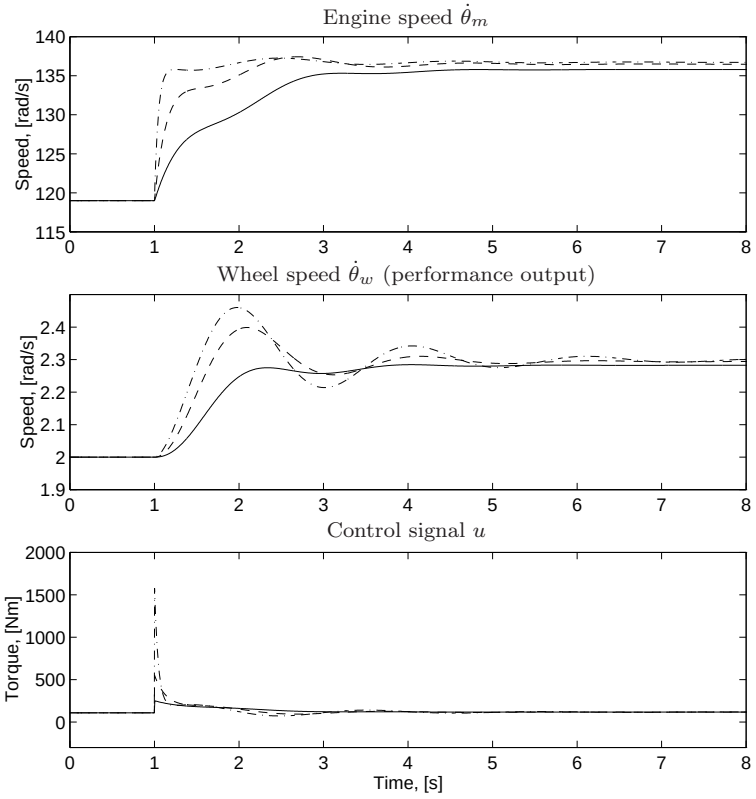

Figure 5.1 *RQV control (5.1) of Model 1. Controller gains $K_p = 8$, $K_p = 25$, and $K_p = 85$ are shown in solid, dashed and dash-dotted lines respectively. Increased gain results in a well behaved engine speed, but an oscillating wheel speed.*

The stationary point $z = r$ is reached if a control signal u_0 is used. This torque is a function of the reference value r and the load l. For a given wheel speed $\dot{\theta}_w$ and load l the driveline has the following stationary point

$$x_0(\dot{\theta}_w, l) = \begin{pmatrix} b_2/k & 1/k \\ i & 0 \\ 1 & 0 \end{pmatrix} \begin{pmatrix} \dot{\theta}_w \\ l \end{pmatrix} = \delta_x \dot{\theta}_w + \delta_l l \tag{5.3}$$

$$u_0(\dot{\theta}_w, l) = \begin{pmatrix} (b_1 i^2 + b_2)/i & 1/i \end{pmatrix} \begin{pmatrix} \dot{\theta}_w \\ l \end{pmatrix} = \lambda_x \dot{\theta}_w + \lambda_l l \tag{5.4}$$

The stationary point is obtained by solving

$$Ax + Bu + Hl = 0 \tag{5.5}$$

for x and u, where A, B, H, and x is given by (4.2) to (4.5).

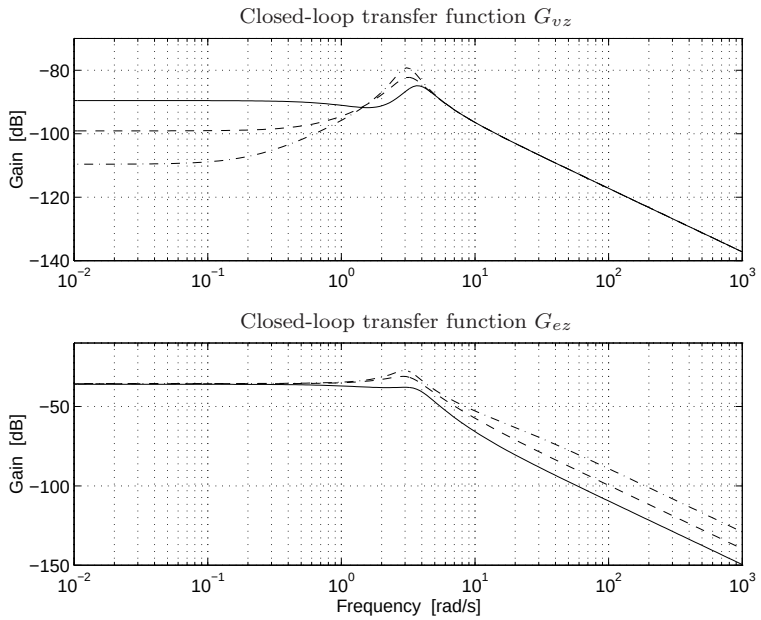

Figure 5.2 *Closed-loop transfer functions G_{vz} and G_{ez} when using the RQV control law (5.1) for the controller gains $K_p = 8$ (solid), $K_p = 25$ (dashed), and $K_p = 85$ (dash-dotted). The resonance peaks increase with increasing gain.*

By using these equations, the cost function can be written such that a control signal u that deviates from the stationary value $u_0(r, l)$ adds to the cost function. The extended cost function is given by

$$\lim_{T\to\infty} \int_0^T (z - r)^2 + \eta(u - u_0(r, l))^2 \tag{5.6}$$

where η is used to control the trade-off between rise time and control signal amplitude.

The controller that minimizes (5.6) has no stationary error, since the load l is included and thus compensated for. However, it is desirable that the stationary error characteristic for the RQV controller is maintained in the speed controller, as mentioned before. A stationary error comparable with that of the RQV controller can be achieved by using only a part of the load l in the criterion (5.6), as will be demonstrated in Section 5.3.1. Furthermore, the following demands should be considered.

- The control signal can not exceed $u_{min} = -300$ Nm or $u_{max} = 2300$ Nm.
- The influence from load and measurement disturbances on the performance output, wheel speed, should be minimized. Load disturbances result from, for instance, road roughness or impulses from towed trailers.

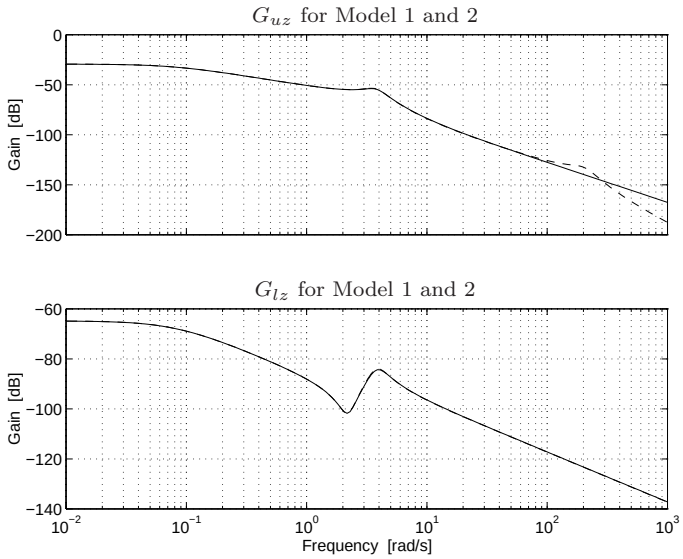

Figure 5.3 *Transfer functions from control signal u and load l to performance output z. Model 1 is shown in solid and Model 2 is shown in dashed. The modeled clutch gives a second resonance peak and a steeper roll-off rate.*

5.3 Speed Control with Active Damping and RQV Behavior

The problem formulation (5.6) will be treated in two steps. First without RQV behavior i.e. using the load l, and then extending to RQV behavior. The problem formulation (5.6) is in this section solved with LQG technique. This is done by linearizing the driveline model and rewriting (5.6) in terms of the linearized variables. A state-feedback matrix is derived that minimizes (5.6). This is done by solving a Riccati equation. The derived feedback law is a function of η which is chosen such that a feasible control signal is used.

The model (4.1)

$$\dot{x} = Ax + Bu + Hl \tag{5.7}$$

is affine since it includes a constant term l. The model is linearized in the neighborhood of a stationary point (x_0, u_0). The linear model is

$$\Delta\dot{x} = A\Delta x + B\Delta u \tag{5.8}$$

where

$$\begin{aligned} \Delta x &= x - x_0 \\ \Delta u &= u - u_0 \\ x_0 &= x_0(x_{30}, l) \end{aligned} \tag{5.9}$$

$$u_0 = u_0(x_{30}, l)$$

where the stationary point (x_0, u_0) is given by (5.3) and (5.4). Note that the linear model is the same for all stationary points.

The problem is to devise a feedback-control law that minimizes the cost function (5.6). The cost function is expressed in terms of Δx and Δu by using (5.9)

$$\lim_{T\to\infty} \int_0^T (M(x_0 + \Delta x) - r)^2 + \eta(u_0 + \Delta u - u_0(r, l))^2 \tag{5.10}$$

$$= \lim_{T\to\infty} \int_0^T (M\Delta x + r_1)^2 + \eta(\Delta u + r_2)^2 \tag{5.11}$$

with

$$\begin{aligned} r_1 &= Mx_0 - r \\ r_2 &= u_0 - u_0(r, l) \end{aligned} \tag{5.12}$$

In order to minimize (5.10) a Riccati equation is solved. Then the constants r_1 and r_2 must be expressed in terms of state variables. This can be done by augmenting the plant model (A, B) with models of the constants r_1 and r_2. Since these models will not be controllable, they must be stable in order to solve the Riccati equation (Maciejowski 1989). Therefore the model $\dot{r}_1 = \dot{r}_2 = 0$ cannot be used because the poles are located on the imaginary axis. Instead the following are used

$$\dot{r}_1 = -\alpha r_1 \tag{5.13}$$

$$\dot{r}_2 = -\alpha r_2 \tag{5.14}$$

which with a low α indicates that r is a slow varying constant.

The augmented model is given by

$$A_r = \begin{pmatrix} & & & 0 & 0 \\ & A & & 0 & 0 \\ & & & 0 & 0 \\ & & & -\alpha & 0 \\ 0 & 0 & 0 & 0 & -\alpha \end{pmatrix}, \tag{5.15}$$

$$B_r = \begin{pmatrix} B \\ 0 \\ 0 \end{pmatrix}, \quad x_r = (\Delta x^T \ r_1 \ r_2)^T \tag{5.16}$$

By using these equations, the cost function (5.10) can be written in the form

$$\lim_{T\to\infty} \int_0^T x_r^T Q x_r + R\Delta u^2 + 2x_r^T N \Delta u \tag{5.17}$$

with

$$\begin{aligned} Q &= (M\ 1\ 0)^T(M\ 1\ 0) + \eta(0\ 0\ 0\ 0\ 1)^T(0\ 0\ 0\ 0\ 1) \\ N &= \eta(0\ 0\ 0\ 0\ 1)^T \\ R &= \eta \end{aligned} \tag{5.18}$$

The cost function (5.10) is minimized by using

$$\Delta u = -K_c \Delta x \tag{5.19}$$

with

$$K_c = Q^{-1}(B_r^T P_c + N^T) \tag{5.20}$$

where P_c is the solution to the Riccati equation

$$A_r^T P_c + P_c A_r + R - (P_c B_r + N) Q^{-1} (P_c B_r + N)^T = 0 \tag{5.21}$$

The control law (5.19) becomes

$$\Delta u = -K_c x_r = -\begin{pmatrix} K_{c1} & K_{c2} & K_{c3} \end{pmatrix} \Delta x - K_{c4} r_1 - K_{c5} r_2 \tag{5.22}$$

By using (5.9) and (5.12) the control law is written

$$u = K_0 x_{30} + K_l l + K_r r - \begin{pmatrix} K_{c1} & K_{c2} & K_{c3} \end{pmatrix} x \tag{5.23}$$

with

$$\begin{aligned} K_0 &= \begin{pmatrix} K_{c1} & K_{c2} & K_{c3} \end{pmatrix} \delta_x - K_{c4} M \delta_x + \lambda_x - K_{c5} \lambda_x \\ K_r &= K_{c4} + K_{c5} \lambda_x \\ K_l &= \begin{pmatrix} K_{c1} & K_{c2} & K_{c3} \end{pmatrix} \delta_l - K_{c4} M \delta_l + \lambda_l \end{aligned} \tag{5.24}$$

where δ_x, δ_l, λ_x, and λ_l are described in (5.3) and (5.4).

When this control law is applied to Example 5.1 the controller gains becomes

$$u = 0.230 x_{30} + 4470 r + 0.125 l - \begin{pmatrix} 7620 & 0.0347 & 2.36 \end{pmatrix} x \tag{5.25}$$

where $\eta = 5 \cdot 10^{-8}$ and $\alpha = 0.0001$ are used. With this controller the phase margin is guaranteed to be at least 60° and the amplitude margin is infinity (Maciejowski 1989). The result is seen in Figure 5.4.

The rise time of the LQG controller is shorter than for the RQV controller. Also the overshoot is less when using LQG control. The driving torque is controlled such that the oscillations in the wheel speed are actively damped. The controlled driving torque makes the engine speed oscillate, as seen in Figure 5.4.

5.3.1 Extending with RQV Behavior

The RQV controller has no information about the load l, and therefore a stationary error will be present when the load is different from zero. The LQG feedback law (5.25) is a function of the load, and the stationary error is zero if the load is known. There is however a demand by the driver that the load should give a stationary error, and only when using a cruise controller the stationary error should be zero.

The LQG controller can be changed such that a load different from zero gives a stationary error. This is done by using $\beta_l l$ instead of the complete load l in (5.23). The constant β_l range from $\beta_l = 0$ which means no compensation for the load, to

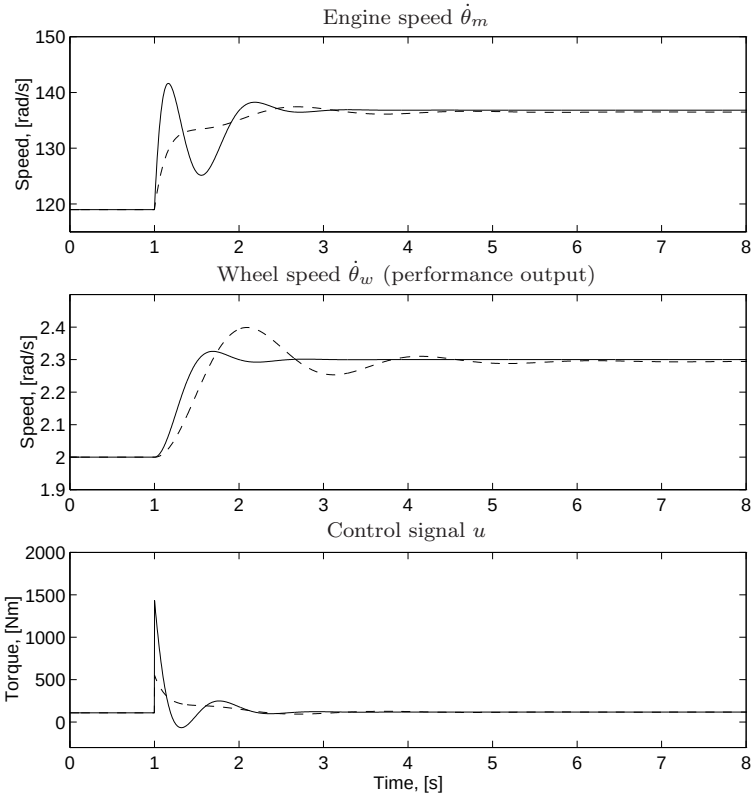

Figure 5.4 *Model 1 controlled with the LQG control law (5.25). RQV control (5.1) with $K_p = 25$ is seen in dashed lines. With active damping, the engine speed oscillates, resulting in a well behaved wheel speed.*

$\beta_l = 1$ which means fully compensation of the load and no stationary error. The compensated LQG control law becomes

$$u = K_0 x_{30} + K_l \beta_l l + K_r r - \begin{pmatrix} K_{c1} & K_{c2} & K_{c3} \end{pmatrix} x \tag{5.26}$$

In Figure 5.5, the RQV controller with its stationary error (remember the reference value $r = 2.3$ rad/s) is compared to the compensated LQG controller (5.26) applied to Example 5.1 for three values of β_l. By adjusting β_l, the speed controller with active damping is extended with a stationary error comparable with that of the RQV controller.

5.4 Influence from Sensor Location

The LQG controller investigated in the previous section uses feedback from all states ($x_1 = \theta_m/i_t i_f - \theta_w$, $x_2 = \dot{\theta}_m$, and $x_3 = \dot{\theta}_w$). This is not possible if only

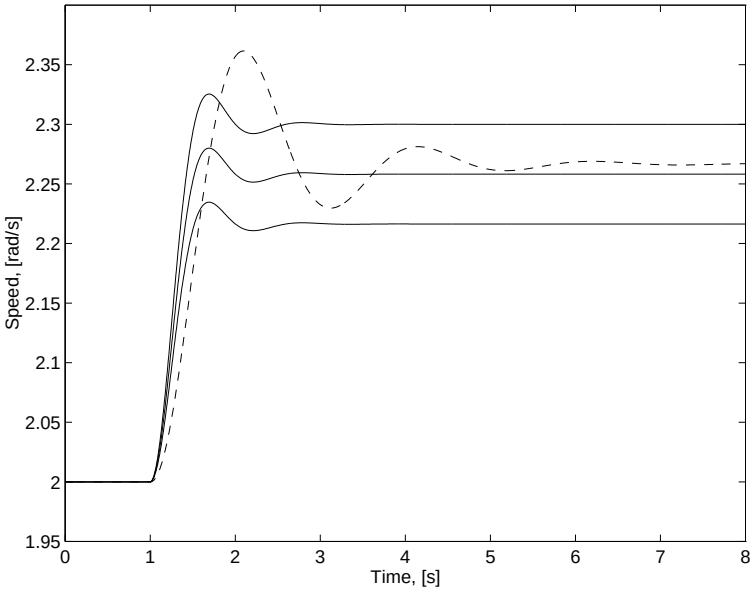

Figure 5.5 *Example 5.1 controlled with the RQV controller (5.1) in dashed line, and the LQG controller with stationary error (5.26) with* $\beta_l = 0,\ 0.5,\ 1$. *The LQG controller achieves the same stationary as the RQV controller by adjusting* β_l.

one sensor is used, which is the case considered in this work. The sensor either measures the engine speed $\dot{\theta}_m$ or the wheel speed $\dot{\theta}_w$. In this section an observer is used to estimate the rest of the states. The observer gain is calculated using LTR technique. Then two different observer problems results depending on which sensor location that is used.

The LQG feedback law (5.23) then becomes

$$u = K_0 x_{30} + K_r r + K_l l - \begin{pmatrix} K_{c1} & K_{c2} & K_{c3} \end{pmatrix} \hat{x} \tag{5.27}$$

with K_0, K_r, and K_l given by (5.24). The estimated states $\hat{x}$ are given by the Kalman filter

$$\Delta\dot{\hat{x}} = A\Delta\hat{x} + B\Delta u + K_f(\Delta y - C\Delta\hat{x}) \tag{5.28}$$

$$K_f = P_f C^T V^{-1} \tag{5.29}$$

where P_f is found by solving the Riccati equation

$$P_f A^T + A P_f - P_f C^T V^{-1} C P_f + W = 0 \tag{5.30}$$

The covariance matrices W and V corresponds to v and e respectively. The output matrix C is either equal to C_m (4.11) when measuring the engine speed, or C_w (4.12) when measuring the wheel speed.

Loop-Transfer Recovery (LTR) is used to recover the properties achieved in the previous design step when all states are measured. This is done by selecting

$$\begin{aligned} V &= 1 \\ W &= \rho B B^T \\ C &= C_m \ \ or \ \ C_w \\ \rho &= \rho_m \ \ or \ \ \rho_w \end{aligned} \tag{5.31}$$

and solving (5.29) and (5.30) for K_f.

When using LQG with feedback from all states, the phase margin φ is at least 60° and the amplitude margin a is infinity as stated before. This is obtained also when using the observer by increasing ρ towards infinity. For Example 5.1 the following values are used

$$\rho_m = 5 \cdot 10^5 \ \Rightarrow \ \varphi_m = 60.5^\circ, \quad a_m = \infty \tag{5.32}$$

$$\rho_w = 10^{14} \ \Rightarrow \ \varphi_w = 59.9^\circ, \quad a_w = 35.0 \tag{5.33}$$

where the aim has been to have at least 60° phase margin.

The observer dynamics is cancelled in the transfer function from reference value to performance output and control signal. Hence, these transfer functions are not affected by the sensor location. However, the observer dynamics will be included in the transfer functions from disturbances both to z and u.

5.4.1 Influence from Load Disturbances

Figure 5.6 shows how the performance output and the control signal are affected by the load disturbance v. There is a resonance peak in G_{vz} when using feedback from the engine speed sensor, which is not present when feedback from the wheel speed sensor is used. The reason to this can be seen when studying the transfer function G_{vz} in (4.20). By using the matrix inversion lemma (4.20) is rewritten as

$$(G_{vz})_{cl} = \frac{G_{vz} + F_y(G_{uy}G_{vz} - G_{uz}G_{vy})}{1 + G_{uy}F_y} \tag{5.34}$$

where G_{ab} means the transfer function from signal a to b, and cl stands for closed loop. The signal y in (5.34) mean the output of the system, i.e. either $\dot{\theta}_w$ or $\dot{\theta}_m$. The controller F_y is given by (4.15) as

$$F_y(s) = K_c(sI - A + BK_c + K_f C)^{-1}K_f \tag{5.35}$$

with C either as C_m for engine speed feedback, or C_w for wheel speed feedback. For the speed controller ($z = \dot{\theta}_w$), Equation (5.34) becomes

$$(G_{vz})_{cl} = \frac{G_{vw}}{1 + G_{uw}F_y} \tag{5.36}$$

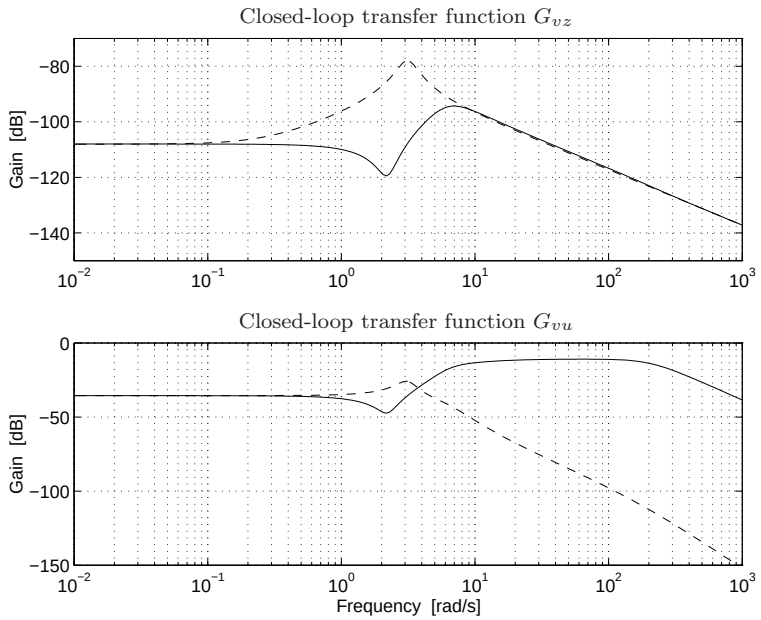

Figure 5.6 *Closed-loop transfer functions from load disturbance v to performance output z and control signal u. Feedback from $\dot{\theta}_w$ is shown in solid and feedback from $\dot{\theta}_m$ is shown in dashed lines. With $\dot{\theta}_m$ feedback the transfer functions have a resonance peak, resulting from the open-loop zeros.*

when the sensor measures the wheel speed, and

$$(G_{vz})_{cl} = \frac{G_{vw} + F_y(G_{um}G_{vw} - G_{uw}G_{vm})}{1 + G_{um}F_y} \tag{5.37}$$

when the sensor measures the engine speed. Hence, when using the wheel speed sensor, the controller is cancelled in the numerator, and when the engine speed sensor is used, the controller is not cancelled.

The optimal return ratio in the LQG step is

$$K_c(sI - A)^{-1}B \tag{5.38}$$

Hence the poles from A is kept, but there are new zeros that are placed such that the relative degree of (5.38) is one, the phase margin is at least 60°, and the gain margin is infinite. In the LTR step the return ratio is

$$F_yG_{uy} = K_c(sI - A - BK_c - K_fC)^{-1}K_fC(sI - A)^{-1}B \tag{5.39}$$

When ρ in (5.31) is increased towards infinity, (5.38) equals (5.39). This means that the zeros in the open-loop system $C(sI - A)^{-1}B$ are cancelled by the controller. Hence, the open-loop zeros will become poles in the controller F_y. This means that

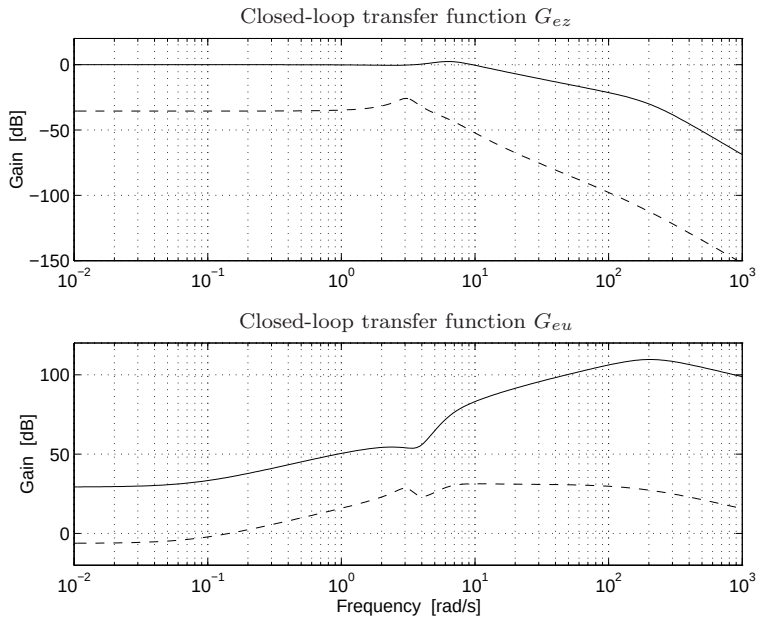

Figure 5.7 *Closed-loop transfer functions from measurement noise e to performance output z and control signal u. Feedback from $\dot{\theta}_w$ is shown in solid and feedback from $\dot{\theta}_m$ is shown in dashed. The difference between the two feedback principles is described by the dynamic output ratio. The effect increases with lower gears.*

the closed-loop system will have the open-loop zeros as poles when using the engine speed sensor. This means that the G_{vz} will have the poles $-0.5187 \pm 3.0753i$ which causes the resonance peak in Figure 5.6.

5.4.2 Influence from Measurement Disturbances

The influence from measurement disturbances e is seen in Figure 5.7. The transfer functions from measurement noise (4.21) can be rewritten with the matrix inversion lemma as

$$(G_{ez})_{cl} = -\frac{G_{uz}F_y}{1 + G_{uy}F_y} \tag{5.40}$$

The complementary sensitivity function is defined for the two sensor alternatives as

$$T_w = \frac{G_{uw}F_y}{1 + G_{uw}F_y}, \quad T_m = \frac{G_{um}F_y}{1 + G_{um}F_y} \tag{5.41}$$

Then

$$(G_{ez})_{cl} \quad = \quad -T_w \quad \text{with} \quad \dot{\theta}_w \quad \text{feedback} \tag{5.42}$$

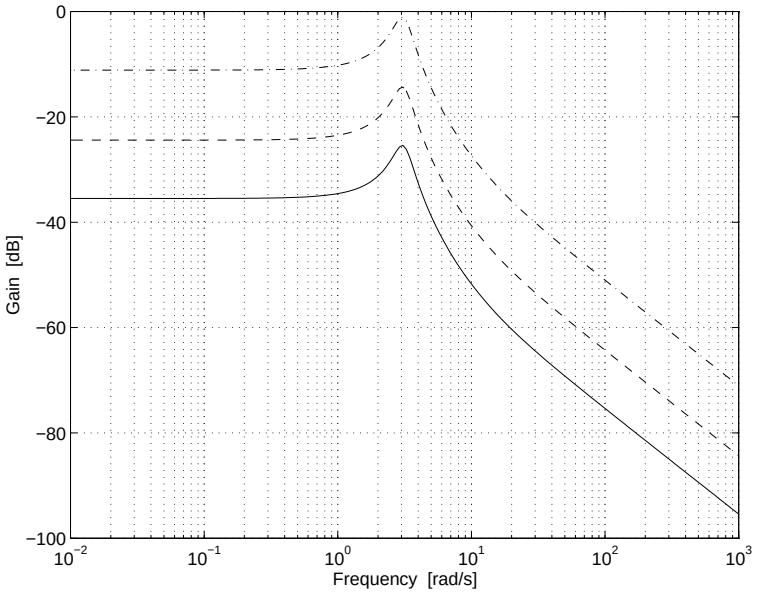

Figure 5.8 *The dynamic output ratio $G_{w/m}$ for gear 1 (solid), gear 7 (dashed), and gear 14 (dash-dotted).*

$$(G_{ez})_{cl} \quad = \quad -T_m \frac{G_{uw}}{G_{um}} = T_m G_{w/m} \quad \text{with} \quad \dot{\theta}_m \quad \text{feedback} \tag{5.43}$$

where the dynamic output ratio $G_{w/m}$ was defined in Definition 4.1. For Model 1 the dynamic output ratio is

$$G_{w/m} = \frac{cs + k}{i(J_2 s^2 + (c + b_2)s + k)} \tag{5.44}$$

where the state-space description in Chapter 4 is used. Especially for low frequencies, $G_{w/m}(0) = 1/i = 1/i_t i_f$. The dynamic output ratio can be seen in Figure 5.8 for three gears.

When ρ in (5.31) is increased towards infinity, (5.38) equals (5.39). Then (5.42) and (5.43) gives

$$(G_{ez})_{cl,m} = (G_{ez})_{cl,w} \, G_{w/m} \tag{5.45}$$

where cl, m and cl, w means closed loop with feedback from $\dot{\theta}_m$ and $\dot{\theta}_w$ respectively.

The frequency range in which the $T_m = T_w$ is valid depends on how large ρ in (5.31) is made. Figure 5.9 shows the sensitivity functions

$$S_w = \frac{1}{1 + G_{uw} F_y}, \quad S_m = \frac{1}{1 + G_{um} F_y} \tag{5.46}$$

and the complementary sensitivity functions T_w and T_m (5.41) for the two cases of feedback. It is seen that $T_m = T_w$ is valid up to about 16 Hz. The roll-off rate at

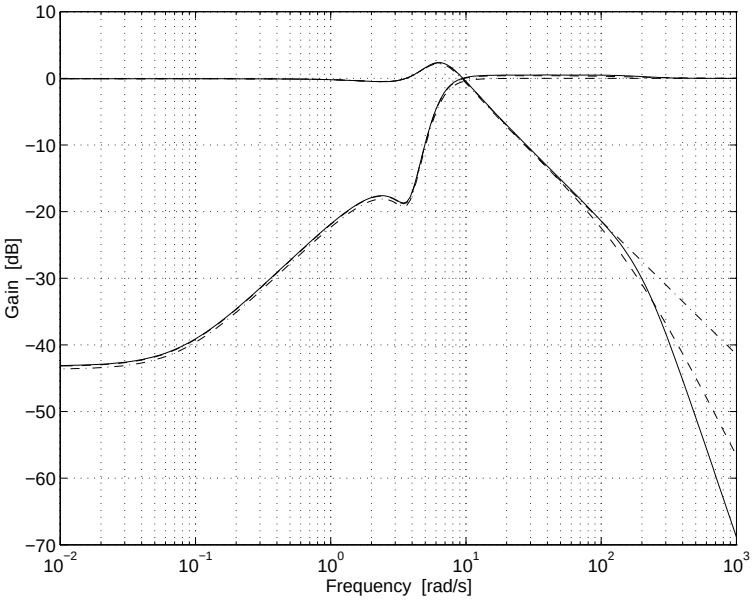

Figure 5.9 *Sensitivity function S and complementary sensitivity function T. The dash-dotted lines correspond to the case with all states known. When only one velocity is measured, the solid lines correspond to $\dot{\theta}_w$ feedback, and the dashed lines correspond to $\dot{\theta}_m$ feedback.*

higher frequencies differ between the two feedback principles. This is due to that the open-loop transfer functions G_{uw} and G_{um} have a different relative degree. G_{uw} has a relative degree of two, and G_{um} has a relative degree of one. Therefore, T_w has a steeper roll-off rate than T_m.

Hence, the difference in G_{ez} depending on sensor location is described by the dynamic output ratio $G_{w/m}$. The difference in low frequency level is equal to the conversion ratio of the driveline. Therefore, this effect increases with lower gears.

5.4.3 Load Estimation

The feedback law with unknown load is

$$u = K_0 x_{30} + K_r r + K_l \hat{l} - \begin{pmatrix} K_{c1} & K_{c2} & K_{c3} \end{pmatrix} \hat{x} \tag{5.47}$$

where $\hat{l}$ is the estimated load. In order to estimate the load, the model used in the Kalman filter is augmented with a model of the load. The load is hard to model correctly since it is a function of road slope. However it can be treated as a slow varying constant. The augmented model is

$$x_4 = l, \quad \text{with} \quad \dot{x}_4 = 0 \tag{5.48}$$

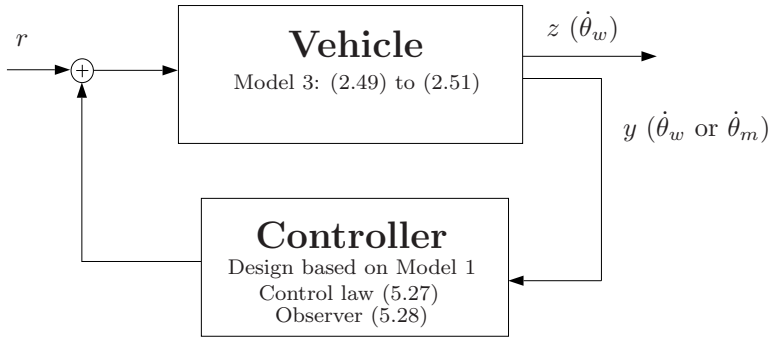

Figure 5.10 *Simulation configuration. As a step for demonstrating feasibility for real implementation, Model 3 is simulated with the controller based on Model 1.*

This gives

$$\dot{\hat{x}} = A_l\hat{x}_l + B_l u + K_f(y - C_l\hat{x}_l) \tag{5.49}$$

with

$$\hat{x}_l = \begin{pmatrix} \hat{x} & \hat{l} \end{pmatrix}, \tag{5.50}$$

$$A_l = \begin{pmatrix} & & & 0 \\ & A & & 0 \\ & & & -1/J_2 \\ 0 & 0 & 0 & 0 \end{pmatrix}, \tag{5.51}$$

$$B_l = \begin{pmatrix} B \\ 0 \end{pmatrix}, \quad C_l = \begin{pmatrix} C & 0 \end{pmatrix} \tag{5.52}$$

The feedback law is

$$u = K_0 x_{30} + K_r r - \begin{pmatrix} K_{c1} & K_{c2} & K_{c3} & -K_l \end{pmatrix} \hat{x}_l \tag{5.53}$$

5.5 Simulations

An important step in demonstrating feasibility for real implementation is that a controller behaves well when simulated on a more complicated vehicle model than it was designed for. Here, the control law based on the reduced driveline model is simulated with a more complete nonlinear model, derived in Chapter 2. The purpose is also to study effects from different sensor locations as discussed in Section 5.4. The simulation situation is seen in Figure 5.10.

The nonlinear Model 3, given by (2.49) to (2.51), is used as vehicle model. The steady-state level for Model 3 is calculated by solving the model equations for the equilibrium point when the load and speed are known.

The controller used is based on Model 1, as seen in the previous sections. The wheel speed or the engine speed is input to the observer (5.28), and the control law (5.27) with $\beta_l = 0$ generates the control signal.

The simulation case presented here is the same as in Example 5.1, i.e. a velocity step response. The stationary point is given by

$$\dot{\theta}_w = 2,\ l = 3000 \quad \Rightarrow \quad x_0 = \begin{pmatrix} 0.0482 & 119 & 2.00 \end{pmatrix}, \quad u_0 = 109 \tag{5.54}$$

where (5.3) and (5.4) are used, and the desired new speed is $\dot{\theta}_w = 2.3$ rad/s. At steady state, the clutch transfers the torque $u_0 = 109$ Nm. This means that the clutch angle is in the area with higher stiffness ($\theta_{c1} < \theta_c \leq \theta_{c2}$) in the clutch nonlinearity, seen in Figure 2.7. This is a typical driving situation when speed control is used. However, at low clutch torques ($\theta_c < \theta_{c1}$) the clutch nonlinearity can produce limit cycle oscillations (Björnberg, Pettersson, and Nielsen 1996). This situation occurs when the truck is traveling downhill with a load of the same size as the friction in the driveline, resulting in a low clutch torque. This is however not treated here. At $t = 6$ s, a load impulse disturbance is simulated. The disturbance is generated as a square pulse with 0.1 s width and 1200 Nm height.

In order to simulate the nonlinear model, the differential equations (2.49) to (2.51) are scaled such that the five differential equations (one for each state) have about the same magnitude. The model is simulated using Runge Kutta (45) (Simulink 1993) with a low step size to catch the effect of the nonlinearity.

Figures 5.11 to 5.13 show the result of the simulation. These should be compared with the same control law applied to Model 1 in Figure 5.4. From these plots it is demonstrated that the performance does not critically depend on the

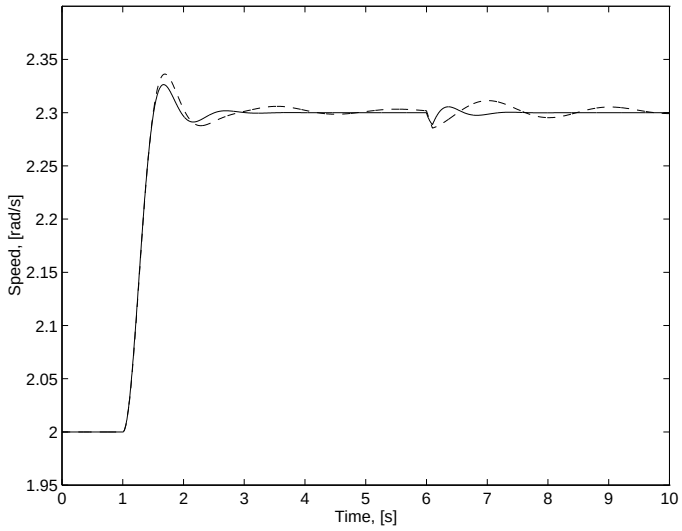

Figure 5.11 *Wheel speed when controlling Model 3 with the LQG control law (5.27) derived from Model 1. The solid line corresponds to $\dot{\theta}_w$ feedback and feedback from $\dot{\theta}_m$ is seen in dashed line. At $t = 6$ s, an impulse disturbance v acts on the load. The design still works when simulated with extra clutch dynamics.*

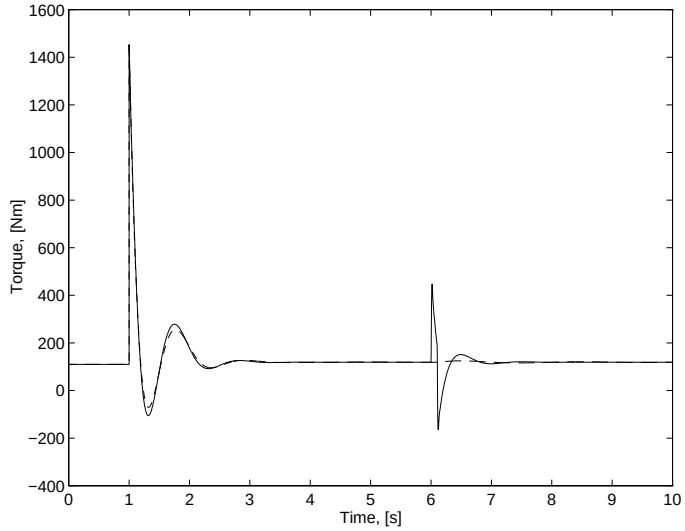

Figure 5.12 *Control signal corresponding to Figure 5.11. There is no difference between the two sensor alternatives in the step response at $t = 1$ s. However, the load impulse (at $t = 6$ s) generates a control signal that damps the impulse disturbance when feedback from the wheel speed sensor is used, but not with engine speed feedback.*

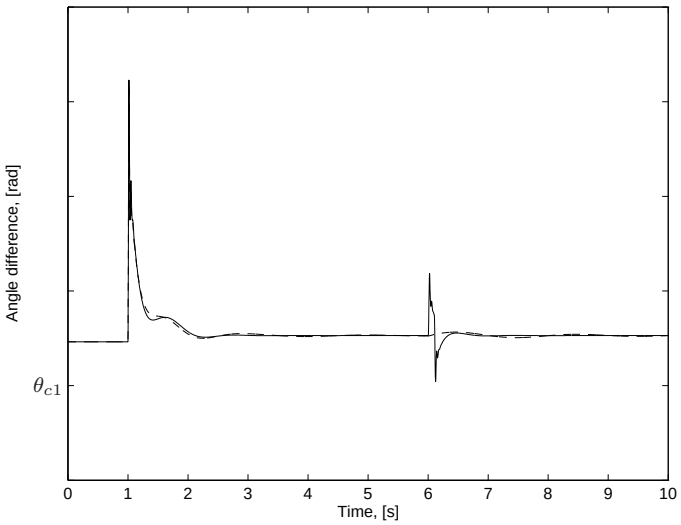

Figure 5.13 *Clutch angle difference corresponding to Figure 5.11. The influence from the clutch nonlinearity can be neglected, because the area with low stiffness ($\theta_c < \theta_{c1}$) is never entered.*

simplified model structure. The design still works if the extra dynamics are added. Further evidence supporting this is seen in Figure 5.13. The area with low stiffness in the clutch nonlinearity ($\theta_c < \theta_{c1}$) is never entered. The load impulse disturbance is better attenuated with feedback from the wheel speed sensor, which is a verification of the behavior that was discussed in Section 5.4.

5.6 Summary

Speed control with active damping and RQV behavior has been proposed in this chapter. RQV control is the traditional way speed control is performed in diesel engines. RQV control gives a certain driving character with a load dependent stationary error when going uphill or downhill. With RQV, there is no active damping of wheel speed oscillations, resulting in vehicle shuffle. An increased controller gain results in more wheel speed oscillations while the engine speed behaves well.

A major contribution in this chapter is a formulation of a criterion for speed control with active damping of wheel speed oscillations and a stationary error giving RQV behavior. To solve the criterion, a linear driveline model with drive shaft flexibility, and parameters estimated from experiments are used. Simulations show that the performance of the design, based on the simplified model, works well for a more complicated model, with a nonlinear clutch characteristics.

An investigation of the influence from different sensor locations on the control design shows that when using LQG/LTR the open-loop zeros are cancelled by the controller. With engine speed feedback this is critical, because the open-loop transfer function has a resonant zero couple. It is shown that this zero couple becomes poles of the transfer functions from load disturbances to wheel speed. This results in undamped load disturbances when engine speed feedback is used. When feedback from the wheel speed sensor is used, no resonant open-loop poles are cancelled. Load disturbances are thus better attenuated with this feedback configuration.

Measurement disturbances are better attenuated when the engine speed sensor is used, than when using the wheel speed sensor. This effect increases with lower gears. Two different closed-loop transfer functions result, depending on feedback configuration. The difference between these two is described by the dynamic output ratio.

In conclusion, even though there are sensor choices, the use of active damping significantly improves the behavior for both sensor cases. Further, the formulation is natural, it allows efficient solution, and there is a simple tuning of the amount of RQV feeling.

6

Gear-Shift Controller Design and Simulations

Traditionally a gear shift is performed by disengaging the clutch, engaging neutral gear, shifting to a new gear, and engaging the clutch again. In todays traffic it is desired to have an automatic gear shifting system, where the complete shift action is controlled by a microprocessor. If the automatic gear shifting system is to work with a clutch and a manually shifted transmission, one of the following strategies can be taken.

- The gear shift is performed with a microprocessor controlling the clutch and the shift event.
- The gear shift is performed without using the clutch (Orehall 1995). In this case the engine is controlled such that the torque in the transmission is zero, whereafter neutral gear is engaged. The engine speed is then controlled to the propeller shaft speed (scaled with the new conversion ratio). Following that, the new gear is engaged, and then the speed controller controls the driveline to the speed demanded by the driver.

When using the second approach, neutral gear is engaged when the transmission transfers zero torque. It is clear that driveline oscillations is an important performance limiting factor if they are not damped out. This is because the system has to wait until satisfactory gear shift conditions are reached, and thus seriously increasing the total time needed for a gear shift. One reason this is not acceptable is that, since there is no torque, the vehicle is free rolling which may be serious with heavy loads and large road slopes. The observation that the vehicle is free rolling, i.e. changing its velocity, when obtaining gear shift conditions shows that the desired control goal is not a stationary point, which has to be handled.

This chapter is devoted to study a new idea that the transmission torque can be estimated and controlled to zero while having active damping. The problem formulation is further discussed in Section 6.1. A model of the transmission is developed and the torque transmitted in the transmission is modeled as a function of the states and the control signal in Section 6.2. Some first primitive attempts are then discussed in Section 6.3.

A key result in this chapter is, in light of the simplistic attempts in Section 6.3, the formulation of the gear-shift control criterion in Section 6.4, and its treatment in Section 6.5. Influence from sensor location and simulations are presented in the sections following.

6.1 Problem Formulation

The gear-shift controller is the controller that drives the transmission torque to zero, while damping oscillations. If a gear shift is commanded when the driveline is oscillating, the gear-shift controller should still drive the transmission torque to zero.

The control signal is restricted to be in the interval between $u_{min} = -300$ Nm and $u_{max} = 2300$ Nm. The time it takes for a gear shift should be possible to optimize. The influence from load and measurement disturbances should be minimized.

6.2 Transmission Torque

The performance output z for the gear-shift controller is the torque transmitted between the cog wheels in the transmission. A more detailed study of the transmission is depicted in Figure 6.1. Here, the input shaft is connected to bearings with a viscous friction component b_{t1}. A cog wheel is mounted at the end of the input shaft which is connected to a cog wheel mounted on the output shaft. The conversion ratio between these are i_t, as mentioned in Chapter 2. The output shaft is also connected to bearings with the viscous friction component b_{t2}.

Two equations describe the inputs and outputs of the transmission

$$J_{t1}\ddot{\theta}_c = M_t - b_{t1}\dot{\theta}_c - z \tag{6.1}$$
$$J_{t2}\ddot{\theta}_t = i_t z - b_{t2}\dot{\theta}_t - M_p \tag{6.2}$$

6.2.1 Transmission Torque for Model 1

By using (2.1)

$$J_m\ddot{\theta}_m = M_m - M_{fr:m} - M_c \tag{6.3}$$

together with (2.12)

$$M_c = M_t, \quad \theta_m = \theta_c \tag{6.4}$$

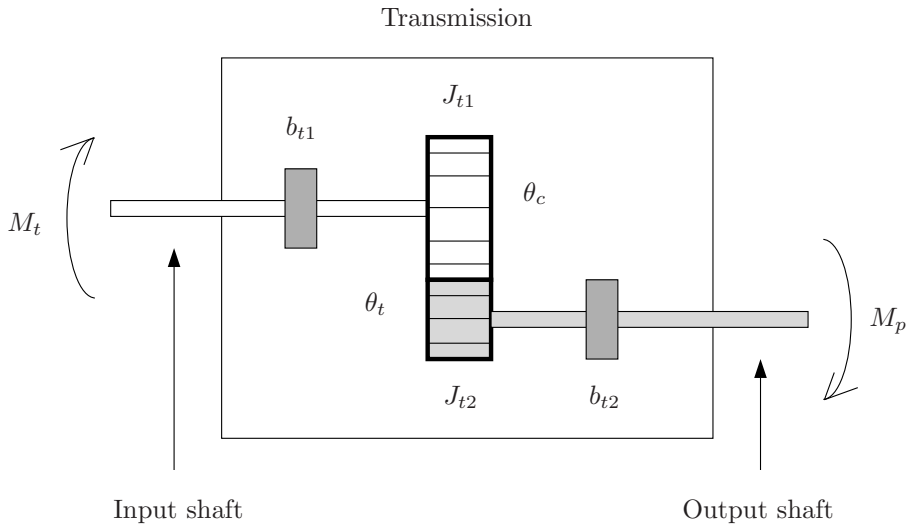

Figure 6.1 *Transmission with two cogwheels with conversion ratio i_t. The cogwheels are connected to the input and output shaft respectively.*

equation (6.1) is expressed in terms of engine speed

$$(J_m + J_{t1})\ddot{\theta}_m = M_m - M_{fr:m} - b_{t1}\dot{\theta}_m - z \tag{6.5}$$

To describe the performance output in terms of state variables, $\ddot{\theta}_m$ (which is not a state variable) is replaced with (2.25)

$$\begin{aligned}(J_m + J_t/i_t^2 + J_f/i_t^2 i_f^2)\ddot{\theta}_m \quad &= \quad M_m - M_{fr:m} - (b_t/i_t^2 + b_f/i_t^2 i_f^2)\dot{\theta}_m \\ &\quad -k(\theta_m/i_t i_f - \theta_w)/i_t i_f \\ &\quad -c(\dot{\theta}_m/i_t i_f - \dot{\theta}_w)/i_t i_f\end{aligned} \tag{6.6}$$

which together with $u = M_m - M_{fr:m}$ gives

$$\begin{aligned}u - b_{t1}\dot{\theta}_m - z \quad &= \quad \frac{J_m + J_{t1}}{J_m + J_t/i_t^2 + J_f/i_t^2 i_f^2}\Big(M_m - M_{fr:m} - (b_t/i_t^2 + b_f/i_t^2 i_f^2)\dot{\theta}_m \\ &\quad -k(\theta_m/i_t i_f - \theta_w)/i_t i_f - c(\dot{\theta}_m/i_t i_f - \dot{\theta}_w)/i_t i_f\Big)\end{aligned} \tag{6.7}$$

From this it is possible to express the performance output as a function of the control signal u and the state variables x, according to the state-space description (4.2) to (4.5).

Definition 6.1 *The performance output for Model 1 is*

$$z \quad = \quad Mx + Du \quad \text{with}$$

$$M^T = \begin{pmatrix} \frac{(J_m+J_{t1})k}{J_1 i} \\ \frac{J_m+J_{t1}}{J_1}(b_1 + c/i^2) - b_{t1} \\ -\frac{(J_m+J_{t1})c}{J_1 i} \end{pmatrix} \tag{6.8}$$

$$D = 1 - \frac{J_m + J_{t1}}{J_1}$$

where the labels from (4.5) are used.

The unknown parameters in (6.8) are $J_m + J_{t1}$ and b_{t1}. The other parameters are estimated in Chapter 3.

One way of estimating these unknowns would be to decouple Model 1 into two models, corresponding to neutral gear. Then a model including the engine, clutch, and the input shaft of the transmission results, in which the performance output z is equal to zero. Trials with neutral gear would then give a possibility to estimate the unknowns.

In the derivation of Model 1 in Chapter 2 the performance output z is eliminated. If z is eliminated in (6.1) and (6.2) and (6.4) is used, the equation for the transmission is

$$(J_{t1}i_t^2 + J_{t2})\ddot{\theta}_m = i_t^2 M_c - i_t M_p - (b_{t1}i_t^2 + b_{t2})\dot{\theta}_m \tag{6.9}$$

By comparing this with the equation describing the transmission in Chapter 2, (2.15)

$$J_t\ddot{\theta}_m = i_t^2 M_c - b_t\dot{\theta}_m - i_t M_p \tag{6.10}$$

the following equations relating the parameters are obtained

$$J_t = i_t^2 J_{t1} + J_{t2} \tag{6.11}$$

$$b_t = i_t^2 b_{t1} + b_{t2} \tag{6.12}$$

For the rest of this chapter the following assumption about the parameters in the transmission is used.

Assumption 6.1 *$J_{t1} = J_{t2}$ and $b_{t1} = b_{t2}$.*

Then (6.11) and (6.12) gives

$$J_{t1} = \frac{J_t}{1 + i_t^2} \tag{6.13}$$

$$b_{t1} = \frac{b_t}{1 + i_t^2} \tag{6.14}$$

In Chapter 3, the estimated combinations of parameters from Model 1 are

$$J_1 = J_m + J_t/i_t^2 + J_f/i_t^2 i_f^2 \tag{6.15}$$

$$b_1 = b_t/i_t^2 + b_f/i_t^2 i_f^2 \tag{6.16}$$

From (6.13) and (6.15) $J_m + J_{t1}$ can be derived

$$\begin{aligned} J_m + J_{t1} &= J_m + \frac{J_t}{1+i_t^2} = J_m + \frac{i_t^2}{1+i_t^2}(J_1 - J_m - J_f/i_t^2 i_f^2) \\ &= J_m \frac{1}{1+i_t^2} + J_1 \frac{i_t^2}{1+i_t^2} - J_f \frac{1}{i_f^2(1+i_t^2)} \end{aligned} \tag{6.17}$$

A combination of (6.14) and (6.16) gives b_{t1}

$$b_{t1} = \frac{b_t}{1+i_t^2} = \frac{i_t^2}{1+i_t^2}(b_1 - b_f/i_t^2 i_f^2) \tag{6.18}$$

For low gears (i_t large), and since J_f and b_f are considerably less than J_1 and b_1, the following assumptions are used

$$J_m + J_{t1} \approx J_1 \frac{i_t^2}{1+i_t^2} \tag{6.19}$$

$$b_{t1} \approx b_1 \frac{i_t^2}{1+i_t^2} \tag{6.20}$$

6.2.2 Transmission Torque for Model 2

The performance output expressed for Model 2 is given by replacing M_t in (6.1) by equation (2.39)

$$M_c = M_t = k_c(\theta_m - \theta_t i_t) + c_c(\dot{\theta}_m - \dot{\theta}_t i_t) \tag{6.21}$$

Then the performance output is

$$z = k_c(\theta_m - \theta_t i_t) + c_c(\dot{\theta}_m - \dot{\theta}_t i_t) - b_{t1} i_t \dot{\theta}_t - J_{t1} i_t \ddot{\theta}_t \tag{6.22}$$

This is expressed in terms of state variables by using (2.45)

$$(J_t + J_f/i_f^2)\ddot{\theta}_t = i_t \left(k_c(\theta_m - \theta_t i_t) + c_c(\dot{\theta}_m - \dot{\theta}_t i_t) \right) \tag{6.23}$$

$$-(b_t + b_f/i_f^2)\dot{\theta}_t - \frac{1}{i_f}\left(k_d(\theta_t/i_f - \theta_w) + c_d(\dot{\theta}_t/i_f - \dot{\theta}_w) \right) \tag{6.24}$$

leading to

Definition 6.2 *The performance output for Model 2 is*

$$z = Mx \quad \text{with} \tag{6.25}$$

$$M^T = \begin{pmatrix} k_c(1 - \frac{J_{t1} i_t^2}{J_2}) \\ \frac{J_{t1} i_t k_d}{J_2 i_f} \\ c_c(1 - \frac{J_{t1} i_t^2}{J_2}) \\ \frac{J_{t1} i_t^2}{J_2}(i_t^2 c_c + b_2 + c_d/i_f^2) - c_c i_t - b_{t1} i_t \\ -\frac{J_{t1} i_t c_d}{J_2 i_f} \end{pmatrix}$$

with states and labels according to to the state-space description (4.6) to (4.8).

In Chapter 3, the following combinations of parameters from Model 2 are estimated.

$$J_2 = J_t + J_f/i_f^2 \tag{6.26}$$
$$b_2 = b_t + b_f/i_f^2 \tag{6.27}$$

From (6.13) , (6.14) , (6.26), and (6.27), J_{t1} and b_{t1} can be derived as

$$J_{t1} = \frac{i_t^2}{1+i_t^2}(J_2 - J_f/i_f^2) \tag{6.28}$$
$$b_{t1} = \frac{i_t^2}{1+i_t^2}(b_2 - b_f/i_f^2) \tag{6.29}$$

which are approximated to

$$J_{t1} \approx \frac{i_t^2}{1+i_t^2}J_2 \tag{6.30}$$
$$b_{t1} \approx \frac{i_t^2}{1+i_t^2}b_2 \tag{6.31}$$

since J_f and b_f are considerably less than J_1 and b_1.

6.2.3 Transmission Torque for Model 3

The performance output for Model 3 is derived in the same way as for Model 2, with the difference that (6.21) is replaced by

$$M_c = M_t = M_{kc}(\theta_m - \theta_t i_t) + c_c(\dot{\theta}_m - \dot{\theta}_t i_t) \tag{6.32}$$

where M_{kc} is the torque transmitted by the clutch nonlinearity, given by (2.48). Then the performance output is defined as

Definition 6.3 *The performance output for Model 3 is*

$$z = (M_{kc},\ \dot{\theta}_t/i_f - \dot{\theta}_w,\ \dot{\theta}_m,\ \dot{\theta}_t,\ \dot{\theta}_w) \begin{pmatrix} 1 - \frac{J_{t1}i_t^2}{J_2} \\ \frac{J_{t1}i_t k_d}{J_2 i_f} \\ c_c(1 - \frac{J_{t1}i_t^2}{J_2}) \\ \frac{J_{t1}i_t^2}{J_2}(i_t^2 c_c + b_2 + c_d/i_f^2) - c_c i_t - b_{t1} i_t \\ -\frac{J_{t1}i_t c_d}{J_2 i_f} \end{pmatrix} \tag{6.33}$$

The parameters not estimated in the definition above are approximated in the same way as for the performance output for Model 2.

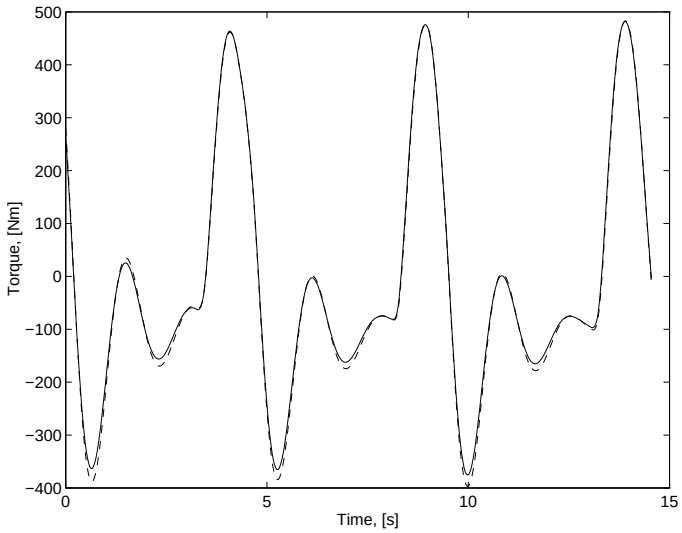

Figure 6.2 *Transmission torque z from parameter estimation of Model 1 and Model 2 on data from Trial 1. The solid line corresponds to Model 1 and the dashed line corresponds to Model 2.*

Comparison

In Figure 6.2 the performance output (6.8) and (6.25) during Trial 1 are shown from the parameter estimation of the linear Models 1 and 2. Figure 6.3 shows the performance output in the frequency domain. The low frequency level differs between the two models, and the main reason to this is the difficulties to estimate the viscous damping coefficients described in Chapter 3. The difference at higher frequencies is a result from the clutch which gives a second resonance peak for Model 2. Furthermore, the roll-off rate of Model 2 is steeper than for Model 1.

6.3 Preliminary Trials

Two preliminary trials will be performed in this section, to study gear-shift control.

6.3.1 Unconstrained Active Damping

A first attempt is to study the performance output, $z = Mx + Du$, with M and D given by (6.8). A control law can be derived since z includes the control signal and D is scalar. If u is chosen as

$$u = -D^{-1}Mx \tag{6.34}$$

$z = 0$ is guaranteed.

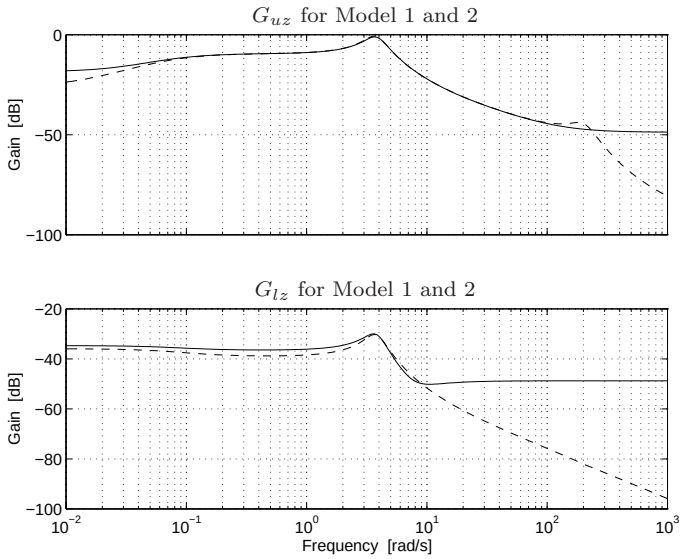

Figure 6.3 *Transfer functions from control signal u and load l to transmission torque z. Model 1 is shown in solid and Model 2 is shown in dashed. The modeled clutch adds a second resonance peak and a steeper roll-off rate.*

Example 6.1 *Consider the truck modeled in Chapters 2 and 3 traveling at a speed of* 3 *rad/s (*5.4 *km/h) with gear 1 and a total load of* 3000 *Nm (≈ 2 % road slope). The stationary point is obtained by using (5.3) and (5.4).*

$$x_{30} = 3,\ l = 3000 \quad \Rightarrow \quad x_0 = \begin{pmatrix} 0.0511 & 178 & 3.00 \end{pmatrix},\quad u_0 = 138 \tag{6.35}$$

In Figure 6.4 the resulting transmission torque z, control signal u, engine, and wheel speed is seen when the control signal is chosen as in (6.34). Unconstrained active damping is achieved which obtains $z = 0$ instantaneously. The wheel speed decreases linearly, while the engine speed is oscillating.

Unconstrained active damping (6.34) generates a control signal that is impossible for the engine to generate. To deal with this situation, it would be desirable to use an control law which also considers that the control signal must be in a certain interval.

It can be noted that despite $z = 0$ is achieved this is not an stationary point, since the speed is decreasing. This means that the vehicle is free rolling which can be critical if lasting too long.

6.3.2 Undamped Gear-Shift Condition

The previous approach is not realizable because of the unrealistic control signal. A second attempt is to explicitly handle the expected vehicle behavior (free rolling)

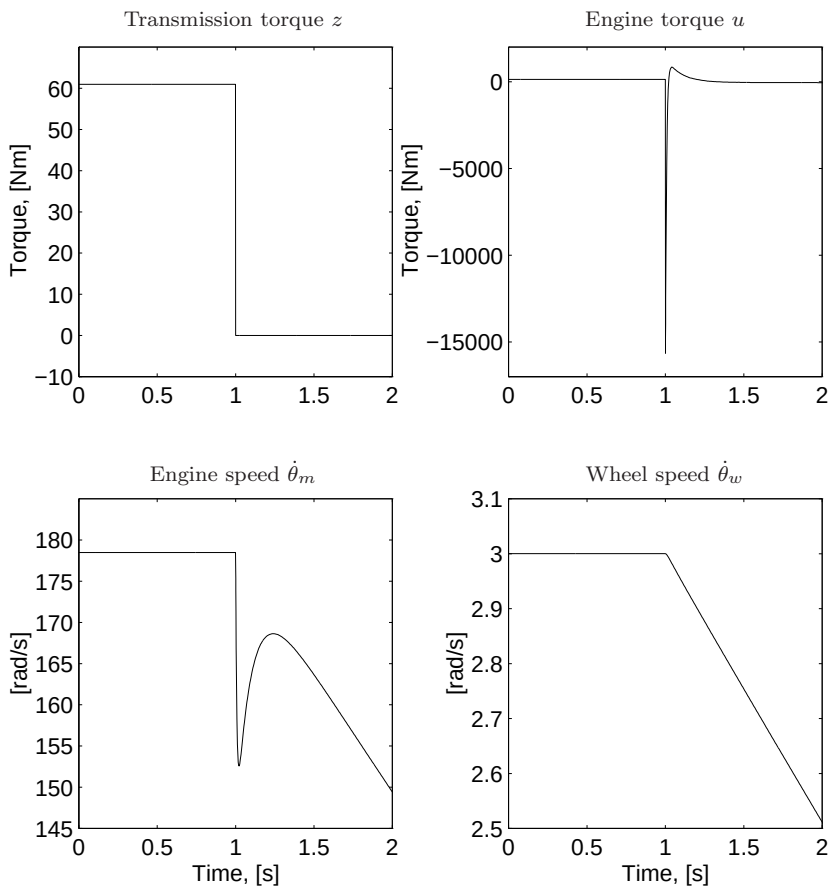

Figure 6.4 *Unconstrained active damping of Model 1. At $t = 1$ s, the control law (6.34) drives the transmission torque to zero. The oscillations in the transmission torque are damped with an unrealizable control signal. The wheel speed decreases linearly.*

when the transmission torque, z, is zero, but without using active damping. This control law is thus derived by considering a stiff driveline, and solving for $z = 0$.

By using the labels according to Chapter 4, the differential equation, describing the stiff driveline is

$$(J_1 i + J_2/i)\ddot{\theta}_w = u - (b_1 i + b_2/i)\dot{\theta}_w - l/i \tag{6.36}$$

This equation is developed by using Model 1 in (2.25) and (2.26), and eliminating the torque transmitted by the drive shaft, $k(\theta_m/i - \theta_w) + c(\dot{\theta}_m/i - \dot{\theta}_w)$. Then by using $\dot{\theta}_m = \dot{\theta}_w i$, (6.36) results.

Equation (6.5) expressed in terms of wheel speed is

$$z = u - b_{t1} i \dot{\theta}_w - (J_m + J_{t1}) i \ddot{\theta}_w \tag{6.37}$$

Combining (6.36) and (6.37) gives the performance output for the stiff driveline.

$$z = (1 - \frac{(J_m + J_{t1})i^2}{J_1 i^2 + J_2})u - (b_{t1} i - \frac{(J_m + J_{t1})i}{J_1 i^2 + J_2}(b_1 i^2 + b_2))\dot{\theta}_w + \frac{(J_m + J_{t1})i}{J_1 i^2 + J_2} l \tag{6.38}$$

The control signal to force $z = 0$ is given by solving (6.38) for u while $z = 0$.

$$\begin{aligned} u_{shift}(\dot{\theta}_w, l) &= \mu_x \dot{\theta}_w + \mu_l l \quad \text{with} \\ \mu_x &= (b_{t1} i - \frac{(J_m + J_{t1})i}{J_1 i^2 + J_2}(b_1 i^2 + b_2))(1 - \frac{(J_m + J_{t1})i^2}{J_1 i^2 + J_2})^{-1} \\ \mu_l &= -\frac{(J_m + J_{t1})i}{J_1 i^2 + J_2}(1 - \frac{(J_m + J_{t1})i^2}{J_1 i^2 + J_2})^{-1} \end{aligned} \tag{6.39}$$

Figure 6.5 shows Example 6.1 applied to Model 1 controlled with the undamped gear-shift condition (6.39). This control law achieves $z = 0$ with a realizable control signal, but the oscillations introduced are not damped. Therefore, the time needed to fulfill the gear-shift condition is not optimized. The performance of this approach is worse if the driveline is oscillating at the time for the gear shift.

6.4 Gear-Shift Control Criterion

Neither of the two approaches in the previous section solve the problem satisfactory. In this section a new idea for gear-shift control is formulated. The transmission torque is estimated and controlled to zero with active damping. The idea is formulated as a cost criterion which uses a combination of the two previous approaches. The criterion is formulated such that active damping is obtained with a control law whose deviation from the undamped gear-shift condition (6.39) adds to the cost function. Let the cost function be

$$\begin{aligned} &\lim_{T \to \infty} \int_0^T z^2 + \eta(u - u_{shift}(\dot{\theta}_w, l))^2 \\ = &\lim_{T \to \infty} \int_0^T (Mx + Du)^2 + \eta(u - \mu_x \dot{\theta}_w - \mu_l l)^2 \end{aligned} \tag{6.40}$$

The controller that minimizes this cost function damps oscillation (since the first parenthesis is minimized), and at the same time, prevents the control signal from having large deviations from the undamped gear-shift condition u_{shift}. The trade-off is controlled by η.

If the driveline is stiff, there is no difference between the two parenthesis in (6.40). Furthermore, the point at which the cost function is zero is no stationary point, since the speed of the vehicle will decrease despite $z = 0$ and $u = u_{shift}$.

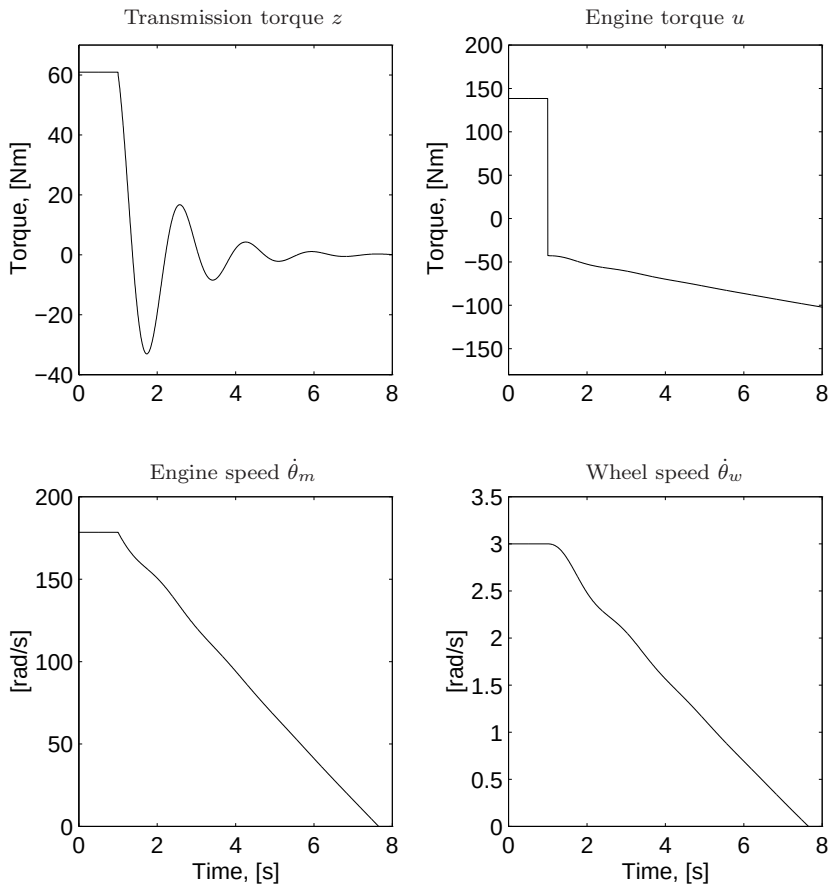

Figure 6.5 *Model 1 controlled with the undamped gear-shift condition (6.39). At $t = 1$ s, a gear shift is commanded. The speed dependent realizable control signal drives the transmission torque to zero. Undamped oscillations in the transmission torque increase the time needed to fulfill the gear-shift condition.*

6.5 Gear-Shift Control Design

The new idea for gear-shift control is in this section given efficient treatment by solving (6.40) for a control law by using LQG technique, using available software. This is done by linearizing the driveline model and rewriting (6.40) in terms of the linearized variables. A state-feedback matrix is derived that minimizes (6.40), by solving a Riccati equation. The derived feedback law is a function of η which is chosen such that a feasible control signal is used.

The linearized driveline model is given by (5.8) and (5.9) in Section 5.3. The

cost function is expressed in terms of Δx and Δu by using (5.9)

$$\begin{aligned} & \lim_{T\to\infty}\int_0^T (M\Delta x + D\Delta u + Mx_0 + Du_0)^2 \\ + \quad & \eta(\Delta u - \mu_x \Delta x_3 + u_0 - \mu_x x_{30} - \mu_l l)^2 \\ = \quad & \lim_{T\to\infty}\int_0^T (M\Delta x + D\Delta u + r_1)^2 + \eta(\Delta u - \mu_x \Delta x_3 + r_2) \end{aligned} \tag{6.41}$$

with

$$\begin{aligned} r_1 &= Mx_0 + Du_0 \\ r_2 &= u_0 - \mu_x x_{30} - \mu_l l \end{aligned} \tag{6.42}$$

The constants r_1 and r_2 are expressed as state variables, by augmenting the plant model (A, B) with models of the constants r_1 and r_2. This was done in (5.13) to (5.16).

By using these equations, the cost function (6.41) can be written in the form

$$\lim_{T\to\infty}\int_0^T x_r^T Q x_r + R\Delta u^2 + 2x_r^T N\Delta u \tag{6.43}$$

with

$$\begin{aligned} Q &= (M\ 1\ 0)^T(M\ 1\ 0) + \eta(0\ 0\ -\mu_x\ 0\ 1)^T(0\ 0\ -\mu_x\ 0\ 1) \\ N &= (M\ 1\ 0)^T D + \eta(0\ 0\ -\mu_x\ 0\ 1)^T \\ R &= D^2 + \eta \end{aligned} \tag{6.44}$$

The cost function (6.43) is minimized by the state-feedback gain

$$K_c = Q^{-1}(B_r^T P_c + N^T) \tag{6.45}$$

where P_c is the solution to the Riccati equation (5.21). The resulting control law is

$$\Delta u = -K_c x_r = -\begin{pmatrix} K_{c1} & K_{c2} & K_{c3} \end{pmatrix}\Delta x - K_{c4} r_1 - K_{c5} r_2 \tag{6.46}$$

using (6.42) gives

$$u = K_0 x_{30} + K_l l - \begin{pmatrix} K_{c1} & K_{c2} & K_{c3} \end{pmatrix} x \tag{6.47}$$

with

$$\begin{aligned} K_0 &= \begin{pmatrix} \lambda_x & \delta_x & \mu_x \end{pmatrix}\Gamma \\ K_l &= \begin{pmatrix} \lambda_l & \delta_l & \mu_l \end{pmatrix}\Gamma \end{aligned} \tag{6.48}$$

where Γ is

$$\Gamma = \begin{pmatrix} 1 - K_{c4}D - K_{c5} \\ \begin{pmatrix} K_{c1} & K_{c2} & K_{c3} \end{pmatrix} - K_{c4}M \\ K_{c5} \end{pmatrix} \tag{6.49}$$

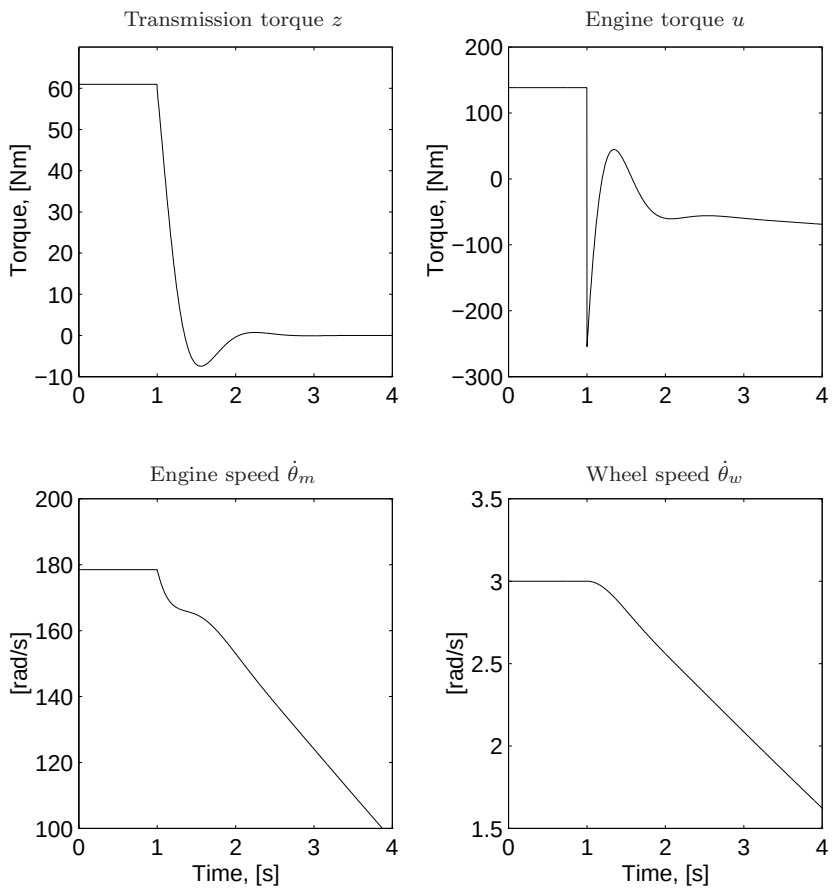

Figure 6.6 *Model 1 controlled with the LQG-control law (6.50), solving the gear-shift criterion (6.40). At $t = 1$ s, a gear shift is commanded. A realizable control signal is used such that the transmission torque is driven to zero, while oscillations are actively damped.*

with λ, δ, and μ given by (5.3), (5.4), and (6.39).

When this control law is applied to Example 6.1 the controller gains becomes

$$u = 2.37 \cdot 10^{-4} x_{30} - 0.0327 l - \begin{pmatrix} 4.2123 & 0.0207 & -1.2521 \end{pmatrix} x \tag{6.50}$$

where $\eta = 0.03$ and $\alpha = 0.0001$ are used. With this controller the phase margin is guaranteed to be at least 60° and the amplitude margin is infinity (Maciejowski 1989). The result is seen in Figure 6.6. By solving the gear-shift criterion (6.40), active damping is obtained with a realizable control signal. The control law is a function of η which is chosen such that the control signal is feasible.

6.6 Influence from Sensor Location

The LQG controller investigated in the previous section uses feedback from all states ($x_1 = \theta_m/i_t i_f - \theta_w$, $x_2 = \dot{\theta}_m$, and $x_3 = \dot{\theta}_w$). This is not possible if only one sensor is used, which is the case considered in this work. The sensor either measures the engine speed $\dot{\theta}_m$ or the wheel speed $\dot{\theta}_w$. In this section an observer is used to estimate the rest of the states. The observer gain is calculated using LTR technique. Two different observer problems results depending on which sensor location that is used. The unknown load can be estimated as in Section 5.4.3.

The LQG feedback law (6.47) becomes

$$u = K_0 x_{30} + K_l l - \begin{pmatrix} K_{c1} & K_{c2} & K_{c3} \end{pmatrix} \hat{x} \tag{6.51}$$

with K_0 and K_l given by (6.48). The estimated state $\hat{x}$ is given by the Kalman filter

$$\Delta\dot{\hat{x}} = A\Delta\hat{x} + B\Delta u + K_f(\Delta y - C\Delta\hat{x}) \tag{6.52}$$

$$K_f = P_f C^T V^{-1} \tag{6.53}$$

where P_f is found by solving the Riccati equation (5.30).

When using the LQG with feedback from all states, the phase margin φ is at least 60°, and the amplitude margin a is infinity, as stated before. This is obtained also when using the observer by increasing ρ towards infinity. For Example 6.1 the following values are used

$$\rho_m = 10^4 \Rightarrow \varphi_m = 77.3^\circ, \quad a_m = 2.82 \tag{6.54}$$

$$\rho_w = 10^{11} \Rightarrow \varphi_w = 74.3^\circ, \quad a_w = 2.84 \tag{6.55}$$

where the aim has been to have at least 60° phase margin.

The observer dynamics is cancelled in the transfer function from reference value to performance output and control signal. Hence, these transfer functions are not affected by the sensor location. However, the dynamics will be included in the transfer functions from disturbances to both z and u.

6.6.1 Influence from Load Disturbances

Figure 6.7 shows how the performance output and the control signal are affected by the load disturbance v. In Section 5.4 it was shown that for the speed controller, the resonant open-loop zeros become poles of the closed-loop system when feedback from the engine speed sensor is used. The same equations are valid for the gear-shift controller except the difference that the D matrix in (6.8) is not equal to zero, as for the speed controller. Hence, also the transfer function DG_{vu} should be added to (5.34). The closed-loop transfer function G_{vu} is given by

$$(G_{vu})_{cl} = -\frac{F_y G_{vy}}{1 + F_y G_{uy}} \tag{6.56}$$

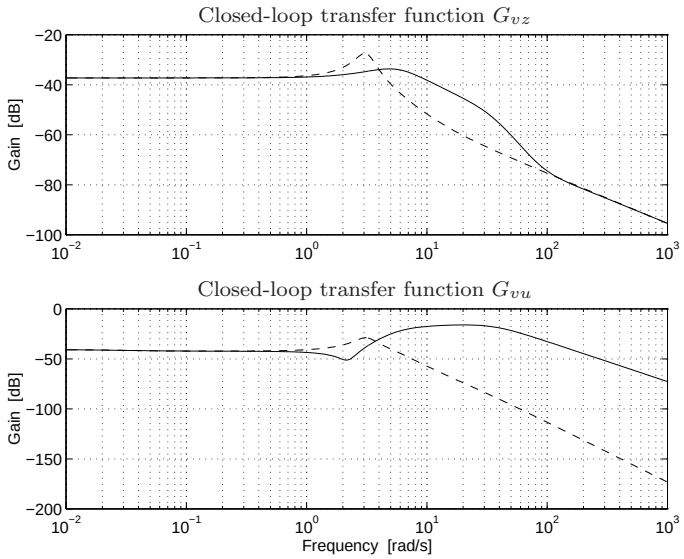

Figure 6.7 *Closed-loop transfer functions from load disturbance v to performance output z and control signal u. Feedback from $\dot{\theta}_w$ is shown in solid and feedback from $\dot{\theta}_m$ is shown in dashed lines. With $\dot{\theta}_m$ feedback the transfer functions have a resonance peak, resulting from the open-loop zeros.*

Thus, the closed-loop transfer function from v to u also has the controller F_y in the numerator. Hence, the closed-loop transfer function from v to z has the open-loop zeros as poles. For $\dot{\theta}_m$ feedback, this means that a resonance peak is present in the transfer functions from v to performance output z and control signal u.

6.6.2 Influence from Measurement Disturbances

The influence from measurement disturbances e are seen in Figure 6.8. According to (5.40) the closed-loop transfer function from e to z is

$$(G_{ez})_{cl} = -\frac{G_{uz}F_y}{1+G_{uy}F_y} \tag{6.57}$$

Then

$$(G_{ez})_{cl} = -T_w\frac{G_{uz}}{G_{uw}} \quad \text{with} \quad \dot{\theta}_w \quad \text{feedback} \tag{6.58}$$

$$(G_{ez})_{cl} = -T_m\frac{G_{uz}}{G_{um}} \quad \text{with} \quad \dot{\theta}_m \quad \text{feedback} \tag{6.59}$$

with T_w and T_m from (5.41).

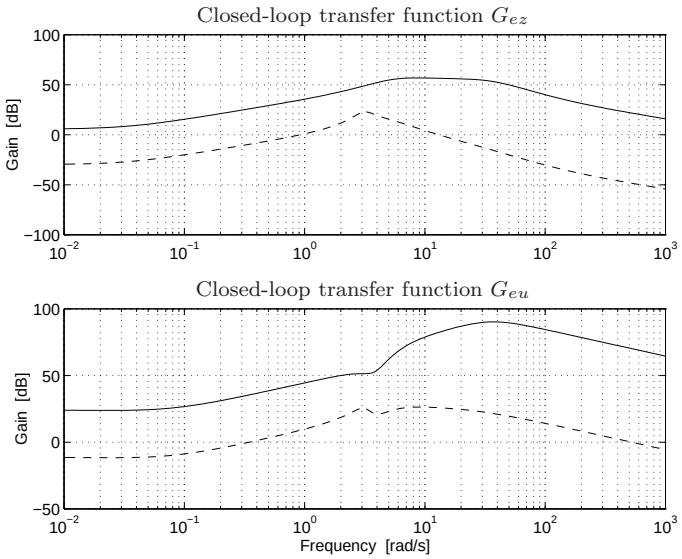

Figure 6.8 *Closed-loop transfer functions from measurement noise e to performance output z and control signal u. Feedback from $\dot{\theta}_w$ is shown in solid and feedback from $\dot{\theta}_m$ is shown in dashed. The difference between the two feedback principles are described by the dynamic output ratio. The effect increases with lower gears.*

When ρ in (5.31) is increased towards infinity, $T_m = T_w$ as was discussed in Section 5.4. Then (6.58) and (6.59) gives

$$(G_{ez})_{cl,m} = (G_{ez})_{cl,w}\, G_{w/m} \tag{6.60}$$

where cl, m and cl, w means closed loop with feedback from $\dot{\theta}_m$ and $\dot{\theta}_w$ respectively. The dynamic output ratio $G_{w/m}$ was defined in Definition 4.1, and is given by (5.44).

The frequency range in which the $T_m = T_w$ is valid depends on how large ρ in (5.31) is made, as discussed in Section 5.4. Figure 6.9 shows the sensitivity functions (5.46) and the complementary sensitivity functions T_w and T_m (5.41) for the two cases of feedback. It is seen that $T_m = T_w$ is valid up to about 2 Hz. The roll-off rate at higher frequencies differ between the two feedback principles. This is due to that the open-loop transfer functions G_{uw} and G_{um} have a different relative degree, as discussed in Section 5.4. T_w has a steeper roll-off rate than T_m, because that G_{uw} has a relative degree of two, and G_{um} has a relative degree of one.

Hence, the difference in G_{ez} depending on sensor location is described by the dynamic output ratio $G_{w/m}$. The difference in low frequency level is equal to the conversion ratio of the driveline. Therefore, this effect increases with lower gears.

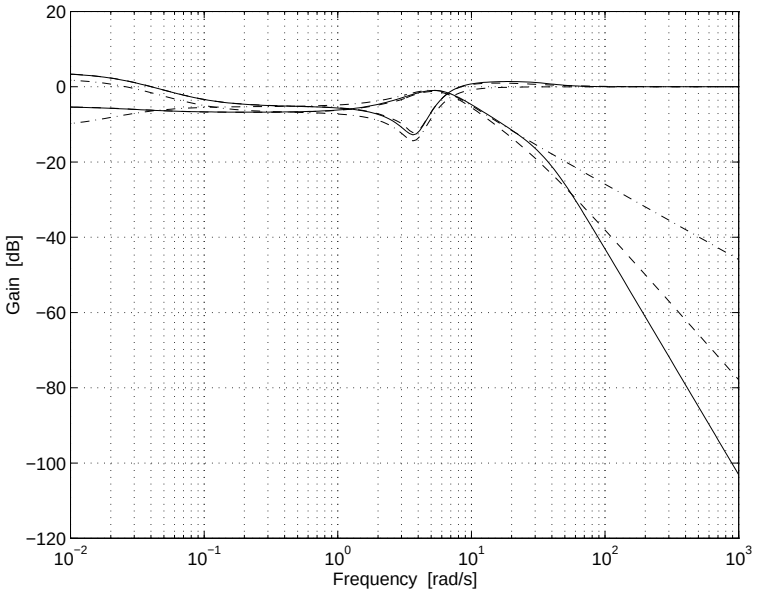

Figure 6.9 *Sensitivity function S and complementary sensitivity function T. The dash-dotted lines correspond to the case with all states known. When only one velocity is measured, the solid lines correspond to $\dot{\theta}_w$ feedback, and the dashed lines correspond to $\dot{\theta}_m$ feedback.*

6.7 Simulations

As in the case of the speed controller, in Section 5.5, the feasibility of the gear-shift controller is studied by simulation on a more complicated vehicle model than it was designed for. The control design is simulated with the nonlinear Model 3, according to Figure 6.10. The effects from sensor placement are also studied in accordance with the discussion made in Section 6.6.

Model 3 is given by Equations (2.49) to (2.51). The steady-state level for Model 3 is calculated by solving the model equations for the equilibrium point when the load and speed are known. In Assumption 6.1, the relationship between the model parameters in the transmission is given. By these, the equation for the transmission torque is calculated using (6.33).

The controller used is based on Model 1, as seen in the previous sections. The wheel speed or the engine speed is input to the observer (6.52), and the control law (6.51) generates the control signal.

Three simulations are performed with the same parameters, given by Example 6.1, (i.e. wheel speed $\dot{\theta}_w = 3$ rad/s, and load $l = 3000$ Nm). In the simulations, a gear shift is commanded at $t = 2$ s. The first simulation is without disturbances. In the second simulation, the driveline is oscillating prior to the gear shift. The oscillations are a result of a sinusoid disturbance acting on the control signal. The

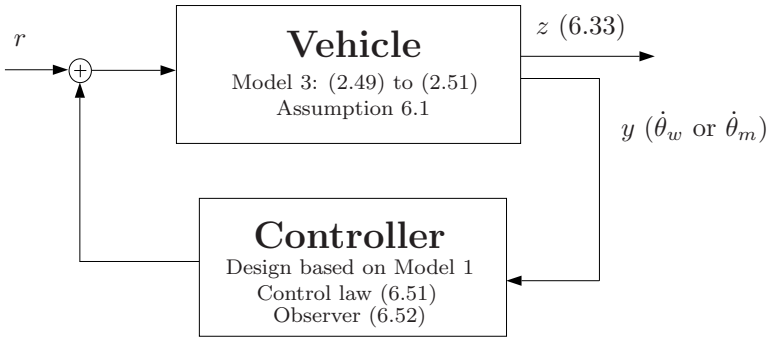

Figure 6.10 *Simulation configuration. As a step for demonstrating feasibility for real implementation, Model 3 is simulated with the controller based on Model 1.*

third gear shift is simulated with a load impulse at $t = 3$ s. The disturbance is generated as a square pulse with 0.1 s width and 1200 Nm height.

In order to simulate the nonlinear model, the differential equations (2.49) to (2.51) are scaled such that the five differential equations (one for each state) have about the same magnitude. The model is simulated using Runge Kutta (45) (Simulink 1993) with a low step size to catch the effect of the nonlinearity.

In Figure 6.11 the simulation without disturbances is shown. This plot should be compared with Figure 6.6, where the design is tested on Model 1. The result is that the performance does not critically depend on the simplified model structure. The design still works if the extra nonlinear clutch dynamics is added. In the simulation, there are different results depending on which sensor that is used. The model errors between Model 1 and Model 3 are handled better when using the wheel speed sensor. However, neither of the sensor alternatives reaches $z = 0$. This is due to the low frequency model errors discussed in Section 6.2. In Figure 6.12 the simulation with driveline oscillations prior to the gear shift is shown. The result is that the performance of the controller is not affected by the oscillations. Figure 6.13 shows the simulation with load disturbance. The disturbance is better damped when using feedback from the wheel speed sensor, than from the engine speed sensor, which is a verification of the discussion in Section 6.6.

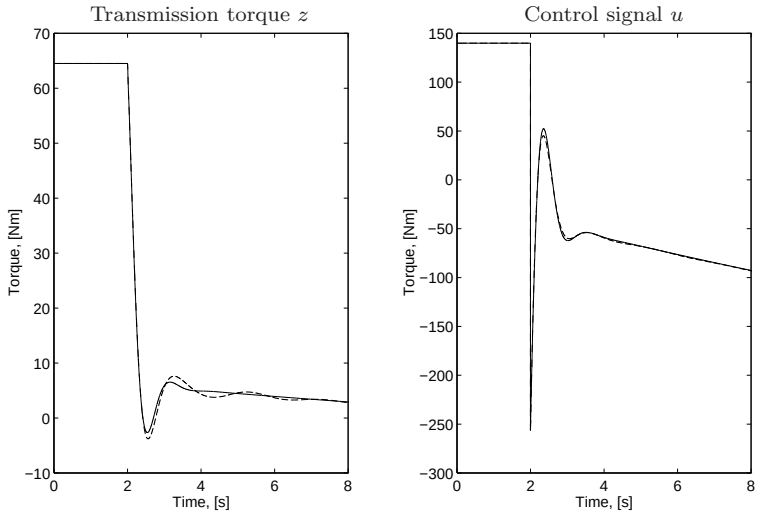

Figure 6.11 *Simulation of Model 3 with observer and control law based on Model 1. Feedback from the wheel speed sensor is seen in solid, and from the engine speed sensor is seen in dashed. The design still work when simulated with extra clutch dynamics.*

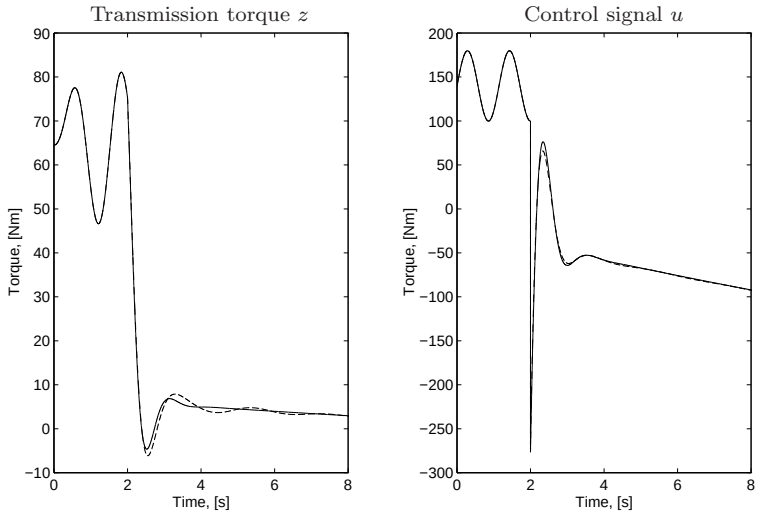

Figure 6.12 *Simulation of Model 3 with observer and control law based on Model 1. Feedback from the wheel speed sensor is seen in solid, and from the engine speed sensor is seen in dashed. The conclusion is that the control law works well despite initial driveline oscillations.*

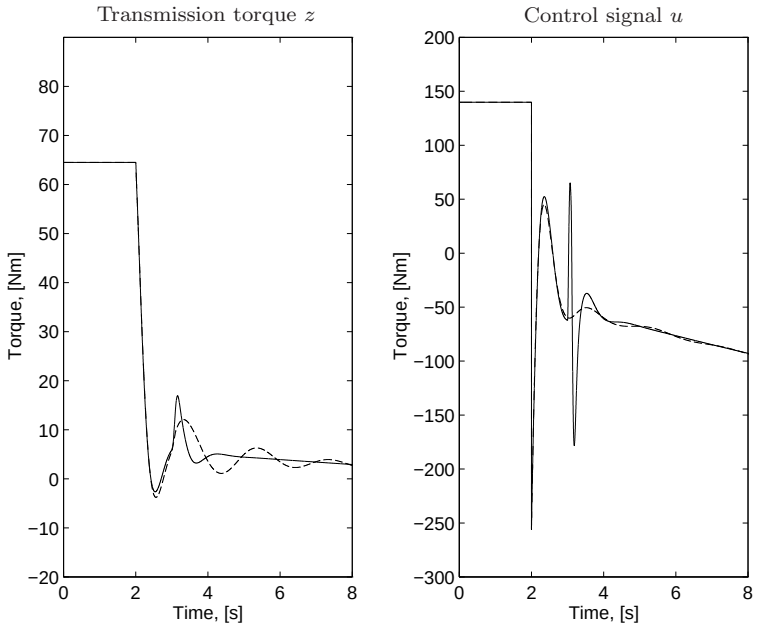

Figure 6.13 *Simulation of Model 3 with observer and control law based on Model 1. An impulse disturbance is acting on the load at $t = 3$ s. Feedback from the wheel speed sensor is seen in solid, and from the engine speed sensor is seen in dashed. The conclusion is that the load disturbance is better attenuated when using feedback from the wheel speed sensor.*

6.8 Summary

Driveline oscillations is a limiting factor in gear shifting with engine control. Based on a model of the transmission torque, a criterion for a gear-shift controller is obtained, that actively damps driveline oscillations. The proposed solution handles the fact that the gear-shift condition is not a stationary point.

When using a driveline model with drive shaft flexibility, it is possible to solve the criterion for a control law that minimizes the cost function. The control law is derived with LQG/LTR technique. Simulations show that the performance of the design, based on the simplified model, works well for a more complicated model with a nonlinear clutch characteristics. However, there can be problems with a low frequency level that gives a stationary error. This difference in level is a result of the difficulty to estimate the driveline friction parameters.

An investigation of the influence, from different sensor locations, on the control design results in the same conclusion as in Chapter 5. When using LQG/LTR the open-loop zeros are cancelled by the controller. This results in undamped load disturbances when engine speed feedback is used. Therefore, load disturbances are better attenuated with feedback from the wheel speed sensor.

Measurement disturbances are better attenuated when the engine speed sensor is used, than when using the wheel speed sensor. This effect increases with lower gears. Two different closed-loop transfer functions result, depending on feedback configuration. The difference between these two is described by the dynamic output ratio.

In conclusion, actively damped transmission-torque control works well also in the case of existing initial oscillations. Furthermore, disturbances occuring during the control action are actively damped, and thus reducing the time needed for a gear shift.

7

Conclusions

The driveline is a fundamental component in a vehicle, and there is currently a strong trend in improving performance by adding functionalities in driveline management systems.

The major contribution of this thesis is a novel gear shifting strategy based on modeling of the transmission torque, and design of a criterion for a controller that drives this torque to zero. This controller is to be used with a new automatic gear shifting system, utilizing engine controlled gear shifting without using the clutch. The proposed solution offers a possibility to optimize the time needed for a gear shift, which is important since the vehicle is free rolling when in gear-shift condition. Furthermore, neutral gear can successfully be engaged also when facing critical load disturbances and initial driveline oscillations.

A second important contribution is the extension of the traditionally used RQV controller. A criterion for a controller that actively damps wheel speed oscillations with a stationary error characteristic for the RQV controller, is obtained. With this controller the performance and driveability is improved since vehicle shuffle is reduced. Furthermore, the formulation is natural, it allows efficient solution, and there is a simple tuning of the amount of RQV feeling.

A basis for these results is the modeling conclusions drawn from experiments and modeling using a heavy truck. A key contribution is the observation that a linear model with stiff clutch and drive shaft flexibility is able to explain the measured engine speed and wheel speed. Extra clutch dynamics is not able to explain more of the experiments for low frequencies. Therefore, the linear model is concluded to be a basis for control design, which is verified by simulations on a model with a nonlinear clutch characteristics.

Another important observation from the experiments is the explanation of the difference between the measured engine speed and transmission speed. The major part of the difference is explained by a simple sensor model. Parameter estimation of a nonlinear model shows that the deviations still left occur when the clutch transfers zero torque.

A common architectural issue in driveline control is the issue of sensor location. Different sensors give the same open-loop poles, but different zeros. An investigation of the influence from different sensor locations on the control design shows that when using LQG/LTR, load disturbances are better damped with feedback from the wheel speed, due to well damped open-loop zeros. Measurement disturbances are better attenuated when the engine speed sensor is used, than when using the wheel speed sensor. The difference is explained by the dynamic output ratio, and increases with lower gears.

There are thus issues to be considered in sensor choice, but the overall conclusion is that the proposed strategies improve performance and driveability in both speed control and gear-shift control.

Bibliography

Björnberg, A., M. Pettersson, and L. Nielsen (1996). Nonlinear driveline oscillations at low clutch torques in heavy trucks. *To be presented at Reglermötet '96 in Luleå, Sweden*.

Bosch (1993). *Automotive Handbook*. Stuttgart, Germany: Robert Bosch GmbH.

Gillespie, T. D. (1992). *Fundamentals of Vehicle Dynamics*. SAE International.

Henriksson, T., M. Pettersson, and F. Gustafsson (1993). An investigation of the longitudinal dynamics of a car, especially air drag and rolling resistance. Technical Report LiTH-ISY-R-1506, Department of Electrical Engineering, Linköping University.

Kubrusly, C. and H. Malebranche (1985). Sensors and controllers location in distributed systems - a survey. *Automatica 21*, 117–128.

Liversidge, J. H. (1952). *Backlash and Resilience within Closed Loop of Automatic Control Systems*. Academic Press.

Ljung, L. (1988). Control Theory 1984-1986. *Automatica 24*, 573–583.

Ljung, L. (1995). *System Identification Toolbox. User's Guide*. MathWorks, Inc.

Maciejowski, J. M. (1989). *Multivariable Feedback Design*. Addison-Wesley.

Meriam, J. L. and L. G. Kraige (1987). *Dynamics*, Volume 2 of *Engineering Mechanics*. John Wiley & Sons.

Mo, C. Y., A. J. Beaumount, and N. N. Powell (1996). Active control of driveability. SAE Paper 960046.

Nwagboso, C. O. (1993). *Automotive Sensory Systems*. Chapman & Hall.

Orehall, L. (1995). Scania opticruise: Mechanical gearchanging with engine control. Truck and Commercial Vehicle International '95.

Pettersson, M. and L. Nielsen (1995). Sensor placement for driveline control. *Preprint of the IFAC-Workshop on Advances in Automotive Control, Ascona, Switzerland*.

Simulink (1993). User's guide. MathWorks, Inc.

Spong, M. W. and M. Vidyasagar (1989). *Robot Dynamics and Control*. John Wiley & Sons.

Suzuki, K. and Y. Tozawa (1992). Influence of powertrain torsional rigidity on NVH of 6x4 trucks. SAE Paper 922482.

Notations

Variables

r	Radius, reference signal
u	Control signal
z	Performance output
x	State vector
y	Sensor output
v	State disturbance, velocity
e	Measurement disturbance
n	Input disturbance
l	Load
θ	Angle
α	Road slope

Symbols

J	Mass moment of inertia
i	Conversion ratio
k	Torsional stiffness

c	Torsional damping
b	Viscous friction component
m	Vehicle mass
$c_{r1},\ c_{r2}$	Coefficients of rolling resistance
c_w	Air drag coefficient
ρ_a	Air density
A_a	Vehicle cross section area
F_a	Air resistance force
F_r	Rolling resistance force
M	Torque, performance output state matrix
A	State-space matrix
B	Input state matrix
C	Output state matrix
H	Load state matrix
D	Performance output control signal matrix
G	Transfer function
$G_{w/m}$	Dynamic output ratio
S	Sensitivity function
T	Complementary sensitivity function
K_c	State-feedback matrix
K_f	Observer gain
φ	Phase margin
a	Amplitude margin

Subscripts

m	Engine
c	Clutch
t	Tranmission
p	Propeller shaft
f	Final drive
d	Drive shafts
w	Wheel
fr	Friction
0	Stationary value
$t1$	Transmission input
$t2$	Transmission output